Study on Optical Access Technologies by Radio-over-Fiber and Precision Time Protocol in Mobile Communication Systems

移動通信システムにおける光ファイバ無線と高精度時刻同期プロトコルを用いた光アクセス技術に関する研究

February 2021

Kazuki TANAKA

田中　和樹

Study on Optical Access Technologies by Radio-over-Fiber and Precision Time Protocol in Mobile Communication Systems

移動通信システムにおける光ファイバ無線と高精度時刻同期プロトコルを用いた光アクセス技術に関する研究

February 2021

Waseda University
Graduate School of Fundamental Science and Engineering
Department of Electronic and Physical Systems,
Research on Radio and Optical Converged Systems

Kazuki TANAKA

田中　和樹

Contents

Chapter 1

Introduction

1-1 Background

The demand of fixed broadband services has increased since the early 2000s. Asymmetric digital subscriber line (ADSL) and very high bit rate digital subscriber line (VDSL) that were mainly used for access links between a central office (CO) and subscribers at the time were almost replaced by fiber to the home (FTTH) using optical access technologies. Point-to-point (PtP) and point-to-multipoint (PtMP) architectures have been utilized in commercial optical access networks. Passive optical networks (PONs) are well-known as cost-effective optical access technologies for one of the PtMP architectures.

Figure 1-1 shows the technology evolution of PON systems [1]. Two standards development organizations (SDOs) of ITU-T and IEEE have standardized some kinds of PON systems to support various data rate requirements. ITU-T G-PON and IEEE G-EPON for 1-Gbit/s class services were standardized in the middle of 2000s and have been mainly used in commercial FTTH services. XG-PON and 10G-EPON for 10-Gbit/s class services were also standardized in around 2010 and have been deployed for commercial services in limited areas. These PON systems are based on time division multiplexing (TDM) and time division multiple access (TDMA). To increase the total system capacity, wavelength division multiplexing (WDM) technologies have been also used. In NG-PON2 that was standardized in 2015, the total system capacity increases up to 40 Gbit/s using four wavelengths whereas the data rate per user is limited to 10 Gbit/s. In 50G-EPON that was standardized in 2020, the data rate per user becomes 50 Gbit/s at maximum using two wavelengths. Currently, a pure TDM-PON system to support 50 Gbit/s is under standardization in ITU-T.

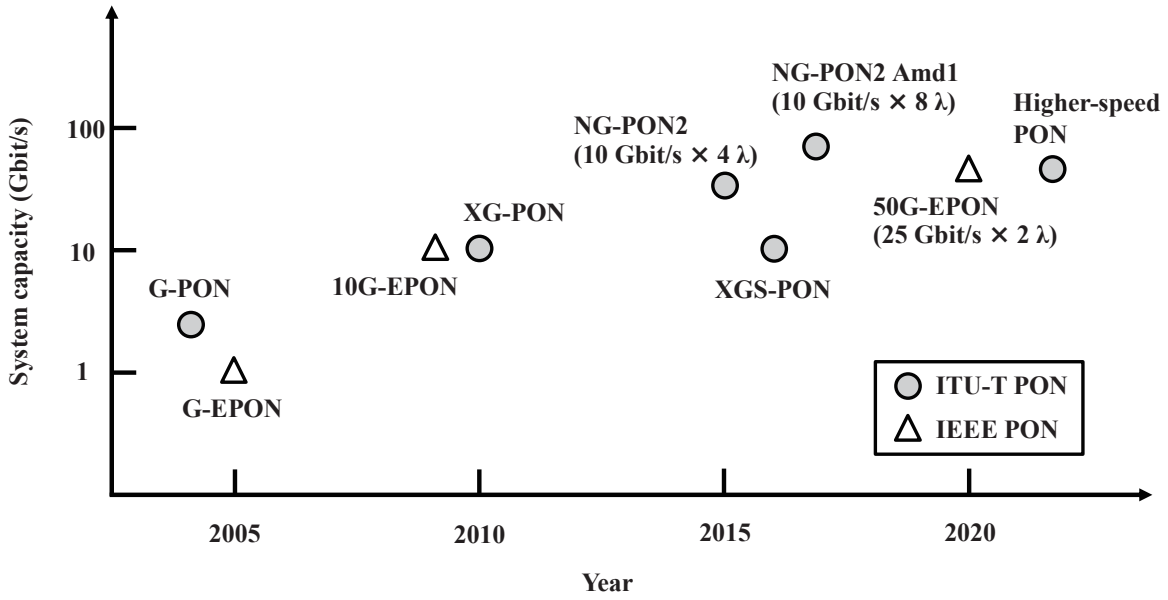

Fig. 1-1 Technology evolution of PON systems in ITU-T and IEEE.

In addition to the expansion of fixed broadband services, the demand of mobile broadband services has been dramatically increasing, and mobile devices such as smartphones are indispensable to life currently. In a recent report, the ownership rate of information and communication equipment in households as of 2018 was shown to be 95.7% for all mobile terminals including 79.2% for smartphones. The rate for smartphones was higher than 74.0% for personal computers and 64.5% for fixed-line phones. Moreover, in the internet usage rates by various individual devices, the rate from smartphones was the highest at 59.5%, and one from personal computers were at 48.2% [2].

Currently, the wireless services provided by domestic telecommunications carriers are mainly based on the 4th generation (4G) mobile communication systems. On the other hand, in some limited areas, commercial services using 5th generation (5G) mobile communication systems have been launched in Japan since 2020. Services are diversified in 5G, and they are classified into three types of enhanced mobile broadband (eMBB), massive-machine type communication (mMTC), and ultra-reliable and low latency communication (URLLC). Requirements are different depending on the service types. The peak data rate for eMBB becomes 20 Gbit/s, the number of simultaneous terminal connections for mMTC becomes one million devices/km^2, and the delay for URLLC becomes 1 ms [3]. For expanding 5G service areas, it will be necessary to aim for excellent configurations from the perspective of

performance and cost in the entire system including wireless and optical systems. Furthermore, in beyond 5G era, each service type from 5G mobile systems will require the performance improvement, and the emergence of completely new service types will also impose difficult transmission conditions on optical access networks (NWs). Table 1-1 shows the predictive peak data rate and delay required in beyond 5G [4], in view of the evolution of mobile communication systems toward 5G. It is noted that the delay shows the value in radio sections between base stations (BSs) and user equipment (UE).

Table 1-1 The peak data rate and delay required in beyond 5G.

Item	Generation		
	4G	5G	Beyond 5G
Peak data rate (Gbit/s)	1	10-20	> 100
Delay (ms)	10	1	0.1

In order to achieve high peak data rates in 5G and beyond 5G, it is essential to use high frequency bands such as millimeter waves where a wide channel bandwidth (BW) can be utilized. In general, a high-frequency signal suffers large signal attenuation due to the radio wave propagation and obstacles, and, as the result of that, it is necessary to densely construct small wireless service areas called small cells in many places. In order to expand service areas promptly to the required sites, available deployed optical access fibers that connect antenna sites to the CO should be effectively and efficiently used, in addition to downsizing and power saving the wireless and optical transmission equipment in antenna sites.

A conventional 4G mobile BS consists of baseband unit (BBU) and remote radio head (RRH). Depending on the allocation of the BBU and RRH, there exist two configurations, distributed radio access network (D-RAN) and centralized RAN (C-RAN) [5]. In D-RAN, both BBU and RRH are deployed near the antenna, and the BBU is connected to a CO by layer 2 (L2) or layer 3 (L3) transmission links that are called mobile backhaul (MBH). In time division duplex (TDD) -based mobile BSs, a global positioning system (GPS) antenna has

been commonly deployed in each BS antenna site, and each of the BSs is synchronized to the precise time from the GPS signal. When much more BSs are deployed in 5G and the future mobile systems, the deployment of GPS antennas will cause higher total system cost and longer coverage expansion period. On the other hand, in C-RAN, BBUs are located in a CO, and one or plural RRHs are placed near each BS antenna. Digitized radio-over-fiber (D-RoF) technologies, that sample and quantize radio waveforms and then transmit the digital signals over a fiber, have been used for the connection between BBU and RRH. The optical transmission between BBU and RRH in C-RAN is called mobile fronthaul (MFH). In the C-RAN architecture, multiple RRHs can be controlled by the cooperative BBUs on the CO side, and, as a result, the transmission characteristics at cell edges can be improved. However, the common public radio interface (CPRI) [6], [7] that has been commonly used for the optical link between BBU and RRH in 4G C-RAN requires an approximately sixteen times higher data rate than the mobile user data rate [8]. Considering the peak data rate of 20 Gbit/s in 5G mobile systems and available optical access technologies, continuously using the conventional CPRI will cause a significant increase in the cost of the optical access links.

1-2 Objective

As described in Section 1-1, in mobile communication systems for 5G and beyond 5G, optical access fiber resources should be efficiently used, that is, an access fiber should be shared with multiple antenna sites. Additionally, in MBH, time synchronization techniques without the deployment of GPS antennas are needed, and, in MFH, simple, cost-effective and large-capacity optical access systems are required avoiding using conventional CPRI links. The detailed purpose of this study on the future MBH and MFH is described as follows.

Precise time synchronization among multiple BSs are required for network handover function, suppression of radio frequency (RF) interference among adjacent cells, advanced wireless technologies including coordinated multi-point (CoMP) [9] and enhanced inter-cell interference coordination (eICIC) [10]. To date, a GPS antenna has been deployed to each BS site, and the GPS signal is used for synchronizing the BS to the precise time. RF cables are commonly used for the connection between the antenna and the BS. When BSs need to be

placed in indoor areas such as subway station, underground town and building, long RF cables must be deployed. However, the deployment for the GPS antennas and RF cables is not easy due to several restrictions such as space, power, and usage. The process sometimes causes higher deployment cost and longer deployment period and, in the worst case scenario, makes the deployment of BSs impossible. Therefore, to solve the deployment issue, technologies to transmit signals for synchronization via MBH will be attractive. Several kinds of the techniques have been studied [11], [12]. Precision time protocol (PTP) defined in IEEE 1588-2008 [11] enables PTP slaves to synchronize to a PTP master in frequency or time over packet-based networks. Most of the current mobile BSs support the PTP function in addition to having GPS input interface for their synchronization However, PTP can effectively work only when the delay of the uplink transmission is the same as that of the downlink transmission, which means conventional TDM-PON systems that have much larger delays in uplink transmission can not be used as the packet-based networks. Another synchronization technique via transmission networks was proposed using TDM-PON systems [12]. In the proposed system, packets for one pulse per second (1PPS) timing and time of date (ToD) from GPS signals are transmitted from an optical line terminal (OLT) in a CO to optical network units (ONUs) in BS deployment sites. Currently available BSs have no 1PPS and ToD input interface for their synchronization. Therefore, equipment that emulates real GPS signals from the 1PPS and ToD signals is required, which will cause system complexity at each BS site and increase the total system cost. Furthermore, in the proposed system, the redundancy of the GPS signal source has not been discussed. To avoid large-scale system failures, such a function should be considered. In chapter 3, a novel time synchronization technique among mobile BSs is proposed. In the proposed technique, TDM-PON and common PTP can be used for MBH and time information transmission to mobile BSs, respectively. The function of the GPS antenna site redundancy is also considered. The proposed technique is experimentally demonstrated using a 10G-EPON [13] prototype.

CPRI that has been used for 4G C-RAN may not be scalable to 5G C-RAN with the large capacity corresponding to 20-Gbit/s mobile user data rate at maximum. Three technical approaches to solve the capacity issue have been studied. The first one is CPRI data compression techniques [14], [15]. CPRI data compression by 50% has been successfully demonstrated. However, CPRI compression basically causes signal deteriorations. Additionally, it will not be effective when the mobile user data rate increases. The second approach is to change the functional splitting point in a mobile BS. The BBU for 4G C-RAN

includes packet data convergence protocol (PDCP), radio link control (RLC), media access control (MAC), and physical layer (PHY) functions whereas the RRH includes an RF function [16]. The tradeoff relationship between required optical link capacity and obtained cooperative operation performance among cells occurs when a splitting point for a mobile BS is selected [16]. When one of the low-layer splitting points such as intra-PHY is chosen, the cooperative operation performance may be acceptable whereas the optical link capacity will not be sufficiently reduced for the mature phase of 5G. Therefore, this approach will not be a fundamental solution. The third approach is intermediate frequency-over-fiber (IFoF) transmission technologies [17], one of the analog radio-over-fiber (A-RoF) technologies, where multiple IF signals are subcarrier multiplexed and then transmitted over a fiber by simple intensity modulation and direct detection (IMDD) scheme. Many papers discussed transmission technologies to increase the IFoF link capacity or simplify the transmission components. For increasing the capacity, various techniques were proposed in terms of solving the issues of RF power fading due to the chromatic dispersion from optical fibers [18]-[20], composite second order distortions [21], [22], nonlinear distortions from optical devices [20], [23], and optical interference noises from multiple optical reflection points. For simplifying the optical transmission components, the use of vertical cavity surface emitting lasers (VCSELs) was proposed [24]. However, few papers discussed filters for extracting each IF channel and frequency converters from IF signals to RF signals which are essential in antenna sites of the downlink transmission. The functions were experimentally demonstrated by analog signal processing [25] and digital signal processing (DSP) [26]-[30]. Concerning the DSP approach, the separation of each IF channel from the others by off-line process [26]-[28], and both extractions of each IF channel and frequency conversions from the IF to the other IF by real-time DSP [29], [30] have been reported. However, the real-time DSP will not have enough performance for 5G and beyond 5G mobile systems where a channel bandwidth of 400 MHz and more, multi-user multiple-input multiple-output (MIMO), and carrier aggregated signals should be considered. The other issues in 5G and the future C-RAN will be the restrictions of deployment spaces and power consumptions especially in antenna sites and the shortage of available access fibers because the number of small cells are expected to dramatically increase. To expand service areas rapidly and configure cost-effective systems, simple equipment for antenna sites and PtMP network architectures will be strongly required. For simplifying antenna sites, using DSP for channel extractions and frequency conversions will be one of the effective ways. Regarding PtMP architectures,

three kinds of access systems have been proposed [31]-[34]. The first system is based on a ring topology using WDM technologies [31]. This kind of system can basically have a function for the protection against network failures and be more reliable whereas the system cost will not be reasonable. The second system is based on a WDM-PON technology with a WDM coupler [32], [33]. An access fiber can be shared by multiple ONUs in such a system. However, most of the deployed access fibers at this moment are based on PtP or PtMP using a power splitter. Therefore, available access fibers can not be effectively applied to such a system, and most of the access fibers for the systems will be newly deployed. The third system is based on a subcarrier multiplexing PON (SCM-PON) technology with a power splitter [34]. Commercially available access fibers can be effectively used in such a system, and the number of newly deployed access fibers can be reduced. However, in the uplink transmission, the transmitted signals may suffer large interference noises at the receiver of an OLT unless a wavelength division multiple access (WDMA) is not applied to the system. It is also obvious in current optical access areas that using tunable optical components for WDM transmission increases the total system cost. Furthermore, in the downlink of SCM-PON systems, wideband optical and electric components are used in each antenna site, which may also increase the system cost. In Chapter 2, a new PtMP MFH architecture that is suitable for 5G is proposed. A feature is to place a relay site to connect a CO and multiple antenna sites. The advantage of the new architecture is investigated in comparison with conventional PtP CPRI-based MFH links. In Chapter 4, the applicability of IFoF transmission technologies to commercially available 4G mobile systems is experimentally evaluated, before studying IFoF systems for 5G and future MFH. In Chapter 5, the proposed PtMP MFH system with over 20-Gbit/s user data rate that is described in Chapter 2 is experimentally demonstrated using real-time field programmable gate array (FPGA) -based DSP equipment for IF channel extractions and frequency conversions at antenna sites. For briefly summarizing the description above, MBH and MFH systems discussed in this thesis are illustrated in Figure 1-2.

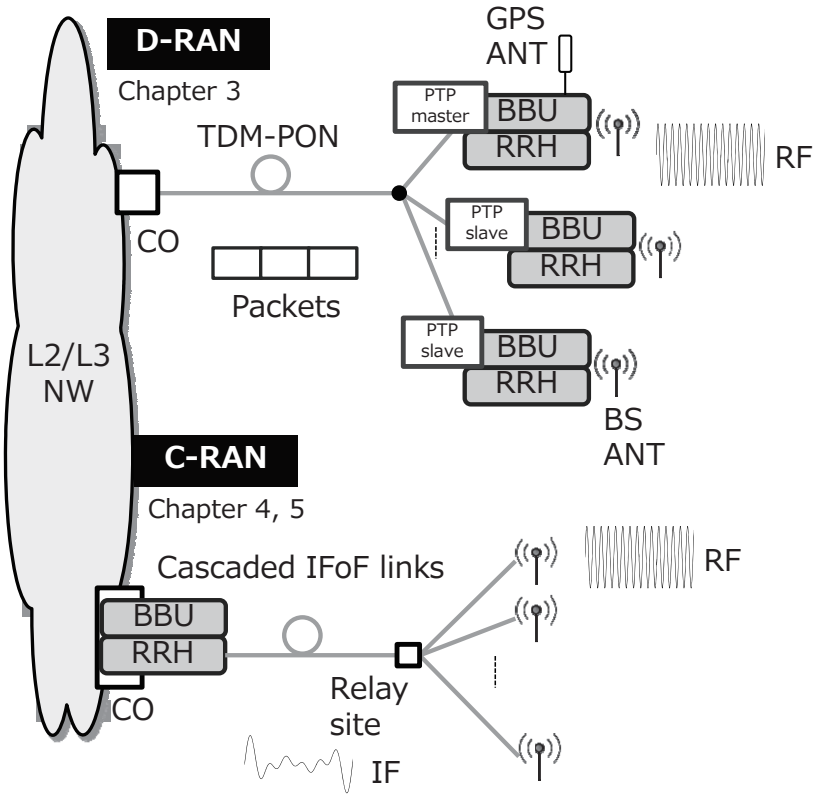

Fig. 1-2 MBH and MFH systems studied in this thesis.

This study mainly discusses two of the issues in D-RAN and C-RAN architectures above. However, the applications of the technologies are not limited to D-RAN or C-RAN in the evolution of mobile systems. In 4G mobile systems, most BSs are based on D-RAN, and the proposed TDM-PON with a time synchronization function can be used as MBH links. When the deployment space or power is insufficient in a certain place, antenna equipment can be separately located from the BBU and RRH by the A-RoF technologies that are studied for C-RAN MFH links. As a result, the service areas for D-RAN will be flexibly and easily expanded especially for indoors. In 5G and the future systems, the ratio of C-RAN to D-RAN will gradually increase. The A-RoF technologies for C-RAN can be applied to the 5G D-RAN in the same manner as the 4G D-RAN. In the initial phase of 5G C-RAN, the functional splitting that was introduced as the second approach to the CPRI capacity issue will be also effective. In the MFH system that uses the functional splitting, the TDM-PON system with a time synchronization function that is studied for D-RAN can be also used. In the mature phase of 5G and also the future C-RAN, A-RoF technologies are expected to be one of the most promising solutions as MFH links. The precise time that is transmitted over TDM-PON by the

proposed technique for D-RAN will be also used as a reference clock for the C-RAN. I strongly believe the technologies discussed in this thesis consistently contribute to the evolution of the future optical access systems for mobile applications.

1-3 Outline of the thesis

This thesis studies optical access technologies for the future MBH and MFH systems in six chapters. Figure 1-3 shows the organization of this thesis. Optical access technologies for MBH are presented in Chapters 2 and 3, and those for MFH are described in Chapters 2, 4, and 5. The contents of each of the chapters are summarized as follows.

In Chapter 1, the evolution of PON systems as optical access technologies is introduced. Main requirements from mobile systems to optical access systems, and issues in MBH and MFH systems are also described. Additionally, the purpose of this thesis is mentioned.

In Chapter 2, basic concepts and technologies for RAN architectures and RoF systems are explained. Then, cascaded IFoF-based systems as a new PtMP architecture for 5G MFH are proposed. Additionally, the proposed systems are compared with conventional CPRI-based MFH systems in terms of required optical fiber resources and system components and functions. The advantages of the proposed systems are clarified.

In Chapter 3, time synchronization technologies using GPS signals and PTP packets are presented. The features of PON technologies such as TDM-PON system and WDM-PON system are also explained. Then, a novel time synchronization technique with a function of GPS antenna site redundancy is proposed. Using a 10G-EPON prototype that implements the proposed functions, the new technique is experimentally evaluated. In addition to the unit tests, the interoperability tests with commercially available PTP slave and time division long term evolution (TD-LTE) BS are conducted. The obtained results verify the applicability of the prototype to the commercial equipment, achieving sufficient absolute time accuracy of 119 ns to a criterion of ±1.5 μs for TD-LTE systems.

In Chapter 4, broadcasting systems and mobile communication systems are presented as use cases of A-RoF technologies. Focusing on the use case of the MFH, the performances of IFoF links for IF channels with 20-MHz channel bandwidths for 4G mobile systems and

100-MHz channel bandwidths for 5G mobile systems are evaluated by numerical calculations in various transmission conditions. From the calculation results, when the optical transmission conditions are properly selected, it is confirmed that 54 IF channels with 100-MHz bandwidths in 64-quadrature amplitude modulation (64-QAM) format can be transmitted over an optical fiber. In addition to the numerical calculations, the performance of IFoF-based links are experimentally evaluated, in order to confirm the applicability to commercial 4G LTE systems and deployed optical fibers. In the experiment, subcarrier multiplexed IF channels with 20-MHz channel bandwidths that consist of one real LTE signal and 23 dummy signals are successfully transmitted over a 7.8-km deployed optical fiber link including two large optical reflection points of -27.9 dB and -21.5 dB.

In Chapter 5, the concept of a cascaded IFoF system with analog and digital hybrid signal processing for 5G and future MFH is presented in detail. The proposed system is compared with SCM-PON system, in terms of bandwidths required in optical-to-electrical converters (O/Es) and electrical-to-optical converters (E/Os) for downlink in various numbers of antenna sites and IF channel bandwidths. The reduction of the bandwidths in the proposed system is clarified. Additionally, real-time FPGA-based DSP equipment for the proposed system is described in detail. The equipment implements the functions of digital filters for extracting each IF channel and frequency converters from each IF to a specific IF. Using the DSP equipment, the cascaded IFoF system with hybrid signal processing is experimentally demonstrated. In the transmission experiments, eighteen 64-QAM orthogonal frequency division multiplexing (OFDM) signals with 400-MHz channel bandwidths are transmitted over 20-km and 1-km optical fibers, and, after the DSP equipment, an error vector magnitude (EVM) criterion for 64-QAM signals of less than 8% is achieved.

Finally, in Chapter 6, conclusions from all of the results that are obtained in this thesis are summarized.

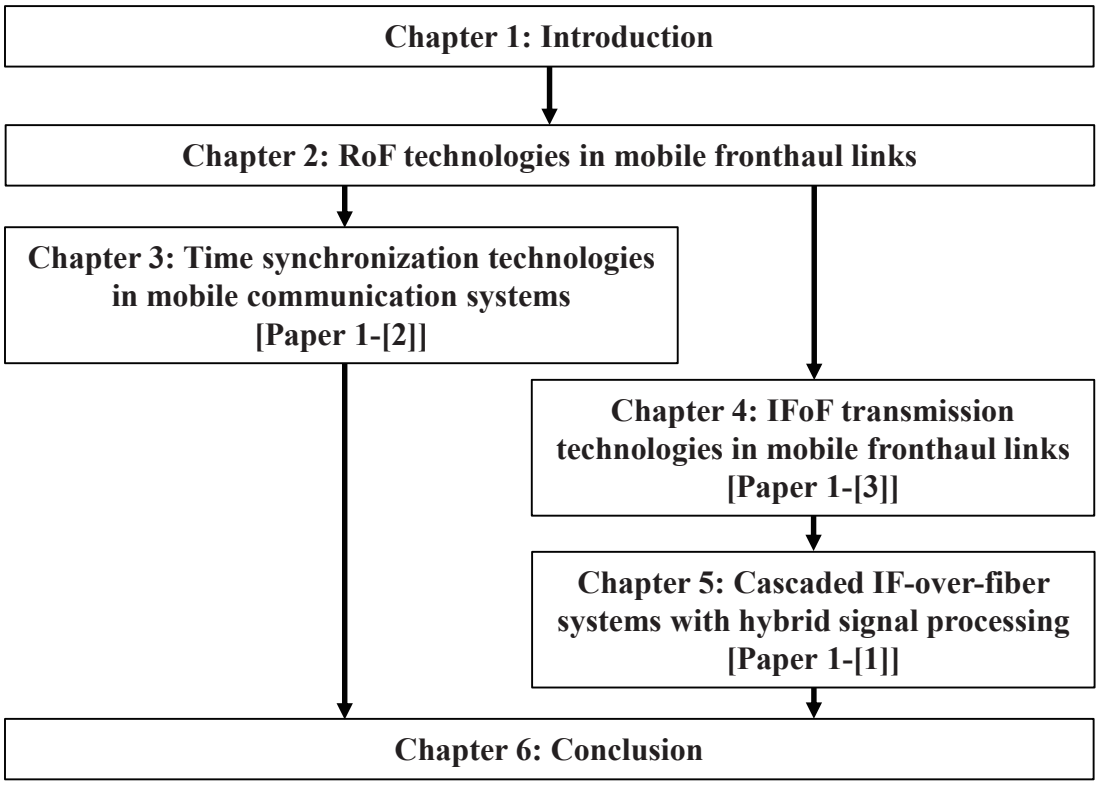

Fig. 1-3 Organization of the thesis.

References

[1] J. S. Wey, "The Outlook for PON Standardization: A Tutorial," *IEEE J. Lightwave Technol.*, vol. 38, no. 1, pp. 31-42, 2020.

[2] Ministry of Internal affairs and Communications, Japan, "White Paper on Information and Communications in Japan," 2019.

[3] Recommendation ITU-R M.2083-0, "IMT Vision – Framework and overall objectives of the future development of IMT for 2020 and beyond," 2015.

[4] K. Tanaka, S. Ishimura, and K. Nishimura, "Radio-over-Fiber Technologies for Mobile Communication Systems," *The Review of Laser Engineering*, vol. 48, no. 1, pp. 6-10, 2020.

[5] S. Namba, T. Matsunaka, T. Warabino, S. Kaneko, and Y. Kishi, "Colony-RAN architecture for future cellular network," in *Proc. Future Network & Mobile Summit*, pp. 1-8, Berlin, Germany, July 2012.

[6] CPRI Specification V7.0, "Common Public Radio Interface (CPRI); Interface Specification," 2015.

[7] A. de la Oliva, J. A. Hernández, D. Larrabeiti, and A. Azcorra, "An Overview of the CPRI Specification and Its Application to C-RAN-Based LTE Scenarios," *IEEE Communications Magazine*, vol. 54, no. 2, pp. 152-159, 2016.

[8] K. Tanaka and A. Agata, "Next-Generation Optical Access Networks for C-RAN," in *Proc. Optical Fiber Communication Conference (OFC)*, Tu2E.1, Los Angeles, CA, Mar. 2015.

[9] H. Zhang, and H. Dai, "Cochannel Interference Mitigation and Cooperative Processing in Downlink Multicell Multiuser MIMO Networks," *EURASIP Journal on Wireless Communications and Networking*, pp. 222-235, 2004.

[10] S. Vasudevan, R. N. Pupala and K. Sivanesan, "Dynamic eICIC — A Proactive Strategy for Improving Spectral Efficiencies of Heterogeneous LTE Cellular Networks by Leveraging User Mobility and Traffic Dynamics", *IEEE Trans. on Wireless Communications*, vol.12, no. 10, pp. 4956–4969, 2013.

[11] IEEE Std 1588-2008, "IEEE Standard for a Precision Clock Synchronization Protocol for Networked Measurement and Control Systems," 2008.

[12] Y. Horiuchi and K. Tanaka, “Precise Time Distribution using Ethernet Passive Optical Network,” in *Proc. 34th European Conference on Optical Communication (ECOC)*, paper We.2.F.7, Brussels, Belgium, Sept. 2008.

[13] IEEE Std 802.3av-2009, “Part 3: Carrier sense multiple access with collision detection (CSMA/CD) access method and physical layer specifications Amendment 1: Physical Layer Specifications and Management Parameters for 10 Gb/s Passive Optical Networks,” 2009.

[14] M. Xu, Z. Jia, J. Wang, L. A. Campos, and G. K. Chang, “Statistical Data Compression and Differential Coding for Digital Radio-Over-Fiber-Based Mobile Fronthaul,” *IEEE J. Opt. Commun. Netw.*, vol. 11, no. 1, pp. A60-A71, 2019.

[15] S. H. Kim, H. S. Chung, and S. M. Kim, “Experimental demonstration of CPRI data compression based on partial bit sampling for mobile front-haul link in C-RAN,” in *Proc. Optical Fiber Communication Conference (OFC)*, W1H5, Anaheim, CA, Mar. 2016.

[16] 3GPP TR 38.801 v2.0.0 Release 14, “Technical Specification Group Radio Access Network; Study on New Radio Access Technology; Radio Access Architecture and Interfaces,” 2017.

[17] ITU-T G-series Reccommendations - Supplement 55, “Radio-over-fibre (RoF) technologies and their applications,” 2015.

[18] S. Ishimura, A. Bekkali, K. Tanaka, K. Nishimura, and M. Suzuki, “1.032-Tb/s CPRI-Equivalent Rate IF-Over-Fiber Transmission Using a Parallel IM/PM Transmitter for High-Capacity Mobile Fronthaul Links,” *IEEE J. Lightwave Technol.*, vol. 36, no. 8, pp. 1478-1484, 2018.

[19] A. Bekkali, S. Ishimura, K. Tanaka, K. Nishimura, and M. Suzuki, “Multi-IF-Over-Fiber System With Adaptive Frequency Transmit Diversity for High Capacity Mobile Fronthaul,” *IEEE J. Lightwave Technol.*, vol. 37, no. 19, pp. 4957-4966, 2019.

[20] P. Li, W. Pan, L. Huang, X. Zou, Y. Pan, Q. Zhou, Y. W. Chen, P. C. Peng, S. Liu, S. Shen, and G. K. Chang, “Multi-IF-Over-Fiber Based Mobile Fronthaul With Blind Linearization and Flexible Dispersion Induced Bandwidth Penalty Mitigation,” *IEEE J. Lightwave Technol.*, vol. 37, no. 4, pp. 1424-1433, 2019.

[21] B. G. Kim, S. H. Bae, and Y. C. Chung, "Adaptive Blind CSO Cancellation Technique for RoF Systems Implemented by Using DMLs," *IEEE Photon. Technol. Lett.*, vol. 30, no. 20, pp. 1745-1748, 2018.

[22] C. Han, M. Sung, S. H. Cho, H. S. Chung, S. M. Kim, and J. H. Lee, "Performance Improvement of Multi-IFoF-Based Mobile Fronthaul Using Dispersion-Induced Distortion Mitigation With IF Optimization," *IEEE J. Lightwave Technol.*, vol. 34, no. 20, pp. 4772-4778, 2016.

[23] H. J. Park, S. Y. Jung, D. W. Kwon, S. H. Cho, H. S. Chung, J. H. Lee, and S. K. Han, "Distortion Mitigation in Multiband OFDM RoF Transmission Employing Blind Post Equalizer," *IEEE Photon. Technol. Lett.*, vol. 28, no. 23, pp. 2708–2711, 2016.

[24] Byung Gon Kim, S. R. Bae, Roan Kim, and Y. C. Chung, "Mobile fronthaul optical link for LTE-A system using directly-modulated 1.5-μm VCSEL," in *Proc. 21st Optoelectronics and Communications Conference (OECC)*, paper TuA2-3, Niigata, Japan, July 2016.

[25] M. Zhu, X. Liu, N. Chand, F. Effenberger, and G. K. Chang, "High-capacity mobile fronthaul supporting LTE-advanced carrier aggregation and 8×8 MIMO," in *Proc. Optical Fiber Communication Conference (OFC)*, M2J.3, Los Angeles, CA, Mar. 2015.

[26] X. Liu, F. Effenberger, N. Chand, L. Zhou, and H. Lin, "Demonstration of bandwidth-efficient mobile fronthaul enabling seamless aggregation of 36 E-UTRA-like wireless signals in a single 1.1-GHz wavelength channel," in *Proc. Optical Fiber Communication Conference (OFC)*, M2J.2, Los Angeles, CA, Mar. 2015.

[27] X. Liu, H. Zeng, N. Chand, and F. Effenberger, "Experimental demonstration of high-throughput low-latency mobile fronthaul supporting 48 20-MHz LTE signals with 59-Gb/s CPRI-equivalent rate and 2-μs processing latency," in *Proc. European Conference on Optical Communication (ECOC)*, We.4.4.3, Valencia, Spain, Sept. 2015.

[28] L. Cheng, X. Liu, N. Chand, F. Effenberger, and G. K. Chang, "Experimental demonstration of sub-Nyquist sampling for bandwidth- and hardware-efficient mobile fronthaul supporting 128×128 MIMO with 100-MHz OFDM signals," in *Proc. Optical Fiber Communication Conference (OFC)*, W3C.3, Anaheim, CA, Mar. 2016.

[29] T. Xu, A. Fumagalli, and R. Hui, "Dynamic optical networks based on digital subcarrier multiplexing," in *Proc. SPIE* 10560, 105600N, 2018.

[30] T. Xu, A. Fumagalli, and R. Hui, "Efficient real-time digital subcarrier cross-connect

(DSXC) based on distributed arithmetic DSP algorithm," *IEEE J. Lightwave Technol.*, vol. 38, no. 13, pp. 3495-3505, 2020.

[31] S. H. Cho, H. Park, H. S. Chung, K. H. Doo, S. Lee, and J. H. Lee, "Cost-effective Next Generation Mobile Fronthaul Architecture with Multi-IF Carrier Transmission Scheme," in *Proc. Optical Fiber Communication Conference (OFC)*, Tu2B.6, San Francisco, CA, Mar. 2014.

[32] M. Xu , J. H. Yan, J. Zhang, F. Lu, J. Wang, L. Cheng, D. Guidotti, and G. K. Chang, "Bidirectional Fiber-Wireless Access Technology for 5G Mobile Spectral Aggregation and Cell Densification," *IEEE J. Opt. Commun. Netw.*, vol. 8, no. 12, pp. B104–B110, 2016.

[33] Y. Zhu, Y. Wu, H. Xu, C. Browning, L. P. Barry, and Y. Yu, "Experimental Demonstration of a WDM-RoF Based Mobile Fronthaul With f-OFDM Signals by Using Directly Modulated 3s-DBR Laser," *IEEE J. Lightwave Technol.*, vol. 37, no. 16, pp. 3875–3881, 2019.

[34] M. Befekadu, S. Straullu, S. Abrate, and R. Gaudino, "Experimental Optimization of DSP-Aggregated Front-hauling Transmission for up to 4x96 LTE radio waveforms," in *Proc. European Conference on Optical Communication (ECOC)*, W.4.P1.SC7.73, Düsseldorf, Germany, Sept. 2016.

Chapter 2

RoF technologies in mobile fronthaul links

2-1 Introduction

In 4G mobile communication systems, C-RANs have been commercially used in some limited areas. CPRI [1], [2] is a well-known MFH interface between BBU and RRH in C-RANs. The CPRI line rate becomes around sixteen times as large as mobile user data rate [3]. Therefore, the high line rate will be a critical issue in 5G C-RANs because the maximum data rate in 5G mobile communication systems is expected to reach 20 Gbit/s. IFoF technologies included in one of the A-RoF technologies have attracted much attention as one of the solutions to the CPRI capacity issue, and many papers studied IFoF transmission technologies and systems for C-RAN MFH [4]-[8]. Additionally, some papers discussed the comparison between A-RoF technologies and D-RoF technologies for mobile applications [9]-[14]. In Ref. [13], [14], D-RoF and A-RoF technologies for MFH links were compared with each other from the viewpoints of required bandwidth, normalized deployment cost, and system complexity. However, the papers to date have not considered the impact of system level functions such as clock distribution and operation, administration and maintenance (OAM). Additionally, a cascaded IFoF-based MFH system as a new MFH for PtMP architecture [15] has not been compared with a conventional CPRI-based MFH system in detail.

In this chapter, conventional D-RoF technologies for MFH links in C-RAN are compared with A-RoF technologies. Firstly, two kinds of RAN architectures, D-RAN and C-RAN, are explained. Then, two kinds of RoF systems, D-RoF and A-RoF, are introduced. Furthermore, a cascaded IFoF system, one of the A-RoF systems, for a simple PtMP architecture is described. Finally, a CPRI-based MFH system using D-RoF technologies is compared with IFoF-based MFH systems using A-RoF technologies from the perspective of system complexity and required fiber resources.

2-2 RAN architectures

In this section, two kinds of RAN architectures, D-RAN and C-RAN, are introduced.

2-2.1 D-RAN architecture

In current 4G mobile communication systems, a D-RAN architecture has been mainly utilized. Figure 2-1 shows a schematic diagram of D-RAN-based mobile system. A base station consists of BBU for higher layer functions and RRH for lower layer functions, and both of the equipment are located at an antenna site. It is noted that, in 5G mobile communication systems, a mobile BS can be split into three parts, central unit (CU), distributed unit (DU), and remote unit (RU) [16]. The BBUs are connected to the mobile core network via L2 or L3 transmission networks including optical access networks between CO and antenna sites. In D-RANs, the transmission networks between BBUs and the mobile core are called MBH. For the downlink transmission, the BBU generates the baseband signals of wireless OFDM signals, and the RRH converts the signals to the RF signals. In most cases, each BS is synchronized to the precise time from GPS by receiving the signal from a GPS antenna. Time synchronization among BSs are required for network handover, suppression of RF interference, and advanced wireless technologies. D-RAN-based BSs independently work with one another.

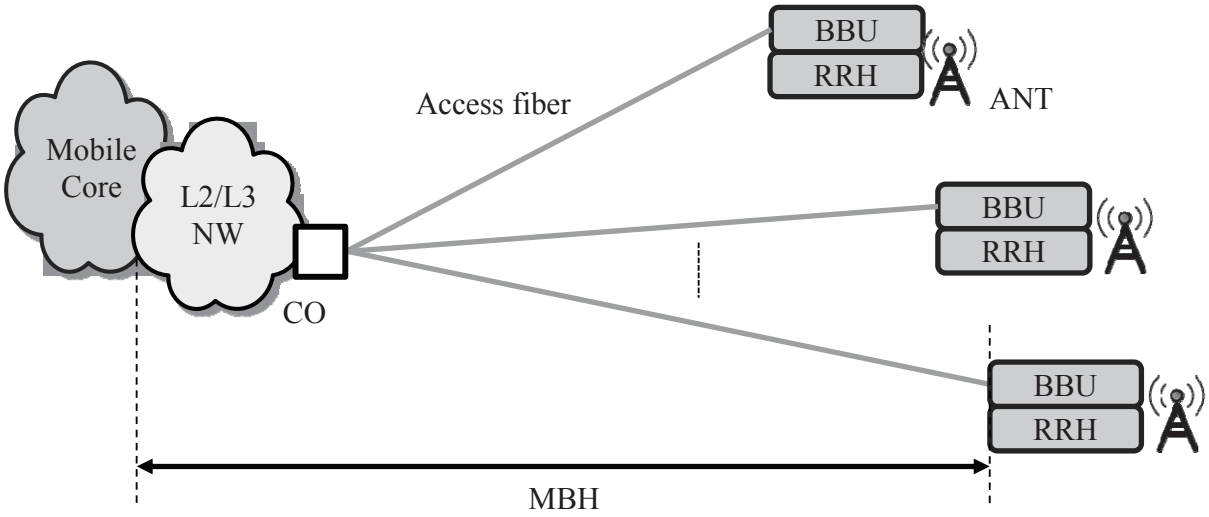

Fig. 2-1 D-RAN architecture.

2-2.2 C-RAN architecture

In 4G mobile communication systems, a C-RAN architecture has been also used mainly in high density urban areas. Figure 2-2 depicts a schematic diagram of C-RAN architecture. The difference between C-RAN and D-RAN is the location of BBUs. In C-RANs, BBUs for plural RRHs are centralized in a CO. In such a configuration, cooperative operations among BSs or cells can be easily performed, and, as a result, interference noises among BSs can be effectively suppressed. Figure 2-3 illustrates a schematic diagram of the functional blocks for a mobile BS [17]. 4G mobile BSs include L1 to L3 functions in the BBUs and an RF function in the RRHs. Therefore, in C-RANs, equipment in antenna sites can be simplified, and the total power consumption and cost are expected to be lower than D-RANs. As a result of that, service areas are expected to expand promptly using C-RANs, which will be a big advantage because the number of small cell sites dramatically increases in the future. However, it is well-known that the functional split between PHY and RF for the conventional CPRI causes more severe requirements for the transmission delay and capacity than the other higher layer functional splits [17]

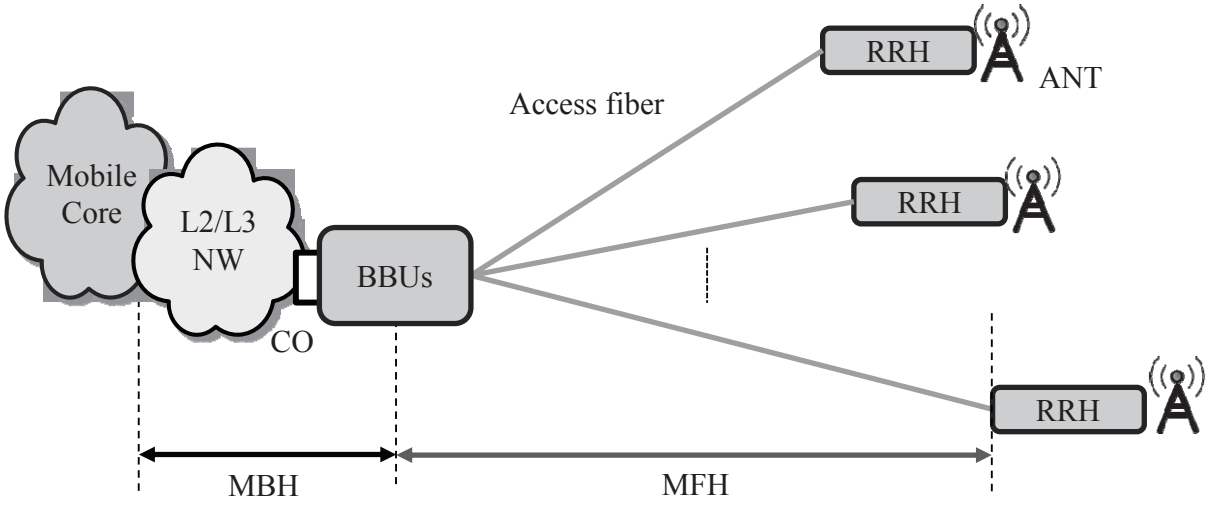

Fig. 2-2 C-RAN architecture.

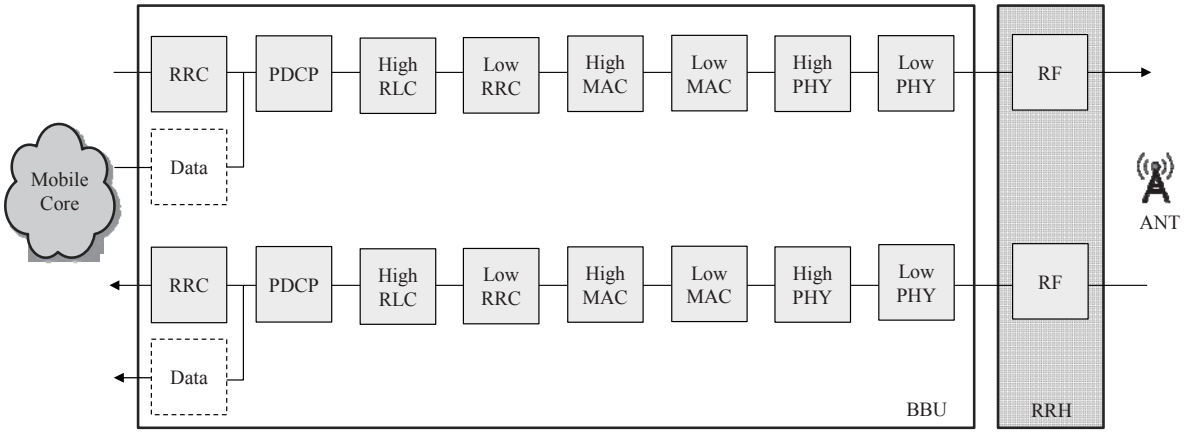

Fig. 2-3 Functional blocks in a mobile BS.

2-3 RoF systems

In this section, two kinds of RoF technologies, D-RoF and A-RoF are introduced. As one of the A-RoF technologies, IFoF technologies are also explained. Additionally, a cascaded IFoF architecture as a new type of PtMP architecture for MFH is proposed.

2-3.1 Digitized RoF transmission

Figure 2-4 shows an example of a D-RoF transmission system for downlink. Digitized analog radio waveforms are generated in a CO or upper networks. The electric digital signal is converted to the optical digital signal by an E/O and transmitted to a remote antenna site over an access fiber. In the antenna site, the optical digital signal is converted to the electric signal by an O/E, and the electric digital signal is converted to the analog signal by a digital-to-analog converter (DAC). The analog signal is finally emitted from an antenna after the signal power is adjusted by an RF amplifier. In D-RoF transmission systems, high-quality wireless signals can be obtained whereas the data rate of the optical digital link is much higher than the user data rate of the analog signal. D-RoF transmission systems have been commercially used for 4G CPRI MFH links and distributed antenna systems (DASs) for blind zones. Figure 2-5 describes the frame structure of CPRI [1], [2]. CPRI 10 ms frames are transmitted between BBUs and RRHs. Each CPRI 10 ms frame consists of 150 hyper frames, and each of the hyper frames with a 66.67-μs time length includes 256 basic frames. Each basic frame with a 260.416-ns time length has a control word (CW) of $1\times n$ byte and in-phase and quadrature (IQ) data block of $15\times n$ byte. CPRI option number is expressed by n. In the CWs, each control word is used for synchronization, L1 in-band protocol, slow and fast control and management (C&M) links, control (ctrl)_antenna carrier (AxC), reservation for future use, or vender specific. The IQ data samples for antenna data streams, that correspond to the digitized analog waveforms mentioned above, are also carried in the IQ data blocks. To date, CPRI line rates from 0.6144 Gbit/s for option #1 to 24.33024 Gbit/s for option #10 have been specified as shown in Table 2-1 [1]. Line coding is necessary for simultaneously transmitting the data and clock on a line in serial data transmission. In CPRI option #1 to #6, 8B/10B line coding is used for serial transmission whereas, in CPRI option #8 to #10, 64B/66B line coding is used. For option #7, in addition to 8B/10B line coding, 64B/66B has been defined. Depending on the antenna design and configuration, operators can select a proper CPRI option. For example, when eight antenna ports and a 200-MHz wireless channel bandwidth are assumed, the required data rate in the CPRI-based MFH link will be around 80 Gbit/s without line coding [17]. Therefore, seven CPRI option #9 links with the capacities of 12.16512 Gbit/s by each link and 85.15584 Gbit/s by all of the links will be one of the selections.

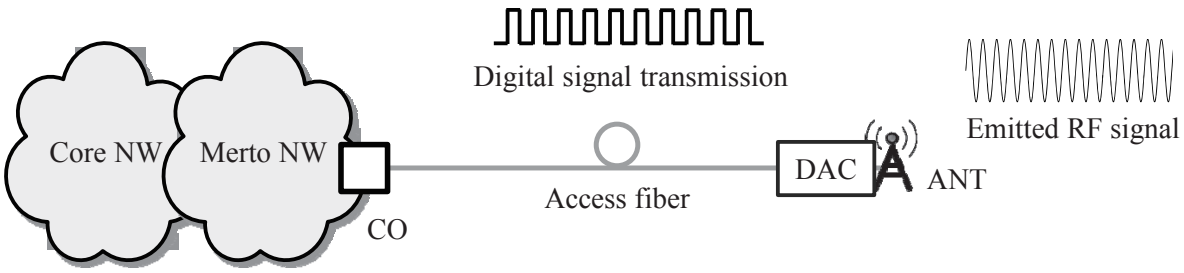

Fig. 2-4 D-RoF transmission system.

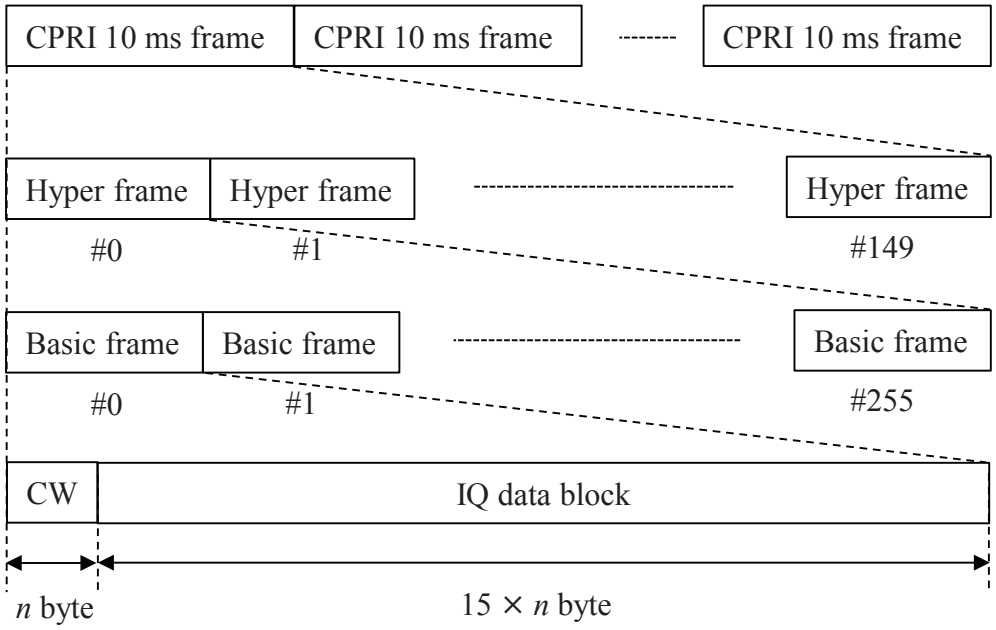

Fig. 2-5 CPRI frame structure.

Table 2-1 CPRI options and line rates.

CPRI option *n*	Line rate (Gbit/s)	Line coding
1	0.6144	8B/10B
2	1.2288	
3	2.4576	
4	3.0720	
5	4.9152	
6	6.1440	
7	9.8304	
7A	8.11008	64B/66B
8	10.1376	
9	12.16512	
10	24.33024	

2-3.2 Analog RoF transmission

Figure 2-6 depicts an example of an A-RoF transmission system for downlink. The analog signal waveform that is emitted from an antenna is generated by a DAC in a CO or upper networks. The analog RF signal is transmitted over a fiber from a CO to an antenna site by E/O and O/E based on analog IMDD scheme. In the antenna site, the analog RF signal can be emitted from the antenna without any changes for the signal format and frequency, after the power is properly adjusted by an RF amplifier. In A-RoF systems, in general, equipment in antenna sites can be simplified. Furthermore, optical transmission with a high spectral efficiency can be easily obtained. The spectral efficiency actually depends on the transmitted wireless signal. However, there exist three demerits in A-RoF systems. First, when the frequency of the RF signal is high, a broadband frequency response is generally required in the E/O and O/E. Such broadband optical components may cause higher optical transmission costs. Second, when multiple antennas are placed in an antenna site, multiple optical

transmission links are required for each of the antennas. Finally, the quality of an RF signal just before being emitted from an antenna may be worse than that in D-RoF systems.

Figure 2-7(a) illustrates a schematic diagram of an IFoF transmission system without SCM. An example of time-domain and frequency-domain signals are also shown in the figure. IFoF transmission technologies are commonly categorized as one of the RoF transmission technologies. In comparison with pure A-RoF systems, the frequency of the signal transmitted over a fiber is changed to an IF. After the optical transmission, a frequency converter for the IF to the RF is needed in an antenna site. The first demerit in A-RoF systems mentioned above can be solved by IFoF transmission systems without SCM at the expense of the simple configuration in antenna sites. Figure 2-7(b) describes an IFoF transmission system with SCM. The number of the antennas are expressed as *M*. In comparison with the system of Figure 2-7(a), multiple IF signals can be transmitted over a fiber without additional wavelengths for a WDM transmission and additional access fibers. Before the optical transmission, some electric components for multiplexing plural IF signals in a frequency domain are required. After the optical transmission, each of the IF signals is extracted by a bandpass filter (BPF) for each of the IFs, and then the frequency of each IF signal is converted to the RF. The equipment in an antenna site may be a little complicated. However, the second demerit in A-RoF systems mentioned above is also expected to be addressed by IFoF systems with SCM. The best selection from A-RoF, IFoF without SCM, and IFoF with SCM will be different depending on the antenna configuration and design.

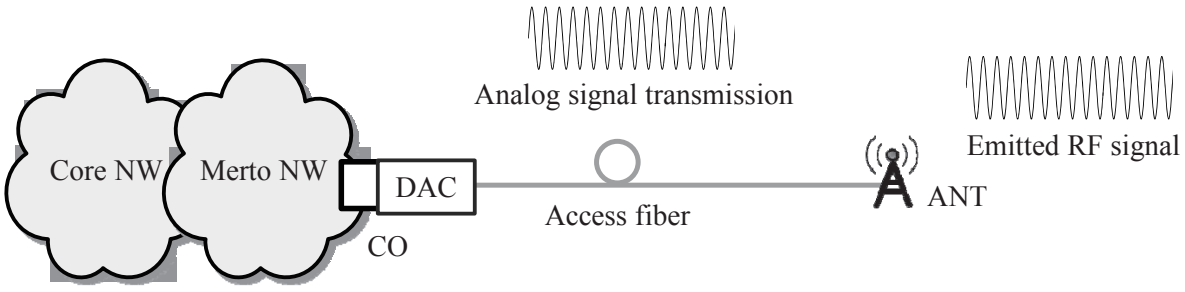

Fig. 2-6 A-RoF transmission system.

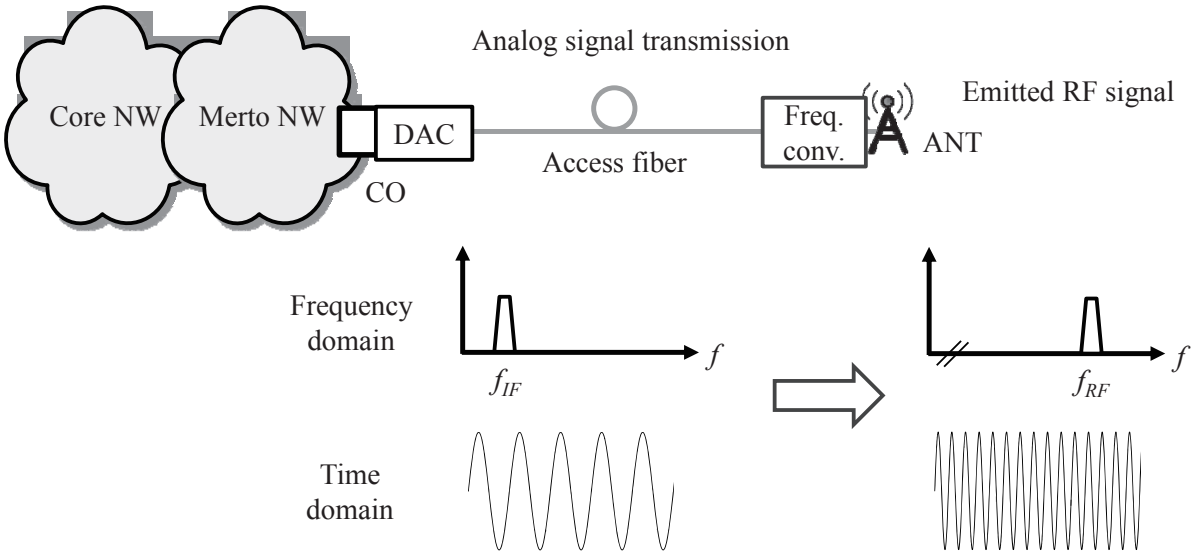

(a)

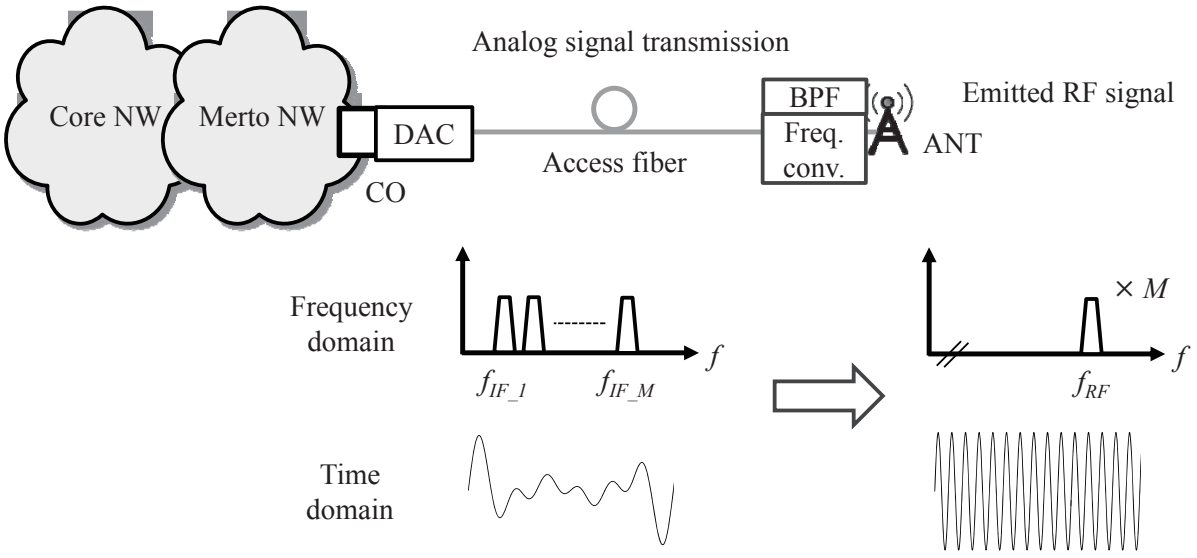

(b)

Fig. 2-7 IFoF transmission systems (a) without SCM and (b) with SCM.

2-3.3 Cascaded IFoF architecture

There are several access network architectures as shown in Figure 2-8. The number of users connected to a CO is expressed by *N*. Figure 2-8(a) depicts an access network based on PtP links. One or multiple access fibers are used for the connection between a CO and each user. When *N* users are connected to the CO, at least *N* fibers are required. In this architecture, the optical transmission for a user is independent of that for the others. Therefore, the communication can be stable. Additionally, even when an access fiber is broken, the influence of that will be limited only to the user on the fiber. However, the cost of access networks will become high. This architecture has been widely used for the MBH and MFH, and also for services for business users. Figure 2-8(b) describes a PtMP access network based on PON. An access fiber that is connected to a CO is shared, via a passive optical splitter, by *N* users. In comparison with the architecture of Figure 2-8(a), a cost-effective optical access network can be expected reducing the number of access fibers. Actually, this kind of PON architecture has been mainly and widely used for FTTH services. In addition, operators and venders are actively studying to use PON for MBH and MFH. However, as a demerit, when an access fiber is broken, the communications between a CO and *N* users will be simultaneously disconnected. Figure 2-8(c) shows another PtMP access network based on cascaded links. There exists a relay site between a CO and *N* users. In the relay site, the optical transmission from the CO is terminated, and then optical signals for *N* users are generated by *N* E/Os. In this architecture, PtP media convertors (MCs) are used in the optical transmission between a CO and a relay site and between a relay site and each user site. Using this architecture, a cascaded IFoF-based system that consists of a broadband and multiple narrowband IFoF links has been proposed as a new PtMP architecture that is suitable for the future MFH [15], [18]. In the following section, the proposed system is compared with a conventional CPRI-based MFH system.

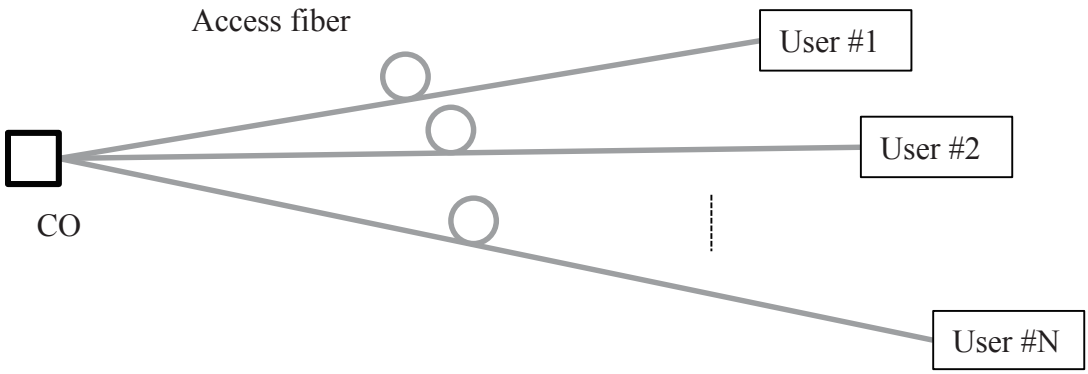

(a)

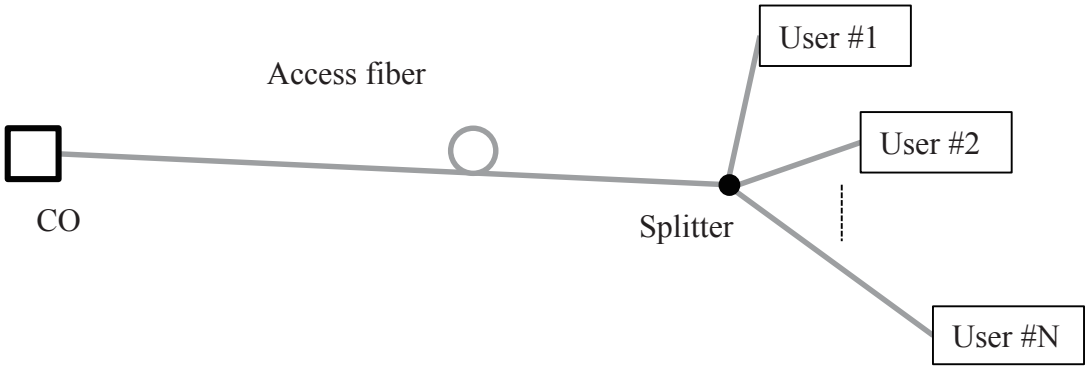

(b)

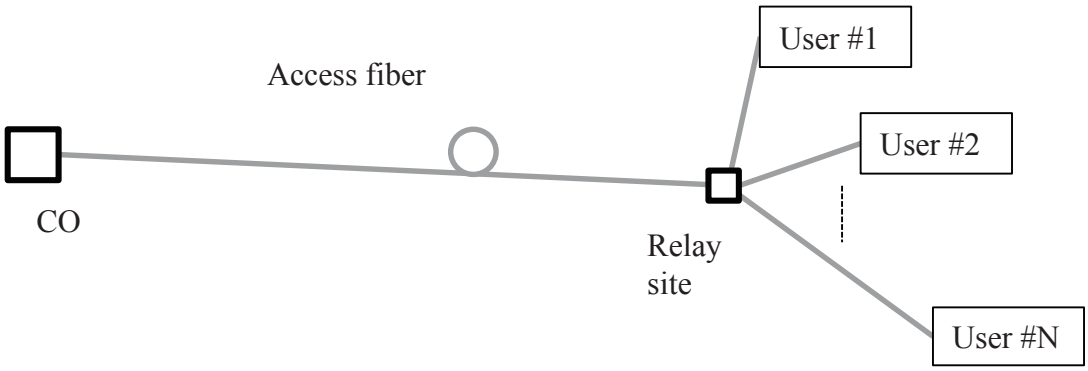

(c)

Fig. 2-8 Optical access network architectures based on (a) PtP links (b) PON and (c) cascaded links.

2-4 Comparative analyses of digitized and analog RoF systems

In this section, CPRI-based MHH links are compared with IFoF-based MFH links including cascaded IFoF links described in the previous section, in terms of system complexity and required optical fiber resources.

2-4.1 Comparison of MFH systems

Focusing on downlink transmission, system configurations of PtP CPRI-based MFH, PtP IFoF-based MFH, and cascaded IFoF-based MFH are explained one by one. The uplink systems are not discussed here because they are considered to take the reverse procedure of the downlink systems. The numbers of antenna elements in each of antenna equipment, RF streams in each antenna site, and antenna sites are expressed as *L*, *M*, and *N*, respectively. Figure 2-9(a) illustrates a conventional PtP CPRI-based MHF system. DUs for the PHY layer functions of a BS is located in a CO whereas RUs for the RF layer functions of a BS is placed in antenna sites. In a CO, CPRI frames that contain the IQ signals of *M* data streams for an antenna site are generated, and the CPRI signals are converted to the optical signals by broadband E/Os. Actual bandwidths required in optical components are described in Section 2-4.2. A WDM technology is applied to the simultaneous transmission of the *M* CPRI signals over an access fiber. The optical transmission length becomes less than 20 km which is equivalent to the maximum transmission length in 4G CPRI links. After the optical transmission, in an antenna site, *M* broadband O/Es convert the CPRI signals to the original electric signals. Then, the IQ signals of the *M* data streams are extracted from the CPRI frames by DSP and converted to the analog IF signals by *M* DACs. The frequency of each IF signal is also converted to an RF by an analog frequency converter. Additionally, analog beamforming (BF) is applied to the RF signals before being connected to *L* antenna elements. CWs in the CPRI frames that are transmitted over the access fiber with the IQ signals are used for conveying information on the BF control. The CWs are also used for synchronizing the RU with the DU and providing operators with minimal OAM functions. When *N* antenna sites are connected to a CO, *N* sets of the components and functions above are required.

Figure 2-9(b) depicts a PtP IFoF-based MFH system. DUs in a CO have PHY and part of RF functions of a BS whereas RUs in antenna sites have some RF functions of a BS. In a CO,

wireless IF signals of *M* data streams for an antenna site are generated and subcarrier multiplexed by DSP, and the digital SCM signal is converted to the analog SCM signal by a high-speed DAC. The SCM signal is multiplexed with a reference clock and an OAM signal in the frequency domain by an analog multiplexer. The reference clock is used for a common clock source for a MFH system. Using the reference clock, the deployment of a GPS antenna to get precise clock in each antenna site is not required. The OAM signal includes information on the BF control at an antenna site. The multiplexed SCM, reference clock, and OAM signals are transmitted to an antenna site over an access fiber by narrowband E/O and O/E. In an antenna site, each signal is separated from the others by a demultiplexer. The reference clock is used for the operation of the RU equipment. The SCM signal is converted to the digital signal by an high-speed analog-to-digital converter (ADC), and each of the *M* IF signals is extracted from the others and converted to an IF signal by simple DSP without modulation and demodulation of the wireless baseband signals. Each of the digital IF signals is converted to the analog signal by a DAC and then converted to an RF signal by an analog frequency converter. In the analog BF process, information on the BF control from the OAM signal is used. Each of the *L* RF signals after the BF process is connected to a specific antenna element. When *N* antenna sites are connected to a CO, *N* sets of the components and functions above are required just like the MFH system of Figure 2-9(a).

Figure 2-9(c) describes a cascaded IFoF-based MFH system. In comparison with Figure 2-9(b), there exists a relay site between a CO and *N* antenna sites where some additional RF functions are implemented. In a CO, an analog SCM signal for each antenna site is generated by DSP and DAC in the same way as the system of Figure 2-9(b). To multiplex the SCM signals for *N* antenna sites in a frequency domain, *N*-1 analog up converters are used for *N*-1 SCM signals. As a result of that, a continuous frequency band is assigned to each antenna site which simplifies the after-mentioned process in a relay site. The *N* SCM signals, a reference clock, and an OAM signal for N antenna sites are multiplexed by an analog multiplexer. The multiplexed signals are transmitted over an access fiber from the CO to a relay site by a set of broadband E/O and O/E. In the relay site, each kind of the signals is separated from the other kinds by an analog demultiplexer. The reference clock and OAM signals are used for the equipment in the relay site and also for one in *N* antenna sites. Therefore, the signals are divided into *N*+1. Each of the *N* SCM signals can be easily extracted and converted to the lowest frequency range by analog BPF and frequency converter. After being multiplexed with the reference clock and OAM signal in a frequency domain, each SCM signal is transmitted to

a specific antenna site over a short fiber by a set of narrowband E/O and O/E. The length of the short fiber will be several kilometers at maximum. The subsequent process in the antenna site is the same as the MFH system of Figure 2-9(b).

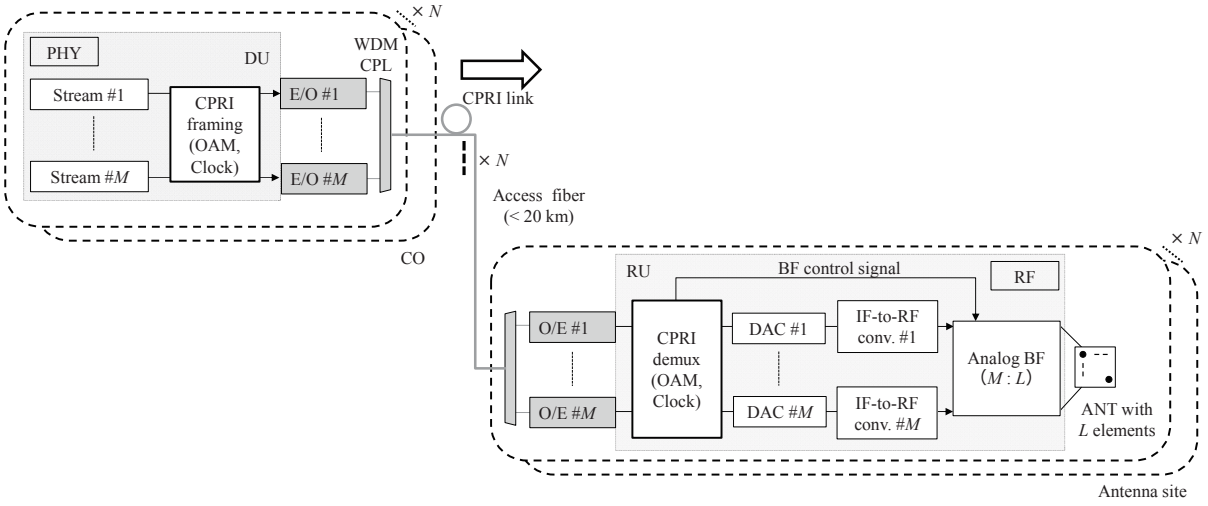

(a)

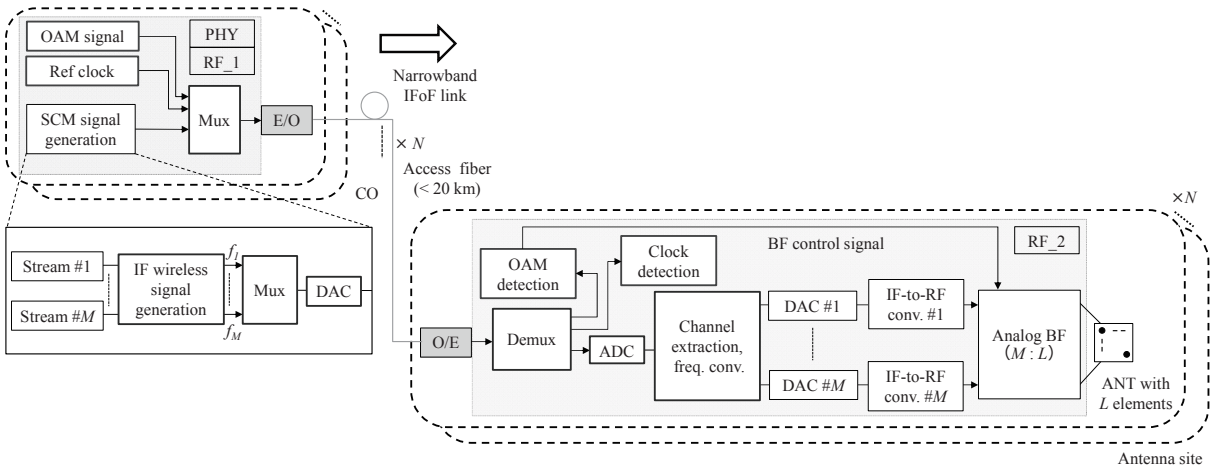

(b)

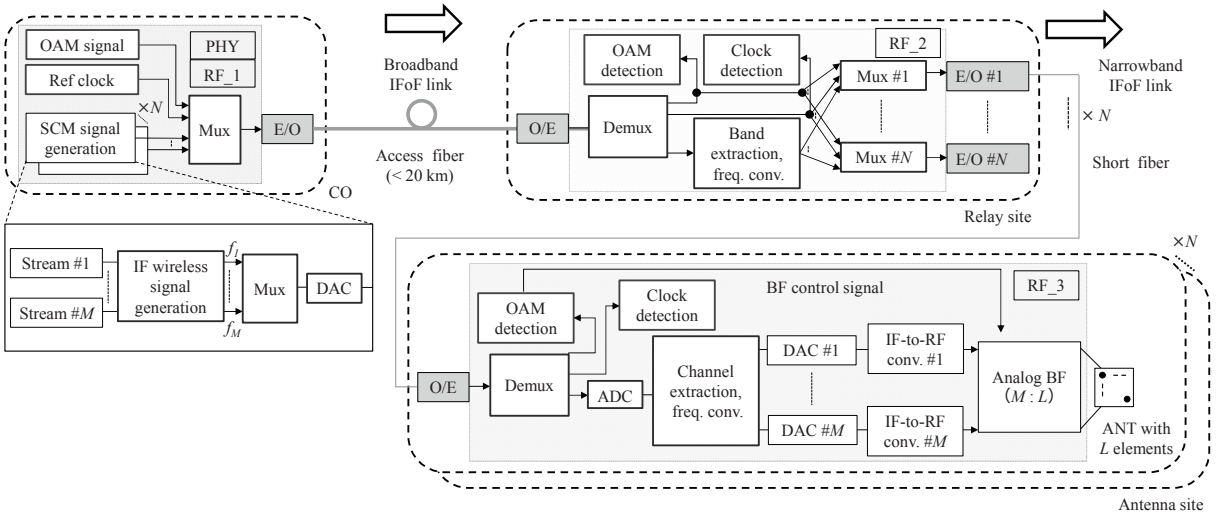

(c)

Fig. 2-9 MFH systems based on (a) PtP CPRI links, (b) PtP IFoF links, and (c) cascaded IFoF links.

2-4.2 System complexity

Three kinds of the MFH systems that are explained in Section 2-4.1 are compared with one another from the perspective of the system complexity including three items of optical transmission, electrical functions and components, and additional functions. Table 2-2 shows an example when L, M, and N are set to 32, 4, and 8, respectively, as typical values.

First, the comparison between PtP CPRI-based system and PtP IFoF-based system is discussed. In the item of optical transmission, a PtP CPRI-based MFH system requires a date rate of about 20 Gbit/s [17] in each broadband E/O and O/E whereas a PtP IFoF-based MFH system requires a BW of 2 GHz in each narrowband E/O and O/E, when an IF channel bandwidth of 400 MHz and the bandwidth ratio of IF signal bands to guard bands of 4:1 are assumed. The data rate of about 20 Gbit/s per RF stream is calculated by an equation [16] of

$$B_{CPRI} = f_s \cdot b_s \cdot 2 \cdot (16/15) \quad , \tag{2.1}$$

where f_s is the sampling rate, b_s is the number of bits per sampling, 2 is the coefficient for I and Q signals, and 16/15 is the additional overhead to the CPRI frame. When f_s and b_s are set to 614.4 MHz and 15, respectively, considering 15.36 MSa/s for 10-MHz BW and 15 bits for LTE, B_{CPRI} becomes 19.6608 Gbit/s. The numbers of E/Os and O/Es can be also reduced from 32 to 8 in the PtP IFoF system. The number of wavelengths for an antenna site is also reduced from 4 to 1. Therefore, the cost of optical components in the PtP IFoF system is expected to be much lower than that in the PtP CPRI system. In the item of electrical functions and components, the PtP CPRI system uses eight sets of the DSP equipment for CPRI framing and demultiplexing whereas the PtP IFoF system needs eight sets of high-speed DACs, ADCs, and DSP equipment for filters and frequency converters. In terms of the data amount processed in an antenna site, the IFoF system will have a smaller load than the PtP CPRI system. For example, when a sampling rate and an amplitude resolution of a high-speed ADC in the PtP IFoF system are assumed to be 4 GSa/s and 12 bit, respectively, the data amount will be around 48 Gbit/s whereas the data amount in PtP CPRI system becomes about 80 Gbit/s from the calculation of 20 Gbit/s × 4 wavelengths. Regarding the item of additional functions, the PtP CPRI system does not need any external signals to the CPRI frames whereas the PtP IFoF system needs to transmit external OAM signal and reference clock in addition to the wireless IF signals. However, the additional OAM signal will not have a large cost impact because commercial community antenna television (CATV) system has a control signal that is similar to the OAM signal.

Second, the comparison between PtP IFoF-based MFH system and cascaded IFoF-based MFH system is discussed. To reduce the number of long access fibers from 8 to 1, the cascaded IFoF system uses eight short fibers and a set of broadband E/O and O/E. The bandwidths of the broadband components will be around 16 GHz when the total bandwidth of the guard bands among wireless IF signals is assumed to be one quarter of the total signal bandwidth of 12.8 GHz that is calculated by 400 MHz × 4 streams × 8 antenna sites. Seven sets of analog up and down converters are also required in the cascaded IFoF system. In general, fiber deployments are considered to have large impacts on the cost and construction period in optical transmission systems. Therefore, especially when many antennas are densely deployed and the number of access fibers are insufficient, the cascaded IFoF systems are expected to be effective for reducing the total deployment cost and construction period.

Table 2-2 Comparison of three kinds of MFH systems in typical conditions.

Comparison item		MFH systems		
		PtP CPRI	PtP IFoF	Cascaded IFoF
Optical transmission	Numbers of broadband E/Os and O/Es	32	0	1
	Required data rate or BW for each of broadband E/O and O/E	20 Gbit/s	-	16 GHz
	Number of wavelengths for an antenna or a relay site	4	1	1
	Number of access fibers from a CO	8	8	1
	Numbers of narrowband E/Os and O/Es	0	8	8
	Required BW for each narrowband E/O and O/E for an analog transmission	0	2 GHz	2 GHz
	Number of wavelengths for an antenna site	0	0	1
	Number of short fibers from a relay site	0	0	8
Electrical functions and components	Numbers of CPRI framing and demultiplexing	8	0	0
	Number of high-speed DACs in a CO	0	8	8
	Number of analog up converters in a CO	0	0	7
	Number of analog down converters in a relay site	0	0	7
	Numbers of high-speed ADCs and DSP in antenna sites	0	8	8
	Numbers of low-speed DACs and IF-to-RF converters in an antenna site	4	4	4
Additional functions	BF control, OAM, and synchronization	By CPRI frames	By OAM signal and reference clock from a CO	

2-4.3 Optical fiber resource

The total fiber length and cost in PtP MFH links and cascaded MFH links are calculated

and compared with each other. The total fiber length for PtP MFH is given by

$$D_{total} = a \cdot N \quad , \tag{2.2}$$

where a is the average access fiber length. In this comparison, the average access fiber length was set to 5 km. The total fiber length for cascaded MFH is described as

$$D_{total} = a + a \cdot \alpha \cdot N \quad , \tag{2.3}$$

where α is the average length ratio of a short fiber to an access fiber. For example, when α is set to 0.1, the short fiber length becomes 0.5 km, considering a 5-km access fiber. Figure 2-10 plots an example of calculation results for the total fiber length. The cascade architecture can effectively reduce the total fiber length as the number of antenna sites N increase and α becomes smaller. This means the cascade architecture becomes more effective when more and more antennas are deployed in small areas. The total fiber length of the cascade links can be less than half that of the PtP links when the number of antenna sites and α are set to four or more and 0.2 or less, respectively, as typical values.

Figures 2-11 shows an example of calculation results for the total fiber cost. The average fiber length of a and α were set to 5 km and 0.1, respectively. The word of dark fiber usage ratio in Figure 2-11 means the ratio of the number of available dark fibers to that of the total access fibers that is described as β. For example, when the ratio of β becomes 25%, one quarter of the total number of access fibers are based on dark fibers whereas the other fibers are based on newly deployed fibers. The new fiber deployment cost of b is assumed to be 45,000 USD/km/fiber that is a little cheaper than 45,000 EUR/km/fiber [19]. Additionally, the indefeasible right of use (IRU) fee of a dark fiber and the operating period are assumed to be 30 USD/month and eight years, respectively. Therefore, the cost of a dark fiber, c, is estimated to be 2,880 USD. The IRU fee assumed here is almost the same as the values in Ref. [20], [21]. In general, the total fiber cost for PtP MFH is expressed by

$$C_{total} = a \cdot b \cdot (N - \beta \cdot N) + c \cdot \beta \cdot N \quad . \tag{2.4}$$

Additionally, when at least one dark fiber is available, the total fiber cost for cascaded MFH is given by

$$C_{total} = a \cdot \alpha \cdot b \cdot N + c \quad . \tag{2.5}$$

when no dark fibers are available, the total fiber cost is described as

$$C_{total} = a \cdot \alpha \cdot b \cdot N + a \cdot b \quad . \tag{2.6}$$

In the PtP links, the total cost can be lower as the dark fiber usage ratio of β increases. In contrast to the situation, cascade links receive no impact of the ratio on the total fiber cost if a dark fiber is available. In 5G and the future mobile systems, more and more small-cells that use high frequencies such as millimeter waves will be formed in small areas, and, as a result, the dark fiber ratio will decline drastically. When the dark fiber usage ratio decreases to 25% and eight antenna sites are included in a MFH system, the total fiber costs of PtP and cascade links are approximately 1.36 MUSD and 0.18 MUSD, respectively.

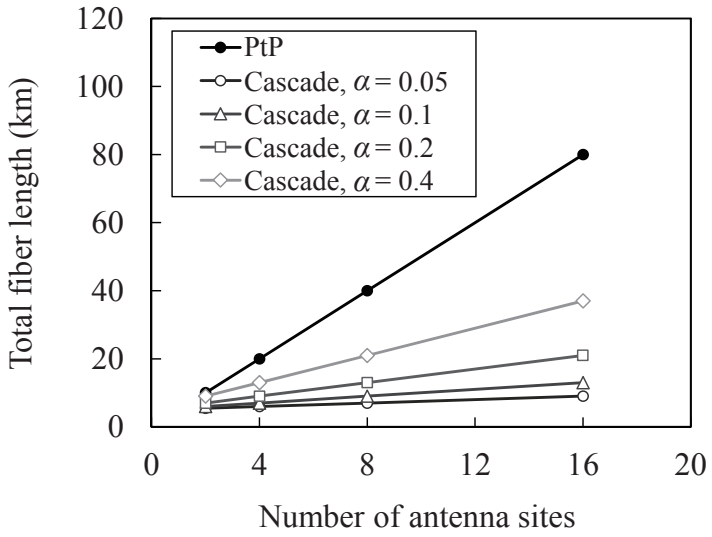

Fig. 2-10 Calculation results of the total fiber length in 5-km access fibers.

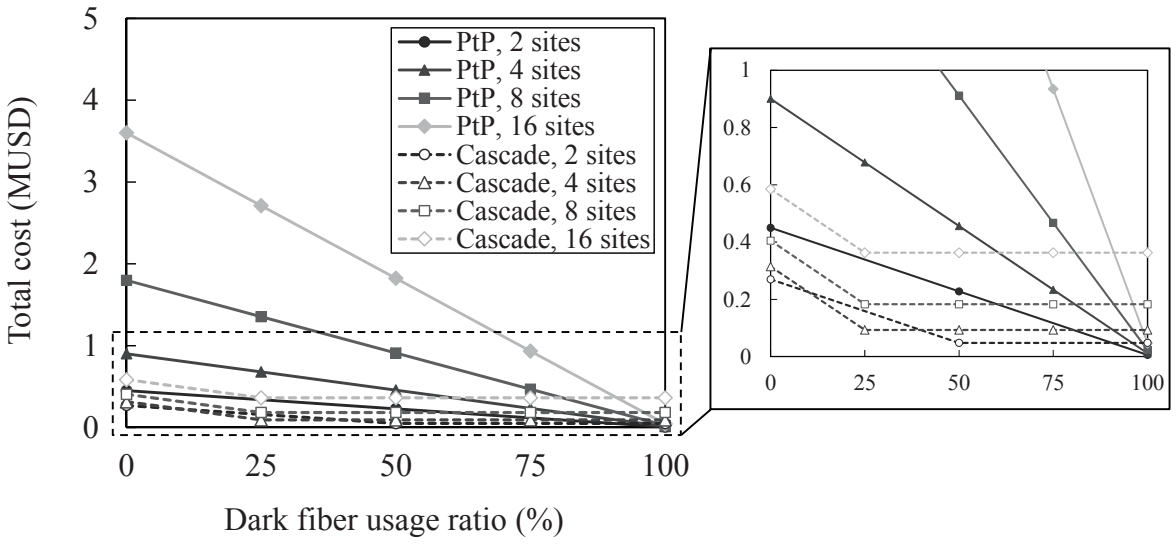

Fig. 2-11 Calculation results of the total fiber cost in 5-km access fibers and α of 0.1.

Figure 2-12 presents an example of the total fiber cost ratio between PtP and cascade MFH links. The ratio of less than 1 means that the total fiber cost in cascade links are lower than that of PtP links. In the calculations, the average access fiber length and the number of antenna sites were set to 5 km and 8. It is obvious that when the dark fiber usage ratio of β is 100%, PtP links have the cost merit in comparison with the cascade links. Additionally, the values of the total fiber cost ratio change depending on α. When a target of the cost ratio is set to 0.5, α of 0.4 can not be accepted irrespective of the dark fiber usage ratio. However, in the future mobile systems, α will be also lower as the number of small-cells increases. Therefore, the cascade links are expected to have a sufficient fiber cost advantage.

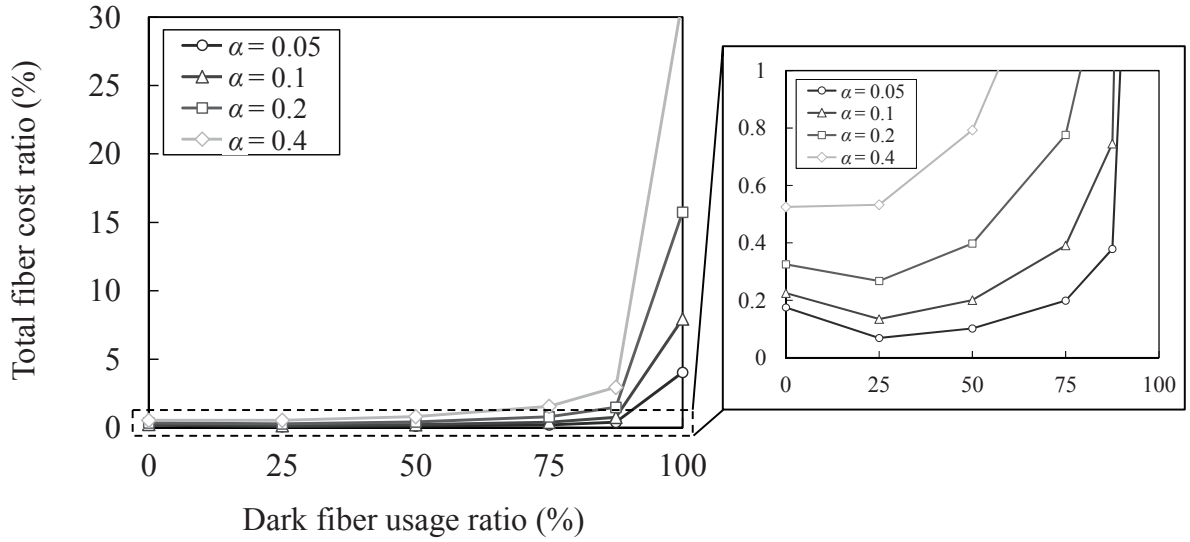

Fig. 2-12 Calculation results of the total fiber cost ratio in 5-km access fibers and eight antenna sites.

2-5 Conclusion

A cascaded IFoF system was proposed and introduced as a PtMP architecture for 5G and the future MFH. A relay site is placed among a CO and multiple antenna sites, and an access fiber between the CO and the relay site can be shared and used by all of the antenna sites. For the downlink, IF signals for all antenna sites are subcarrier multiplexed in the CO and transmitted to the relay site over the access fiber by a wavelength. In the IFoF channel allocation, a continuous frequency band that can include multiple IF channels is assigned to each antenna site to simplify the filtering and frequency conversion processes.

IFoF-based MFH systems including the cascaded IFoF architecture were compared with conventional PtP CPRI-based MFH systems from the perspective of system complexity and fiber resources. In comparison with PtP CPRI-based systems, PtP IFoF-based systems did not use any broadband optical components that will have relatively large cost impacts whereas the IFoF-based systems needed narrowband optical components and external OAM and reference clock distribution functions that will have relatively small cost impacts. Furthermore, in comparison with PtP IFoF systems, cascaded IFoF systems effectively reduced the number of access fibers to only one while using a pair of broadband E/O and O/E, short transmission

links between the relay site and plural antenna sites, and some electric components. The total fiber lengths and costs in PtP and PtMP MFH architectures were also estimated by calculations under typical conditions. When the length ratio of the short fiber to the access fiber of 0.2 or less, and four and more antenna sites were assumed, the total fiber length of the PtMP architecture was less than 50% of that of the PtP architecture. Additionally, when eight antenna sites, access fiber length of 5 km, and the dark fiber usage ratio of 25% were assumed, the total fiber cost of the PtMP architecture was reduced to about 13% of the total fiber cost of the PtP architecture. From the studies in this Chapter, the potential of the cascaded IFoF system for simpler and more cost-effective 5G MFH was shown.

References

[1] CPRI Specification V7.0, "Common Public Radio Interface (CPRI); Interface Specification," 2015.

[2] A. de la Oliva, J. A. Hernández, D. Larrabeiti, and A. Azcorra, "An Overview of the CPRI Specification and Its Application to C-RAN-Based LTE Scenarios," *IEEE Communications Magazine*, vol. 54, no. 2, pp. 152-159, 2016.

[3] K. Tanaka and A. Agata, "Next-Generation Optical Access Networks for C-RAN," in *Proc. Optical Fiber Communication Conference (OFC)*, Tu2E.1, Los Angeles, CA, Mar. 2015.

[4] N. Shibata, T. Murakami, K. Ishihara, T. Kobayashi, J. Kani, J. Terada, M. Mizoguchi, Y. Miyamoto, and N. Yoshimoto, "256-QAM 8 wireless signal transmission with DSP-assisted analog RoF for mobile front-haul in LTE-B," in *Proc. Optoelectronics and Communications Conference (OECC)*, pp. 129-131, Melbourne, Australia, July 2014.

[5] X. Liu, H. Zeng, N. Chand, and F. Effenberger, "Efficient Mobile Fronthaul via DSP-Based Channel Aggregation," *IEEE J. Lightwave Technol.*, vol. 34, no. 6, pp. 1556-1564, 2016.

[6] P. Li, W. Pan, L. Huang, X. Zou, Y. Pan, Q. Zhou, Y. W. Chen, P. C. Peng, S. Liu, S. Shen, and G. K. Chang, "Multi-IF-Over-Fiber Based Mobile Fronthaul With Blind Linearization and Flexible Dispersion Induced Bandwidth Penalty Mitigation," *IEEE J. Lightwave Technol.*, vol. 37, no. 4, pp. 1424-1433, 2019.

[7] M. Sung, S. H. Cho, J. Kim, J. K. Lee, J. H. Lee, and H. S. Chung, "Demonstration of IFoF-Based Mobile Fronthaul in 5G Prototype With 28-GHz Millimeter wave," *IEEE J. Lightwave Technol.*, vol. 36, no. 2, pp. 601-609, 2018.

[8] B. G. Kim, S. H. Bae, H. Kim, and Y. C. Chung, "DSP-based CSO cancellation technique for RoF transmission system implemented by using directly modulated laser," *Optics Express*, vol. 25, no. 11, pp. 12152-12160, 2017.

[9] D. Wake, A. Nkansah, and N. J. Gomes, "Radio Over Fiber Link Design for Next Generation Wireless Systems," *IEEE J. Lightwave Technol.*, vol. 28, no. 16, pp. 2456-2464, 2010.

[10] J. E. Mitchell, “Integrated Wireless Backhaul Over Optical Access Networks,” *IEEE J. Lightwave Technol.*, vol. 32, no. 20, pp. 3373-3382, 2014.

[11] J. Wang, Z. Yu, K. Ying, J. Zhang, F. Lu, M. Xu, L. Cheng, X. Ma, and G. K. Chang, “Digital Mobile Fronthaul Based on Delta–Sigma Modulation for 32 LTE Carrier Aggregation and FBMC Signals,” *IEEE J. Opt. Commun. Netw.*, vol. 9, no. 2, pp. A233–A244, 2017.

[12] I. A. Alimi, A. L. Teixeira, and P. P. Monteiro, “Toword an Efficient C-RAN Optical Fronrhaul for the Future Networks: A Tutorial on Technologies, Requirements, Challenges, and Solutions,” *IEEE Commun. Surv. Tutor.*, vol. 20, no. 1, pp. 708-769, 2018.

[13] C. Ranaweera, E. Wong, A. Nirmalathas, C. Jayasundara, and C. Lim, “5G C-RAN With Optical Fronthaul: An Analysis From a Deployment Perspective,” *IEEE J. Lightwave Technol.*, vol. 36, no. 11, pp. 2059-2068, 2018.

[14] K. Ikeda, C. Lim, A. Nirmalathas, and C. Ranaweera, “A Comparison of Optical Transport Technologies for Wireless Communications Using Optical Ground Wire in Smart Grid,” in *Proc. International Conference on Smart Grid (icSmartGrid)*, Newcastle, Australia, Dec. 2019.

[15] K. Tanaka, H. Y. Kao, S. Ishimura, K. Nishimura, T. Kawanishi, and M. Suzuki, “Cascaded IF-over-Fiber Links with Hybrid Signal Processing for Analog Mobile Fronthaul,” *IEEE J. Lightwave Technol.*, vol. 38, no. 20, pp. 5656-5667, 2020.

[16] ITU-T G-series Reccommendations - Supplement 66, “5G wireless fronthaul requirements in a passive optical network context,” 2018.

[17] 3GPP TR 38.801 v2.0.0 Release 14, “Technical Specification Group Radio Access Network; Study on New Radio Access Technology; Radio Access Architecture and Interfaces,” 2017.

[18] K. Tanaka, A. Bekkali, H. Y. Kao, S. Ishimura, K. Nishimura and M. Suzuki, “First experimental demonstration of 5G mobile fronthaul consisting of cascaded IF-over-fiber links, frequency converters and a channel selector,” *in Proc. European Conference on Optical Communication (ECOC)*, Tu4B.6, Roma, Italy, Sept. 2018.

[19] C. F. Silva, and V. S. Ribeiro, “Business Evaluation for FUTON-like Architectures,” *in Proc. EUROCON 2011 - International Conference on Computer as a Tool*, Lisbon, Portugal, April 2011.

[20] https://www.ntt-east.co.jp/release/detail/20180316_01_01.html.

[21] https://www.ntt-west.co.jp/news/1806/180611a_1.html.

Chapter 3

Time synchronization technologies in mobile communication systems

3-1 Introduction

In 5G and future mobile communication systems, heterogeneous networks [1], where many small cells that use high frequencies such as millimeter waves are placed in a macro cell, will be utilized. In the heterogeneous network, the small cells are mainly used for transmitting user data traffic whereas the macro cell is used for transmitting control signals. To increase the data capacity, more and more small cells are required. In such a situation, TDM-PONs [2], [3], one of the PtMP architectures, will be effective for reducing the number of access fibers and access network costs, not only for FTTH services but also for mobile services. In mobile communication systems, time synchronization among BSs is indispensable for the network handover, RF interference suppression, and advanced technologies of CoMP [4] and eICIC [5]. GPS signals have been commonly used for the purpose. However, when the number of small cells dramatically increases in the future, new time synchronization techniques will be required to avoid the complexity and difficulty in deploying GPS antennas and RF cables. PTP [6] is a new technology for time synchronization over packet networks. However, PTP can not be used over TDM-PON systems because, in PTP, symmetric transmission delays are strictly required in uplink and downlink transmission. The other technique, where information on 1PPS and ToD is transmitted in packets from an OLT to ONUs, has been proposed [7]. However, this technique makes equipment configuration in antenna sites complex and has no reference clock redundancy functions. When a reference clock is shared with many BSs, reference clock redundancy functions will be mandatory to avoid large-scale system failures.

In this chapter, a TDM-PON system with a time synchronization function by PTP packets for multiple mobile BSs is proposed and presented in detail. A time synchronization technique by GPS signals and one by PTP packets are firstly introduced. Then, the features of

TDM-PON and WDM-PON systems for PtMP network architectures are explained. Next, the network architecture and operational principle of a proposed time synchronization technique using IEEE EPON and PTP are described. Finally, a 10G-EPON prototype that implements the proposed function is evaluated, and the effectiveness of itself is confirmed. Additionally, the technique is verified by interoperability tests between the prototype and commercial equipment of PTP slave and 4G mobile BS.

3-2 Synchronization technologies for mobile base stations

In this section, two kinds of precise time synchronization techniques, GPS and PTP, for mobile BSs are explained [8]. Additionally, time synchronization over IEEE EPON that is specified in IEEE 802.1AS is described. Before explaining those techniques, the meaning of time synchronization is clarified.

3-2.1 Time synchronization

Figure 3-1 shows three kinds of synchronization. Signal #1 and #2 are generated by different equipment with each other. Each equipment is considered to have an oscillator and a clock internally. Figure 3-1(a) illustrates an example of frequency synchronization. The signal #1 and signal #2 include a pulse signal with time intervals of T_1 and T_2, respectively. The timing difference between signal #1 and signal #2 is expressed by $\Delta\varphi$. When the relationship between signal #1 and signal #2 is in frequency synchronization, T_1 and $\Delta\varphi$ are equivalent to T_2 and not zero, respectively. Figure 3-1(b) depicts phase synchronization. In phase synchronization, the condition where $\Delta\varphi$ is equivalent to zero is added to the condition of the frequency synchronization. Figure 3-1(c) shows time synchronization. In time synchronization, in addition to the condition of the phase synchronization, the time of a pulse in the signal #1 is the same as that in the signal #2. In the future, most of the mobile communication systems will require precise time synchronization in addition to frequency synchronization.

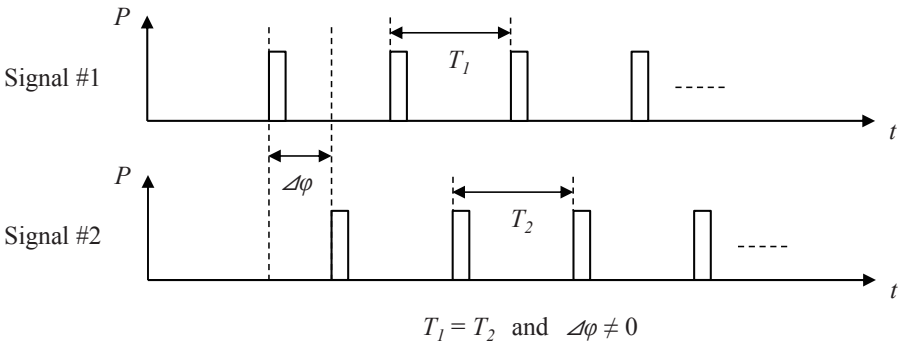

(a)

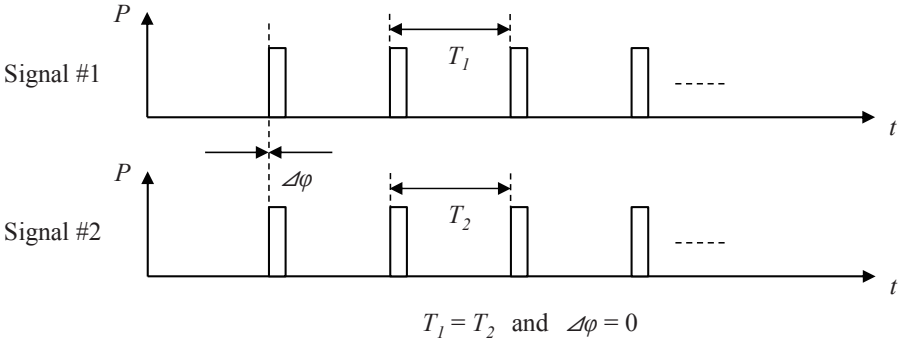

(b)

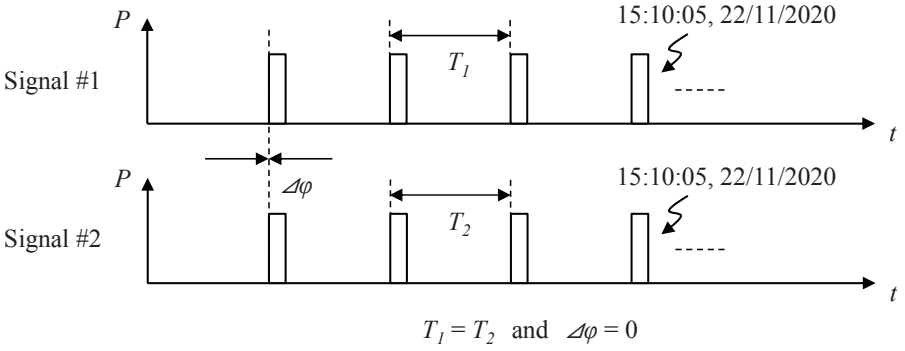

(c)

Fig. 3-1 Three kinds of synchronization: (a) frequency synchronization, (b) phase synchronization, and (c) time synchronization.

3-2.2 GPS signal

GPS, part of the global navigation satellite systems (GNSSs), have been widely used for time synchronization among mobile BSs. Figure 3-2 shows the system configuration for time synchronization by GPS. Each GPS satellite has ultra-stable oscillators or atomic clocks based on cesium (Cs) and rubidium (Rb) and knows its accurate location and clock of (x_{ti}, y_{ti}, z_{ti}, t_{ti}). A GPS receiver (Rx) for time synchronization has a stable oven controlled crystal oscillator (OCXO) with a holdover function. The time synchronization can be performed by broadcasting signals from at least four GPS satellites to a GPS receiver. The GPS signals use a carrier frequency of 1575.42 MHz and code division multiple access (CDMA) by pseudo random noise (PRN) code. The broadcasting signal from each GPS satellite includes information on its accurate location and clock of (x_{ti}, y_{ti}, z_{ti}, t_{ti}). A GPS receiver estimates its location and clock of (x_r, y_r, z_r, t_r) using the broadcasting signals from four or more GPS satellites. It is obvious that when the GPS receiver has an ultra-stable clock of Cs or Rb, three GPS satellites are sufficient for time synchronization. However, in general, such a clock is expensive and difficult to be implemented in each GPS receiver for mobile systems. After the estimation, the receiver provides a mobile BS with reference clocks such as 1PPS and ToD. In order to capture four and more GPS satellites, each BS should place the GPS antenna outdoors and use RF cables for the connection between the GPS antenna and itself. The synchronization accuracy depends on the quality of the received GPS signals.

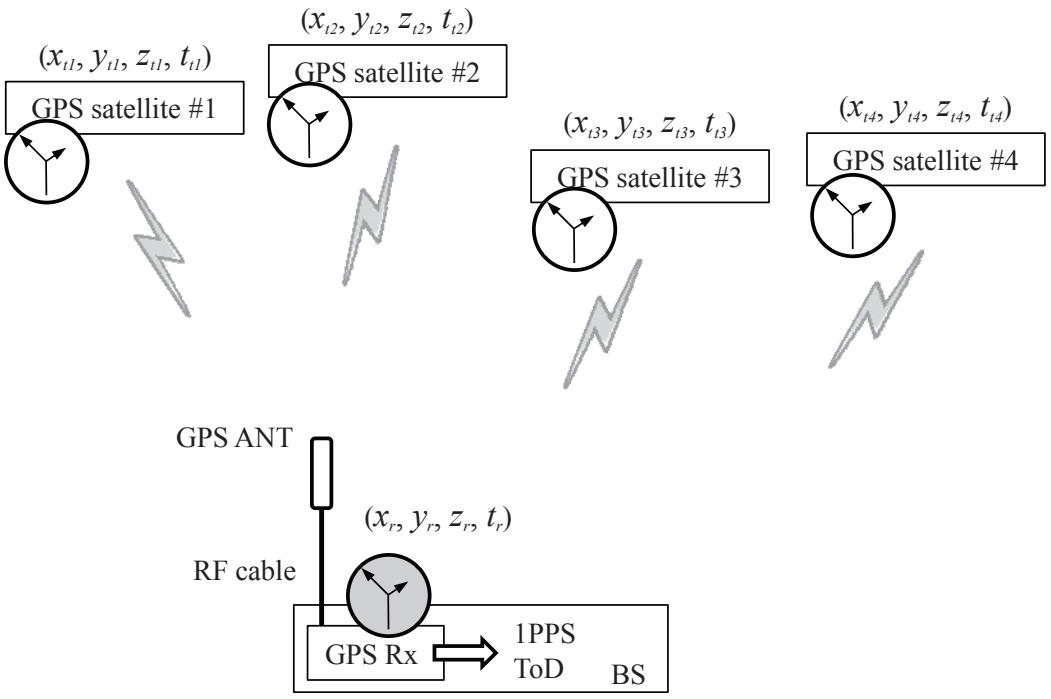

Fig. 3-2 Time synchronization by GPS signals.

3-2.3 Synchronization techniques over transmission networks

There exist several synchronization techniques over transmission networks, network time protocol (NTP), synchronous Ethernet (Sync-E) [9], [10], IEEE 1588 [6], IEEE802.1AS [11]. In NTP, NTP packets are transmitted between the client and the server by the client request. The NTP client can calculate the transmission delay by the packets and set its local time to the server's time considering the transmission delay. This technique is based on software timestamping, and the time accuracy is limited to the order of milliseconds. Sync-E is a technology that is only used for frequency synchronization. Ethernet equipment clock (EEC) in an Ethernet switch is synchronized in physical layer, and the frequency synchronization is not affected by any traffic conditions. The frequency accuracy is ±4.6 parts per million (ppm) in free-running status, which is much better than ±100 ppm from existing Ethernet. For the synchronization by Sync-E, all of the equipment in the transmission network should support the function. IEEE 1588 is a packet-based time and frequency synchronization technique. IEEE 1588 is also called PTP. In PTP, packets for time information are transmitted between

the master and the slave. High synchronization accuracy of less than 1.5μs, that is a requirement from TD-LTE, can be expected by the hardware timestamping. Much attention has been paid for this technology, and the equipment with the PTP function has increased. IEEE 802.1 AS is a subset of IEEE 1588 and specifies synchronization over EPON and wireless local area network (LAN). Table 3-1 shows requirements for time accuracy from mobile communication systems [12]. In this chapter, PTP for mobile applications is studied, targeting time accuracy of less than 1.5 μs for TD-LTE.

Table 3-1 Time accuracy requirements.

Application	Time accuracy
CDMA2000	±3 μs to ±10 μs
TD-LTE (Large cell)	±5 μs
TD-LTE (small cell)	±1.5 μs
TD-SCDMA	
WiMAX TDD	±1 μs
Some LTE-A features	±500 ns to ±1.5 μs

3-2.4 Principle of PTP

Figure 3-3 illustrates a general packet flow between PTP maser and PTP slave for time synchronization. A PTP master sends a sync message to a PTP slave. In the sync massage, information on the transmitting time in the master of t_1 is included. A follow_up message that includes precise time of t_1 may be additionally transmitted to the slave. In the slave, the Sync message is received and the reception time of t_2 is registered. Then, the slave sends a delay request message to the master. In the message, information on the transmitting time in the slave of t_3 is included. The delay request message is received by the master, and the reception time of t_4 is registered. Additionally, the master sends a delay response message to the slave.

The message includes information on t_4. Through this process, the slave can know t_1, t_2, t_3, and t_4. The slave can also calculate the transmission delay from the master and the time offset by the following equations (3.1) and (3.2), respectively.

$$Delay = \frac{(t_2 - t_1) + (t_4 - t_3)}{2} \tag{3.1}$$

$$Offset = (t_2 - t_1) - Delay = \frac{(t_2 - t_1) - (t_4 - t_3)}{2} \tag{3.2}$$

Finally, the slave corrects the local time by the calculated offset value. It is noted that PTP assumes the transmission delay from a PTP slave to a PTP master is the same as that from the PTP master to the PTP slave. Conventional TDM-PONs basically have an asymmetric transmission delay between uplink and downlink because of the dynamic bandwidth allocation (DBA) algorithm for uplink. The transmission delays of downlink and uplink from common G-PON and G-EPON systems are about several tens of microseconds and the order of milliseconds, respectively. In the uplink transmission, large packet jitters are also caused by the DBA algorithm. Therefore, PTP can not be applied to conventional TDM-PONs.

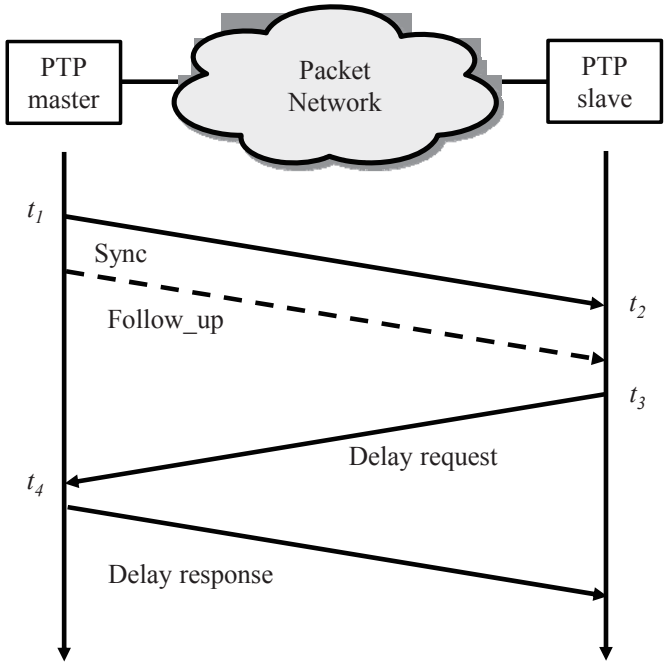

Fig. 3-3 PTP packet transmission between PTP master and PTP slave.

In PTP networks, there are three kinds of PTP clocks [6]. The first one is an ordinary clock (OC) which has a single PTP port in a domain. An OC works as a grand master (GM) clock with the time source of a synchronization network or as a slave clock. The second one is a boundary clock (BC) which has a common local clock, and embedded PTP slave and master in the equipment. The PTP slave terminates PTP packets from the outside GM and synchronizes the local clock to the outside GM. The PTP master in the BC transmits the PTP packets that are regenerated by the synchronized local clock to an outside PTP slave. The third one is a transparent clock (TC) that is classified into end-to-end TC and peer-to-peer TC. In an end-to-end TC, a residence time that is the time difference of the arrival and departure of a PTP packet in a TC, is calculated, and the information on the residence time is added to the correction field of the PTP message. In an outside PTP slave, the correction field can show the total residence time from plural TCs on the link between PTP master and PTP slave. In a peer-to-peer TC, the link delay at ingress ports of a TC is measured by a peer delay mechanism [6]. The information on the link delay and the residence time in the TC is added to the correction field of a PTP message. In the outside PTP slave, the correction field can show the total link delay and the total residence time from plural TCs on the link between PTP master and PTP slave. Therefore, delay request and delay response messages are not needed.

PTP is originally designed for various kinds of applications that are not limited in communication services, and, as a result, the protocol is a little bit complex. Therefore, various PTP profiles have been already standardized and prepared to meet the system requirement of each application. Each of the profiles specifies a set of required options, prohibited options, and the ranges and defaults of configurable attributes. For telecommunication services, some PTP profiles have been standardized in ITU-T as “PTP Telecom Profile”. ITU-T G.8265.1 [13] supports frequency synchronization over packet networks of telecommunication companies. In phase and time synchronization, G.8275.1 [14] and G. 8275.2 [15] specify PTP Telecom Profiles for full timing support and partial timing support, respectively. Figure 3-4(a) and (b) describes synchronization networks based on G.8275.1 and G.8275.2 respectively. The packet network for G.8275.1 consists of plural BCs. On the other hand, in the packet network for G.8275.2, common packet switches without PTP functions, BCs, and TCs are included. To date, time synchronization by PTP has been actively studied in SDOs.

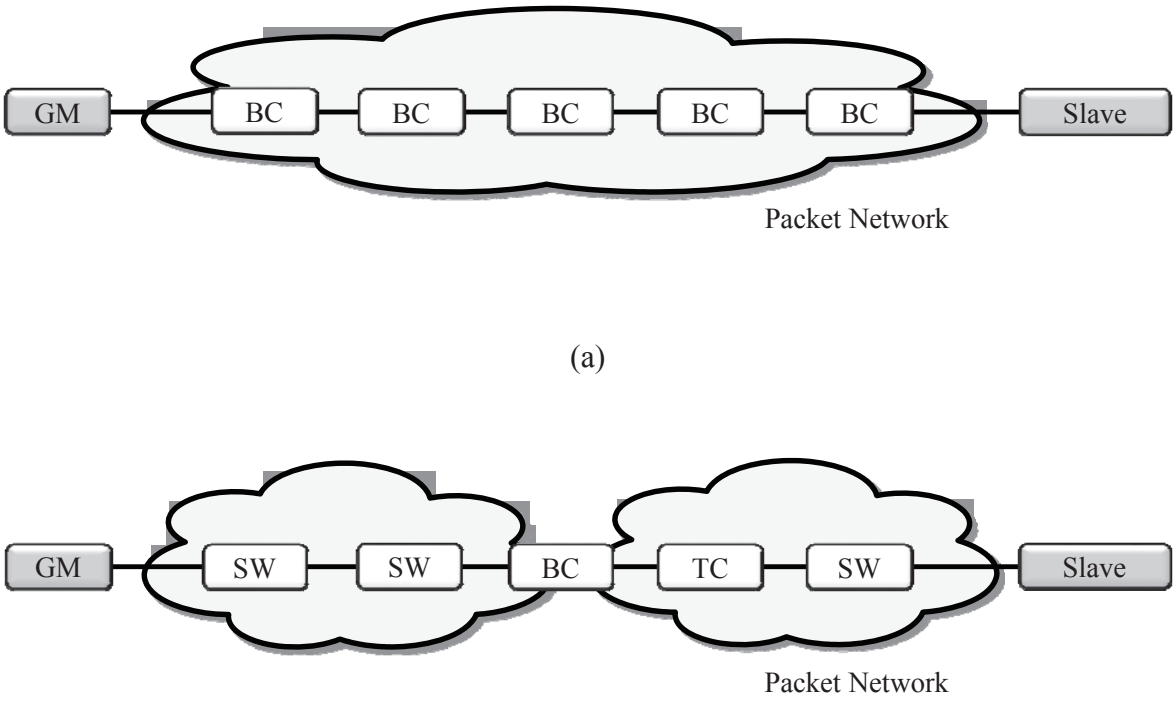

Fig. 3-4 PTP-based synchronization networks specified (a) in ITU-T G.8275.1 and (2) in ITU-T G.8275.2.

3-2.5 Principle of IEEE 802.1AS for EPON

Common IEEE EPON systems [2] have no functions for transmitting time information. Considering the use of EPON systems for mobile applications, such functions were strongly required to simplify the synchronization systems for plural BSs and specified in IEEE 802.1AS. In IEEE 802.1AS, an OLT works as a clock master whereas the ONUs that are connected to the OLT operate as the clock slaves. Therefore, precise time should be sent to the OLT, and then the time information is transmitted to the ONUs via the OLT. Figure 3-5 briefly depicts the process for time synchronization over EPON systems [16]. First, an OLT is provided with precise time by GPS or PTP. Second, the OLT synchronizes its local clock with the precise time. Third, the OLT calculates the one-way transmission delay from the OLT to

the ONU_i by the round-trip time (RTT) between the OLT and ONU_i which is described as RTT_i. In the calculation process, the multipoint control protocol (MPCP) messages in common EPON systems are used, as shown in Figure 3-6. There is a local counter in each of the OLT and the ONU_i. The value of the local counter is expressed by 32 bits and increases every 16 nanoseconds. The counter is reset every 68.72 seconds after it becomes the maximum value. The OLT sends the ONU_i a MPCP message with a time stamp of A when the local counter of the OLT is in A. After receiving the MPCP message, the ONU_i sets the value of its local counter to A. The ONU_i sends a MPCP message with a time stamp of B when the local counter of the ONU_i is in B. The OLT receives the MPCP message from the ONU_i when the local time of the OLT is in C. From the values of A, B, and C, the OLT can calculate the RTT_i by (C-A) - (B-A) = (C-B). When the refractive indexes of the downlink and uplink wavelengths are n_d and n_u, respectively, the downlink transmission delay from the OLT to the ONU_i is expressed by

$$RTT_i \frac{n_d}{n_d + n_u} \quad . \tag{3.3}$$

Fourth, the OLT calculates the synchronized time at the ONU_i of $T_{X,i}$ to the ONU_i local counter value of X by an equation of

$$T_{X,i} = T_{X,o} + RTT_i \cdot \frac{n_d}{n_d + n_u} \quad , \tag{3.4}$$

where $T_{X,o}$ is the time when the OLT transmits the MPCP message with a time stamp of X to the ONU_i. Fifth, the OLT sends the ONU_i the information on the relationship between X and $T_{X,i}$. Sixth, the ONU_i sets its local time to T by an equation of

$$T = T_{X,i} + (Y - X) \cdot T_{granularity} \quad , \tag{3.5}$$

where Y is the ONU_i local counter value at the timing of the setting, and $T_{granularity}$ is the time granularity of the counter of 16 ns. Finally, the ONU can provide a BS with precise time

information. The time synchronization performance that is obtained by the process above is deteriorated by the local counter inaccuracy, the RTT drift, and the propagation delay difference between uplink and downlink [16]. The maximum time error in an EPON system with a 20 km SMF was estimated to be 121 ns which consisted of the local counter inaccuracy of 8 ns, the RTT drift of 96 ns, and the propagation delay of 17 ns [16]. The RTT drift is the dominant factor, and, as a result, the influence of the fiber length is considered to be sufficiently small in real systems. The splitting ratio in an EPON system is also considered not to be related to the time accuracy because the time synchronization process for one of the ONUs is independent of that for the other ONUs.

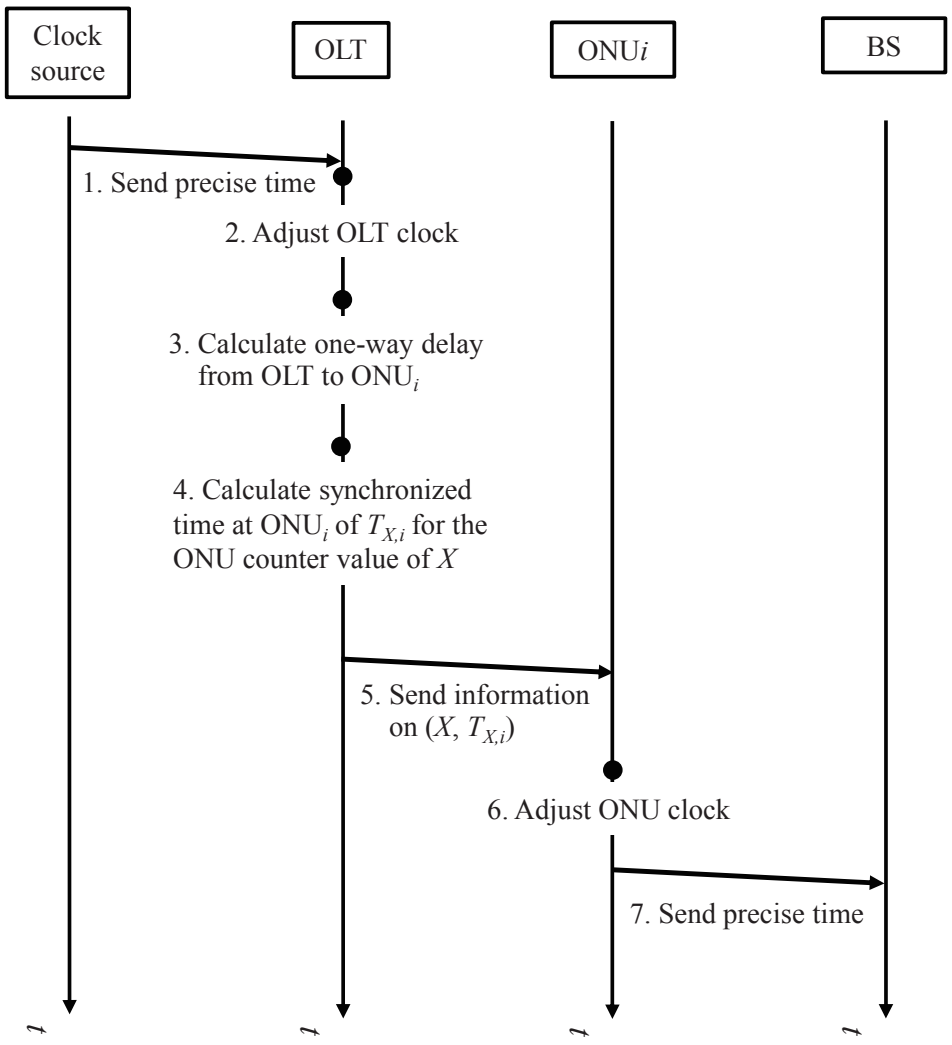

Fig. 3-5 Process for time synchronization over EPON systems.

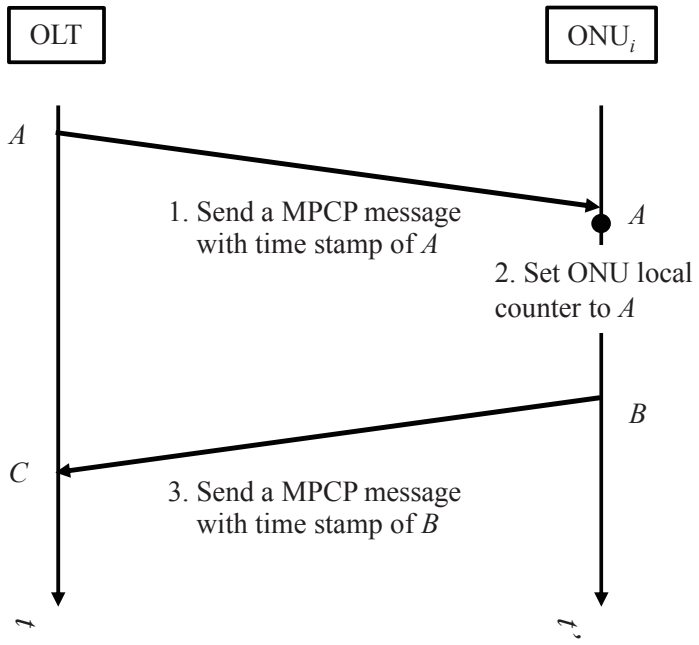

Fig. 3-6 RTT measurement in EPON systems.

3-3 Optical access systems

In this section, two kinds of PON systems that have been standardized in ITU-T and IEEE, i.e., TDM-PON and WDM-PON, are explained.

3-3.1 TDM-PON system

TDM-PON systems [2], [3], [17] have been mainly used for FTTH services all over the world. Figure 3-7(a) shows an overview of the downlink transmission. An OLT is located in a CO and connected to plural ONUs via an optical power splitter. Data traffic for plural ONUs are multiplexed in a time domain, and the TDM packets are transmitted over an access fiber from an OLT. The access fiber is connected to a splitter, and each of the outputs is connected to a specific ONU. For the splitter, eight branches have been widely used. When a splitter with four branches is located in the CO, the total number of the branches becomes 32. In each

ONU, the packet data for itself are sent to the end-user side whereas the packets for the other users are discarded in the ONU. Figure 3-7(b) shows the uplink transmission. To avoid the packet collisions among plural ONUs at the power splitter, the OLT controls the transmission timing and the amount of the data of each ONU by DBA algorithm. Thanks to the process, the OLT can successfully receive TDM packets from all ONUs. The wavelength for uplink transmission is different from that for downlink transmission. Therefore, in TDM PON systems, only one fiber can be shared by plural ONUs for bidirectional transmission, which is important for cost-effective access networks.

TDM-PON systems can be also applied to mobile services. Actually, the systems have been commercially used for 4G mobile services in some areas. However, the large delay for the uplink transmission using conventional DBA algorithm may be a problem for some applications that require low latencies. For the URLLC in 5G mobile systems, the delay in the wireless transmission section should be less than 1 ms. To reduce the uplink transmission delay in a TDM-PON system, cooperative DBAs between a PON system and BSs have been proposed [18], [19]. In MFH systems where BBU and RRHs are connected to OLT and ONUs, respectively, the OLT decided BW allocations to the ONUs by information on not the conventional data amount reported from the ONUs but the wireless scheduling from the BBU [18]. In MBH systems where BBUs are connected to ONUs, the OLT used information on the wireless scheduling that was also sent to the OLT via ONUs and decided the BW allocations to the ONUs before the uplink data from UEs arrive at the ONUs [19]. In both cases, the waiting time in ONUs for uplink transmission will be eliminated or reduced.

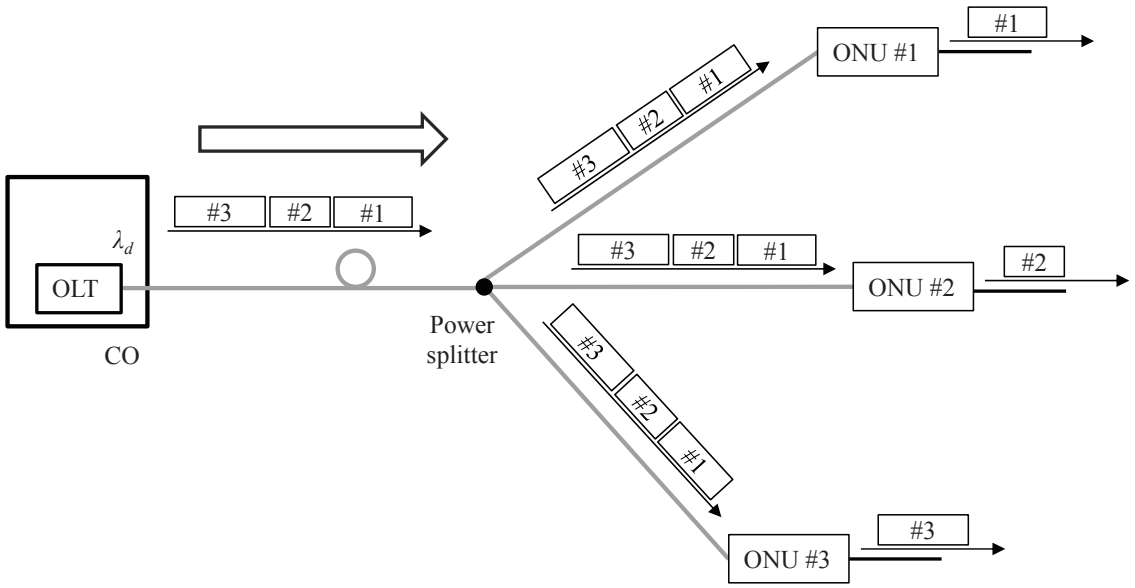

(a)

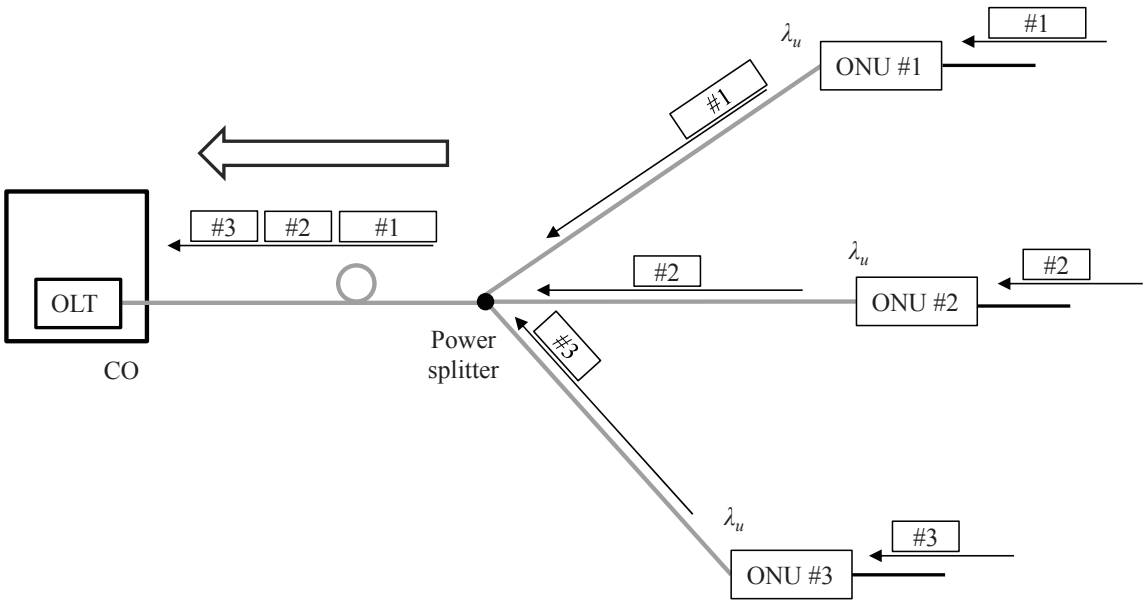

(b)

Fig. 3-7 TDM-PON system (a) for the downlink transmission and (b) for the uplink transmission.

3-3.2 WDM-PON system

Figure 3-8 shows an overview of a WDM-PON system that uses tunable laser diodes (LDs) [17]. An OLT is located in a CO and connected to plural ONUs via an arrayed waveguide grating (AWG). An AWG is a kind of passive wavelength router. In the figure, the number of ONUs is expressed by *N*. An OLT has *N* wavelengths in total for *N* ONUs, and the optical signals are multiplexed by a multiplexer (Mux). After passing through a WDM coupler (CPL) for separating downlink and uplink transmission, the WDM signal is transmitted over a fiber. An AWG separates each wavelength from the others, and each optical signal is transmitted to a specific ONU. The uplink transmission takes the opposite process of the downlink. In a WDM-PON system, the bandwidth of a wavelength is occupied by an ONU, which can provide each user with stable and large-capacity services. However, the system cost of WDM-PON is generally considered to be higher than that of TDM-PON due to expensive tunable components. In the future, TDM-PON and/or WDM-PON systems should be used depending on service requirements

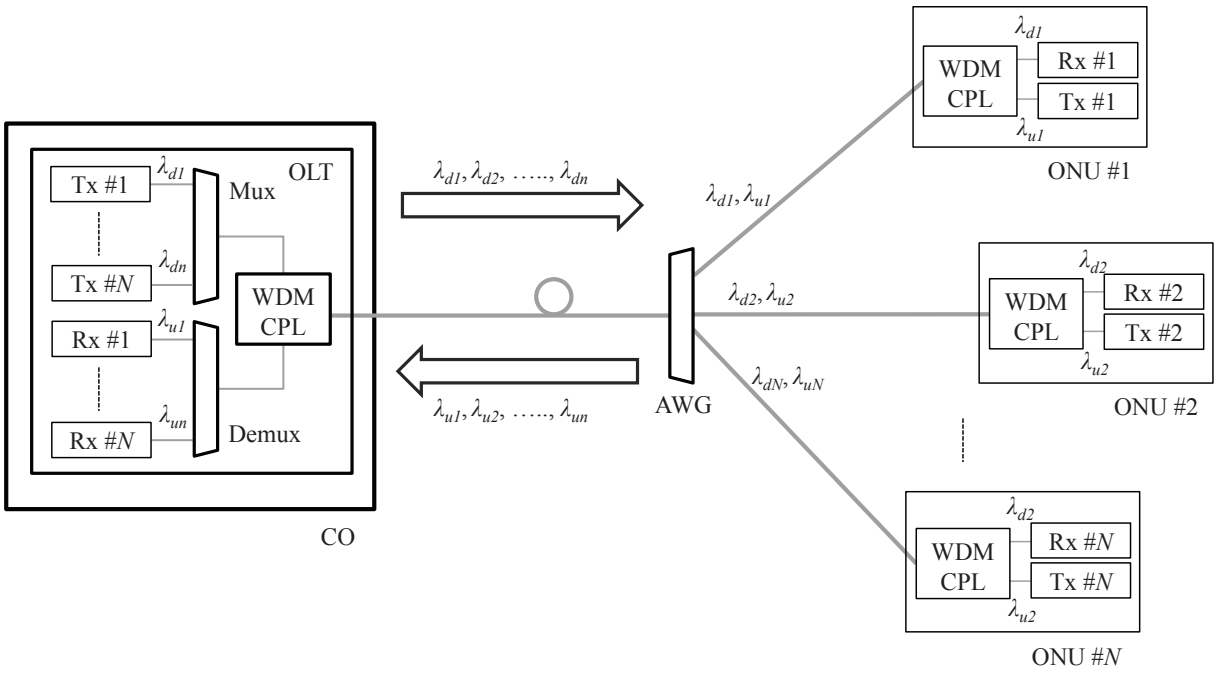

Fig. 3-8 WDM-PON system.

3-4 TDM-PON systems with time synchronization functions

In this section, the overviews of mobile and optical access networks are explained. Then, a new time synchronization technique using IEEE EPON and PTP is proposed, and the synchronization process is explained in detail [8].

3-4.1 Network architecture

Most of the commercial mobile networks consist of mobile core and MBH [20]. Figure 3-9 shows a conceptual diagram of mobile networks. The mobile core network [20] includes mobility management entity (MME), policy and charging rules function (PCRF), serving general packet radio service support node (SGSN), home subscriber server (HSS), serving gateway (S-GW) and packet data network gateway (P-GW). The mobile core is logically connected to BSs over MBH systems that are based on layer 2 or layer 3 packet networks.

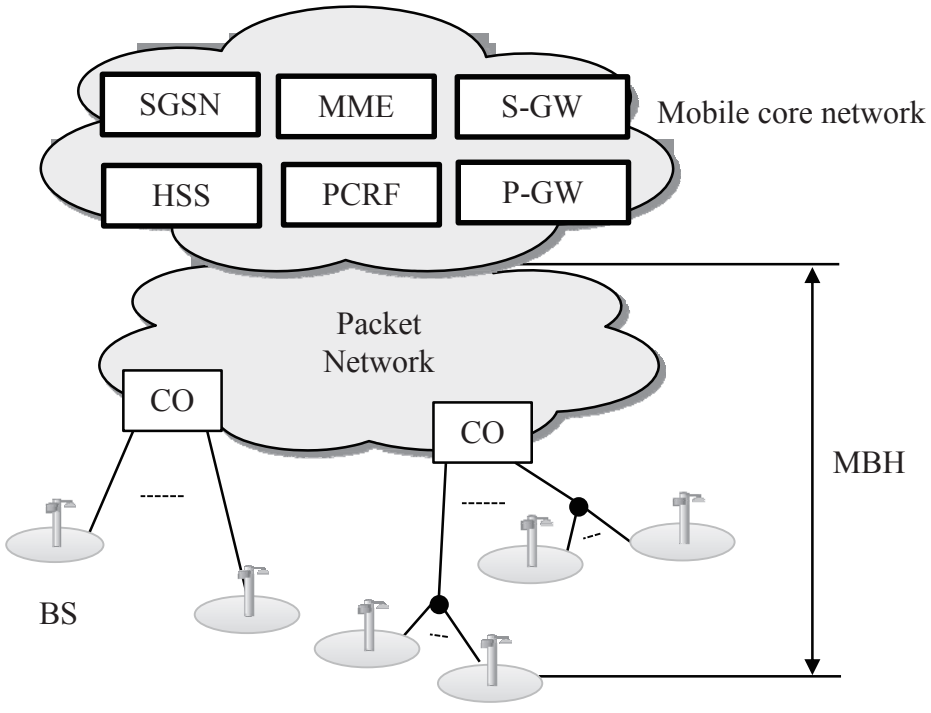

Fig. 3-9 Overview of mobile networks.

Figure 3-10 shows optical access networks for the connection between BSs and COs. In most of the commercial mobile networks, MCs for PtP optical Ethernet links have been used. When multiple mobile systems such as global system for mobile communications (GSM), wideband code division multiple access (W-CDMA), LTE and LTE-Advanced (LTE-A) are located in a BS site, layer 2 switch (L2SW) can be effectively used for multiplexing the packets and enhancing the bandwidth utilization efficiency. In high-density urban areas, PON systems will be useful for using an access fiber efficiently. In various PON systems, TDM-PON systems that have been widely used for commercial FTTH services will be especially attractive because of the high maturity and the cost effectiveness. A concern about the use of TDM-PON systems is a risk of large-scale system failure when the trunk fiber between CO and optical splitter has a problem.

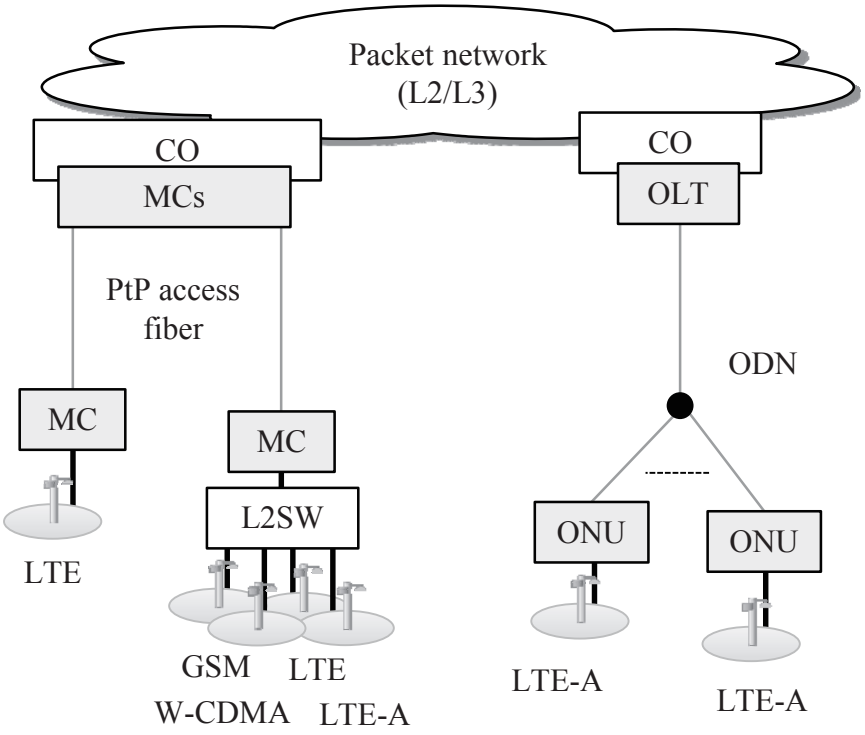

Fig. 3-10 Optical access networks to connect mobile BSs to COs.

As described in Section 3-1, the difficulty in deploying RF cables between GPS antennas and indoor and/or underground BSs is an important issue. To address the issue, time synchronization through transmission networks such as PTP can be effectively used. When PTP is applied to a TDM-PON system, three options for the location of a GM can be considered. Figure 3-11 shows the three options of in a site in packet networks, in a CO, and in a BS site.

When one of the options is selected, time accuracy, GM redundancy, and difficulty in deploying GPS antennas should be considered. In the option 1, time accuracy is one of the concerns. Additionally, when an active GM is switched to the other GM, large difference in absolute time will be another concern. These are because part of available packet SWs may not support PTP, and they may cause large packet delays and jitters. To completely address the concerns, packet SWs that do not support PTP should be replaced by ones with PTP functions. However the replacement process will need a big budget. The advantage of the option 1 is the reduction of the number of GMs in the whole system.

In the option 2, especially in Japan, the deployments of GPS antenna and RF cable may be difficult in some cases because COs are managed by an owner, and most operators can not use the space and facility as they hope. When GPS antenna and RF cable are deployed in a CO, negotiations with the owner are indispensable, which may take long time. In the worst case scenario, the deployments are not permitted after long discussion. Additionally, the site redundancy of GPS antenna and GM will be another issue.

In the option 3, both GPS antenna and GM are placed in a BS site, and the deployment place can be flexibly selected. The site redundancy of GMs and GPS antennas can be also taken by placing the equipment in plural BS sites. One technical issue is time accuracy as explained in Section 3-2.4. Therefore, when the technical issue is solved, the option 3 will be the best option for operators that do not have and manage COs.

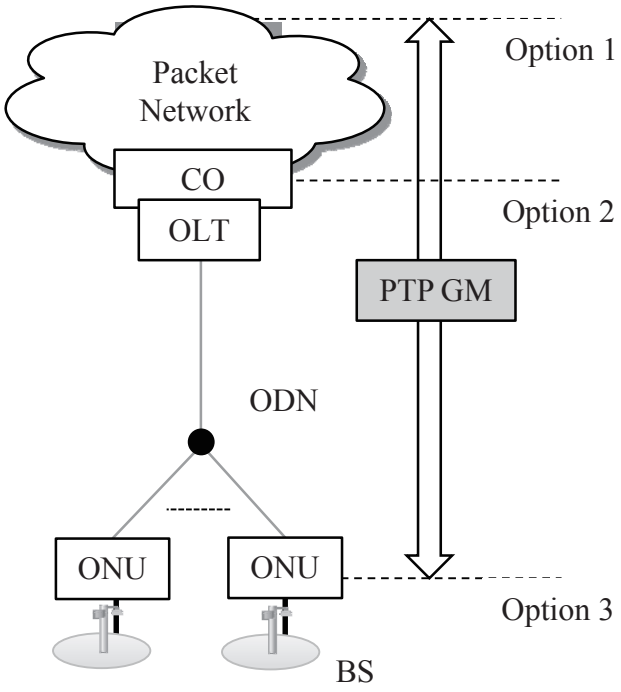

Fig. 3-11 Three options for the location of a PTP GM.

3-4.2 Proposal for time synchronization technique over EPON

PTP can operate successfully when each node in a network implements a BC function [6]. A BC generally includes its local clock and the functions of PTP slave and master. The PTP slave of a BC terminates PTP packets from the outside PTP master, and the local time of the BC is adjusted by the received time information. The PTP master of the BC regenerates PTP packets by the adjusted precise local clock and sends them to the outside PPT slave. The basic idea of a proposed time synchronization technique over EPON is based on the concept of a BC function. Time synchronization schemes in a TDM-PON system such as IEEE 802.1AS can synchronize the local time of each ONU with that of the OLT. Therefore, the local time of an OLT corresponds to that of a BC node.

Figure 3-12 depicts an overview of a proposed EPON system with time synchronization and GPS site redundancy functions. The option 3 in Figure 3-11 is applied to the proposed system for the location of PTP GMs. The ONUs connected to PTP GM and slave are described as master ONU (M-ONU) and slave ONU (S-ONU), respectively. A GPS antenna

and a PTP GM that is connected to the GPS antenna are deployed in one of the ONU sites in an optical distribution network (ODN). For GPS site redundancy, at least two sets of the GPS antenna and PTP GM will be prepared for a CO. In the time synchronization process, PTP is used only between ONUs and PTP equipment. Time information is sent from M-ONUs to an OLT by internet protocol (IP) packets whereas it is distributed from the OLT to S-ONUs by IEEE 802.1AS. Announce messages from PTP GMs [6] are also transmitted on the EPON system by IP packets.

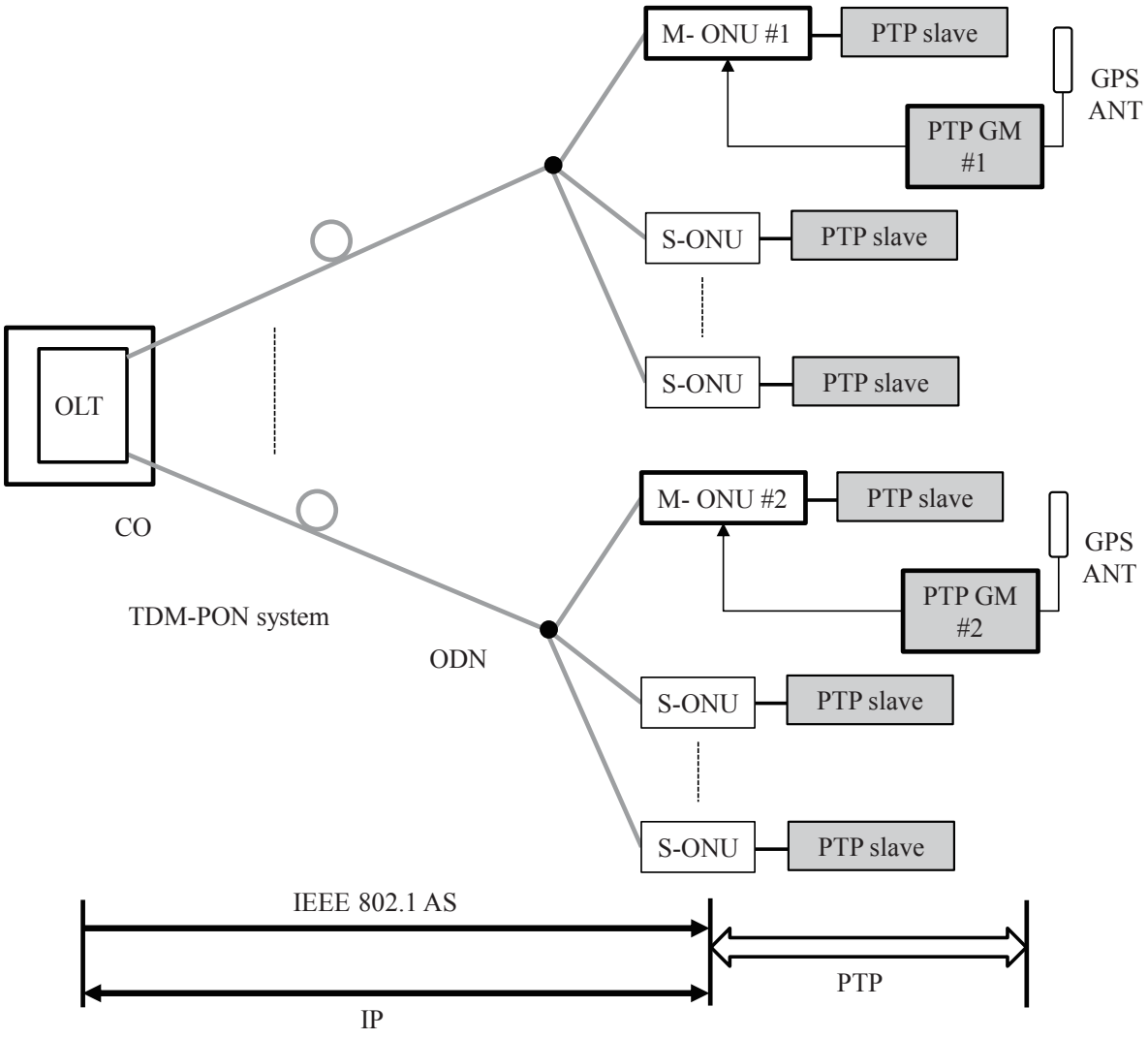

Fig. 3-12 Overview of the TDM-PON with time synchronization and GPS site redundancy functions.

Figure 3-13 illustrates the process of the proposed time synchronization scheme in detail. First, an OLT synchronizes the local clocks of ONUs with its local clock by IEEE 802.1AS. The local time in each ONU can become the same as that in the OLT. Second, PTP GMs send PTP packets that include precise time information from GPS signals to M-ONUs. Third, M-ONUs compare their local time with the precise time from GMs and calculate the time difference. Fourth, information on the time difference is encapsulated in IP packets and sent to the OLT. More specifically, the information on t_2-t_1 and t_4-t_3 in PTP process is used. Fifth, the OLT adjusts its local time by clock servo algorithm [21]. Sixth, the OLT synchronizes the local clocks of the S-ONUs with its local clock by IEEE 802.1AS again. The first to the sixth processes are repeated to gradually perform the synchronization. Finally, S-ONUs regenerate PTP packets and synchronize PTP slaves with its local time. The S-ONUs operates as GMs from the PTP slave perspective. In the proposed system, a GM is directly communicated with only one specific M-ONU, which can reduce the required PTP slave accommodation capacity in the GM and also the GM cost. Additionally, the proposed system does not suffer the delay and jitter in a TDM-PON system because the M-ONU transmits not the absolute time of a GM but the time difference between GM and OLT.

Regarding the GM site redundancy, an OLT has a lookup table to show the priority of GMs and information on PTP announce messages from the GMs. The OLT selects one of the GMs following the lookup table. When an active GM has a problem, the OLT switches the active GM to the other one with the second highest priority. The OLT maintains its local clock during the switching process, to prevent the PTP slaves from losing PTP packets.

A concern over the proposed synchronization technique may be influence on the data throughput. However, the packet rate of synchronization messages in conventional PTP is around 1 to 128 packets per second [15]. Additionally, the common packet rate in IEEE 802.1AS is one to several packets per second. The influence of these packets will be negligible.

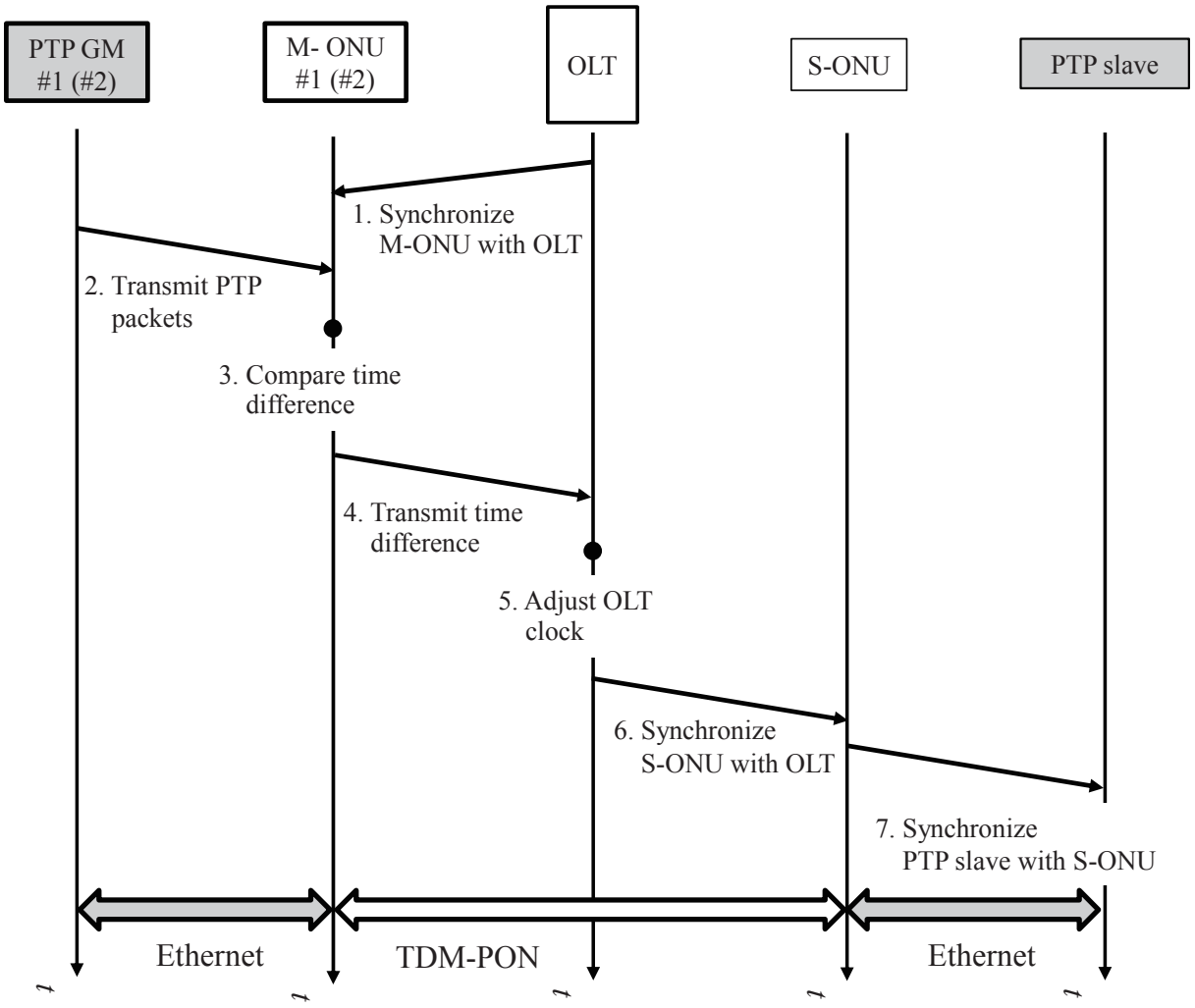

Fig. 3-13 The detail of time synchronization process for a PTP slave.

3-5 Transmission experiments

In this section, the effectiveness of the proposed time synchronization technique is experimentally confirmed. The performance of a 10G-EPON prototype that has the time synchronization function is firstly evaluated. Then, the prototype is connected to commercial PTP slave and TD-LTE BS that supports PTP, and the time accuracy in each of the commercial equipment is measured [8].

3-5.1 PTP packets over conventional TDM-PON

Figure 3-14(a) depicts an experimental setup to measure the time accuracy that is obtained by PTP and conventional TDM-PON. There are a PTP GM and a PTP slave. The PTP GM is synchronized with the precise time from a GPS signal. PTP packets between the GM and the slave are transmitted via ONU #1, OLT Card #1, OLT Card #2, and ONU #2. The timing difference of 1PPS signals between the GM and the slave is measured by a universal counter (UC). Figure 3-14 (b) shows the timing difference measured for 72 hours. The rage of the timing difference was -89 μs to +69 μs which is much larger than a criterion of ±1.5 μs. The transmission delay from the GM to the slave is almost equivalent to that from the slave to the GM. However, the transmission from the ONUs to the OLT has large packet jitters, which caused the bad time synchronization performance. Through this experiment, it was experimentally confirmed that PTP can not be applied to conventional TDM-PONs.

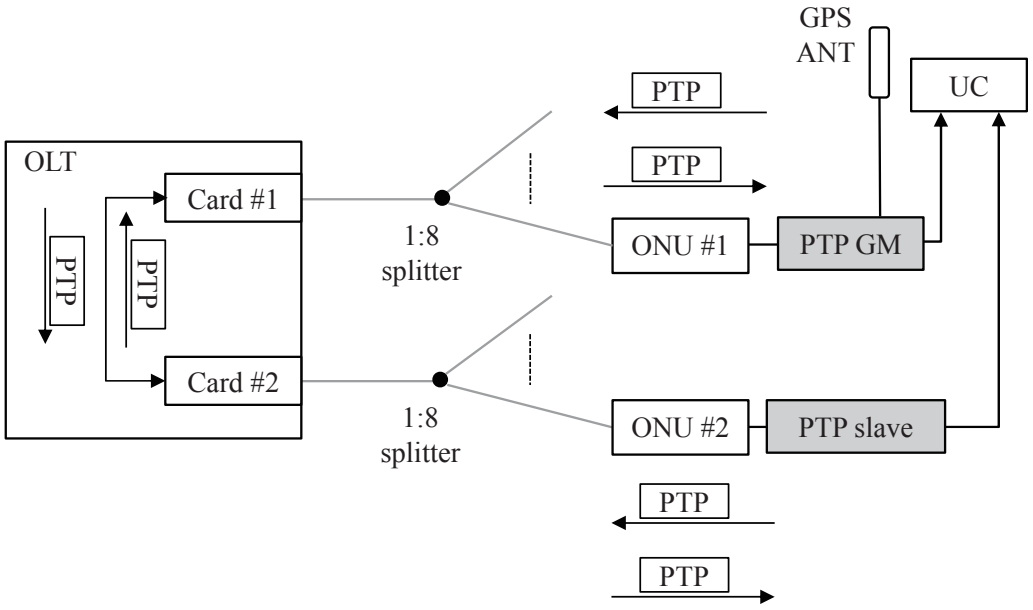

(a)

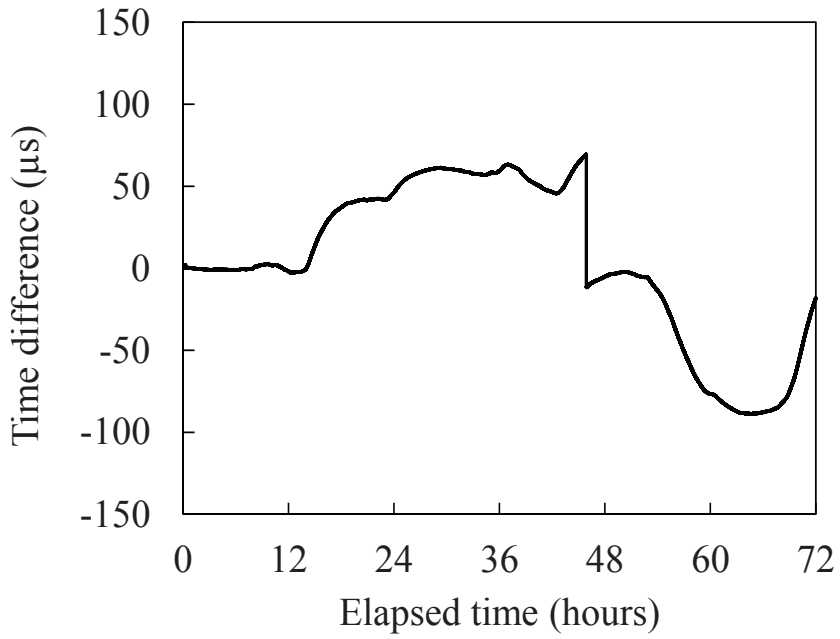

(b)

Fig. 3-14 Time accuracy obtained by PTP and conventional TDM-PON; (a) experimental setup and (b) experimental result.

3-5.2 Unit tests of 10G-EPON prototype

In this section, a 10G-EPON prototype that implements the proposed time synchronization function is evaluated in three kinds of unit tests. Main target specifications in the prototype are shown in Table 3-2.

Table 3-2 Main target specifications in the 10G-EPON prototype.

Item		Specification
OLT/ONU (Common)	**Supported standards**	**10G-EPON specified in IEEE802.3av IEEE802.1AS IEEE1588-2008 (PTP), ITU-T G8265.1, ITU-T G8275.1**
	Transmission rate	**10.3125 Gbit/s for uplink and downlink**
	Fiber length	**20 km**
	Loss budget	**> 29 dB**
	Synchronization	**Phase: < ±1.0 μs Frequency: < 16 ppb**
OLT	**NNI**	**10G-LR/SR, 1000Base-X**
	EPON ports	**32**
	Splitting ratio	**128**
ONU	**UNI**	**10GBase-LR/SR, 1000Base-X, 1000Base-T**
	RF output	**1PPS, 10MHz**

Figure 3-15(a) describes the first experimental setup. In the experiment, various SMF lengths of 2 km, 10 km, and 20 km were used. The ODN with a 20-km SMF accommodates an M-ONU and an S-ONU #3. The other ODNs with 10-km SMF and 2-km SMF connect an OLT to an S-ONU #2 and an S-ONU #1, respectively. In each ODN, a 1:8 optical power splitter was includes to emulate a common optical loss in PON systems. The transmission rate of sync messages between the GM and the M-ONU was set to 32 times per second. In order to evaluate the time accuracy of each S-ONU, the 1PPS timing signal from each S-ONU was compared with that from the GM by oscilloscope (OCS). Figure 3-15(b) shows the accumulated experimental results for three minutes. Minimum and maximum fluctuations were measured to be 10 ns from S-ONU #3 and 14 ns from S-ONU #2, respectively.

Maximum absolute time offset was 11 ns in S-ONU #1. The values were less than 16 ns of the time quanta (TQ) in 10G-EPON systems. Therefore, the synchronization process was found to work properly as designed. In comparison with a time accuracy criterion of ±1.5 μs, it was experimentally verified that the prototype, that transmits the information on the time difference between M-ONU local time and GPS precise time from M-ONU to OLT, can provide S-ONUs with sufficiently accurate time in the short term, and the time accuracy is independent of the fiber lengths.

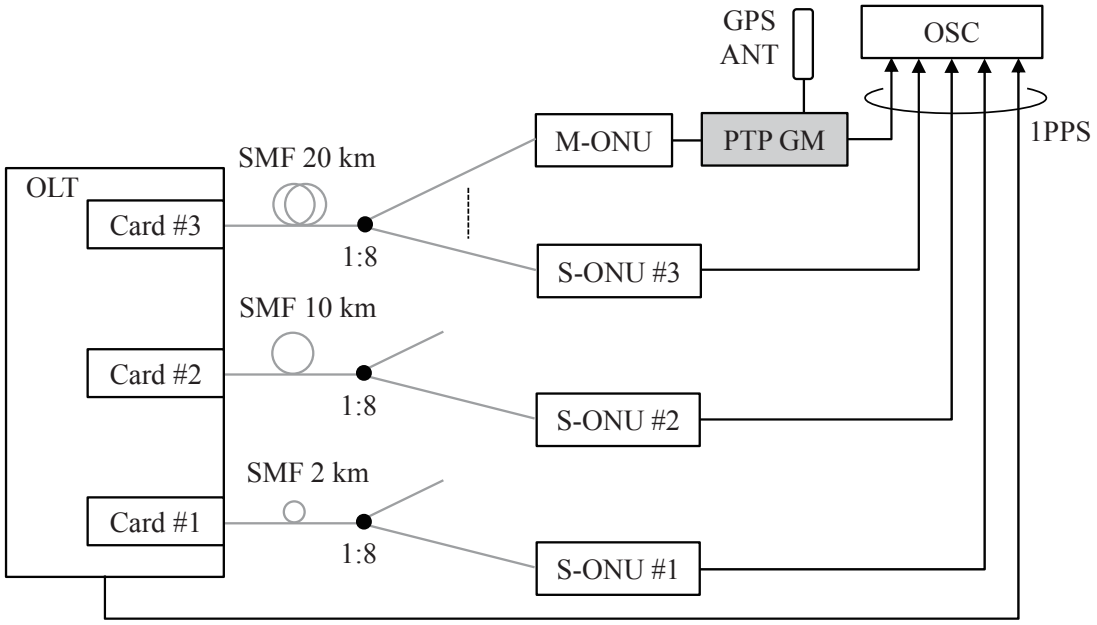

(a)

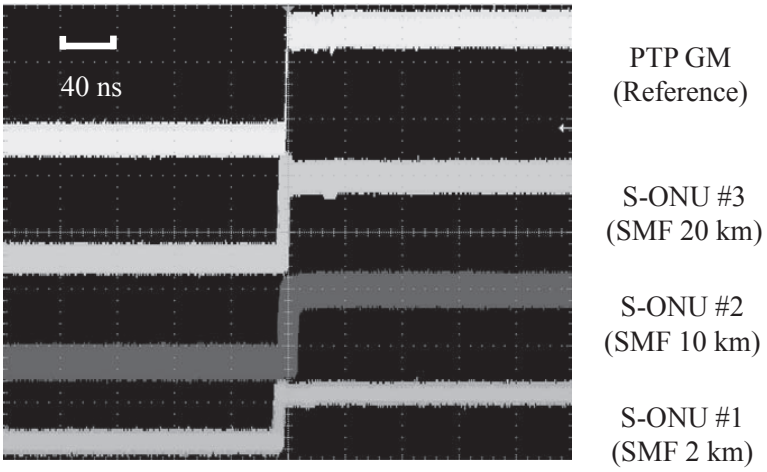

(b)

Fig. 3-15 Comparison of 1PPS timing signals after SMF 2 km, SMF 10 km, and SMF 20 km transmission; (a) experimental setup and (b) experimental result.

Second, Figure 3-16(a) describes an experimental setup to measure the operational stability for a long term. This experiment was carried out to confirm the system reliability against large traffic and packet jitters. An ODN with 2-km SMF and 1:8 optical power splitter was prepared for an S-ONU #1 whereas the other ODN with 20-km SMF and 1:8 optical power splitter was prepared for an M-ONU and an S-ONU #2. 1PPS timing signals from the S-ONU #1 and the S-ONU #2 were compared with the 1PPS output from the PTP GM for 72 hours by a UC. During the measurement, dummy traffic with random frame sizes was transmitted on each of the ODNs. The load for S-ONU #1 was set to 100% for both downlink and uplink whereas that for M-ONU and S-ONU #2 was set to 50% for downlink and 100% for uplink. Setting PTP packets to a high priority class in the PON, no PTP packet losses were found. Figure 3-16(b) shows the obtained time accuracy in S-ONU #1 and S-ONU #2. Maximum values for absolute time difference and fluctuation were 13 ns and 17 ns, respectively. In comparison with the short-term measurement, no big difference was observed. It was also experimentally confirmed that the time accuracy of each S-ONU is independent of the data traffic in addition to the fiber lengths.

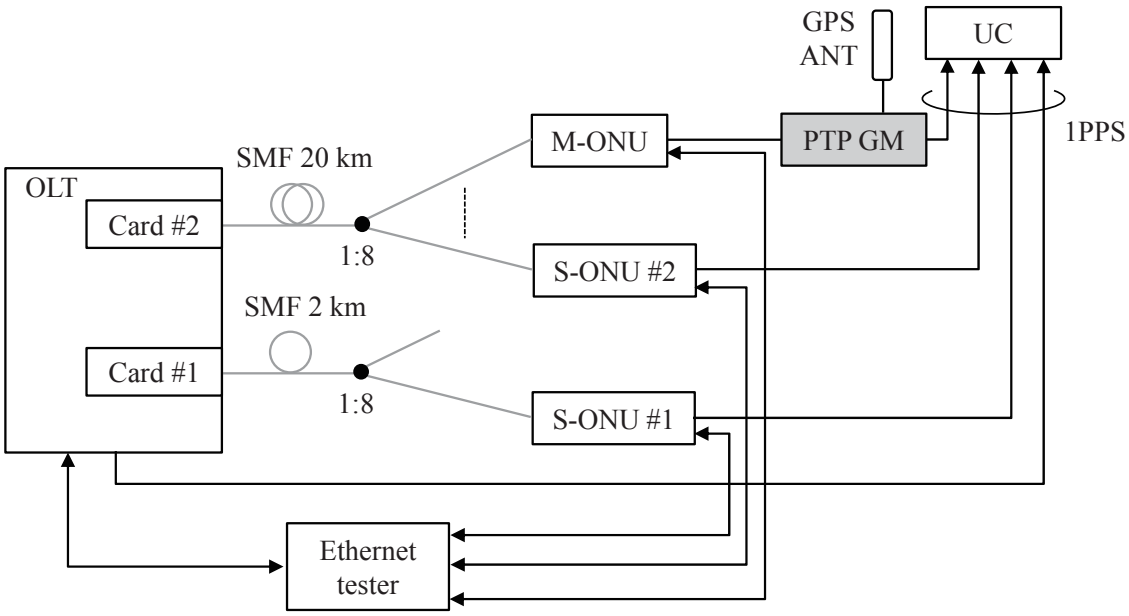
GPS
ANT
UC
1PPS
PTP GM
M-ONU
SMF 20 km
OLT
Card #2
1:8
S-ONU #2
SMF 2 km
Card #1
1:8
S-ONU #1
Ethernet
tester

(a)

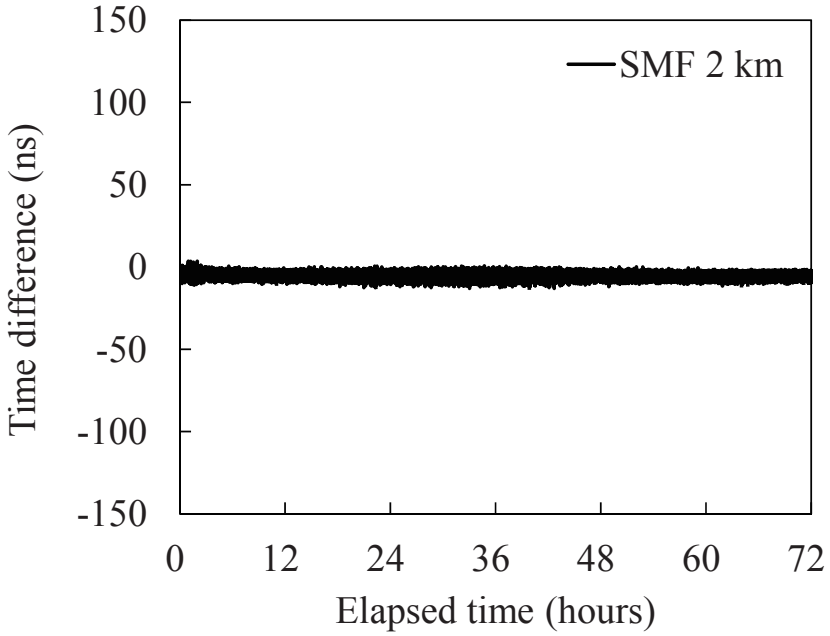
SMF 2 km
Time difference (ns)
150
100
50
0
-50
-100
-150
0
12
24
36
48
60
72
Elapsed time (hours)

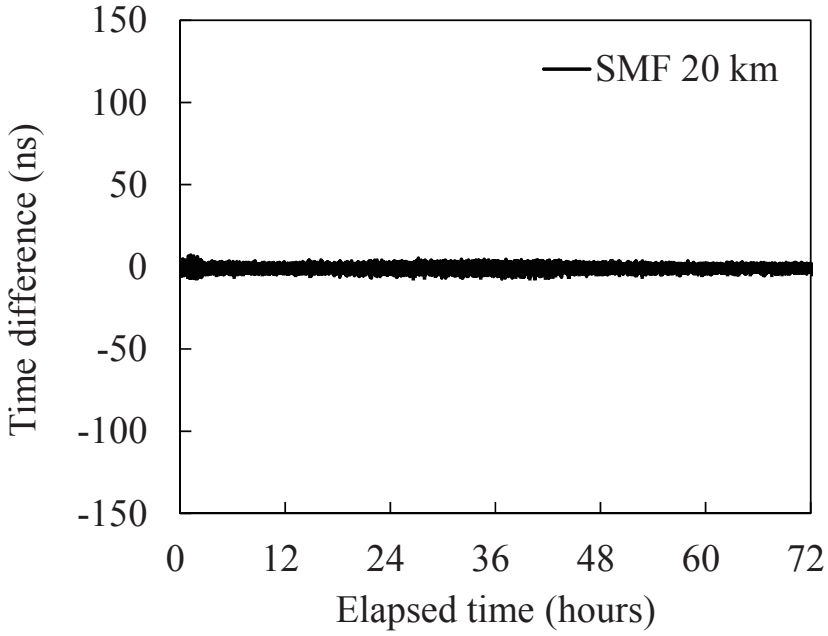

(b)

Fig. 3-16 Time stability of S-ONUs; (a) experimental setup and (b) experimental results.

Finally, Figure 3-17(a) presents an experimental setup to evaluate a switchover function between M-ONUs. An ODN with 20-km SMF and 1:8 optical splitter was connected to M-ONU #1, M-ONU #2, and S-ONU. Each M-ONU was connected to a PTP GM that was synchronized with the precise time of a GPS signal. M-ONU #1 and M-ONU #2 were assigned to the highest priority and the second highest priority, respectively. In the experiment, the 1PPS timing signal from an OLT was compared to that from a PTP GM #1 by a UC. The offset value to each M-ONU was not properly adjusted to clarify the influence of the switchover. Figure 3-17(b) describes the experimental result. When the M-ONU #1 was disconnected, the M-ONU #2 was automatically selected as a reference clock by the OLT. As a result, the OLT was synchronized to the time in the M-ONU #2 within 60 s. From this experiment, the site redundancy function of PTP-GMs was experimentally verified.

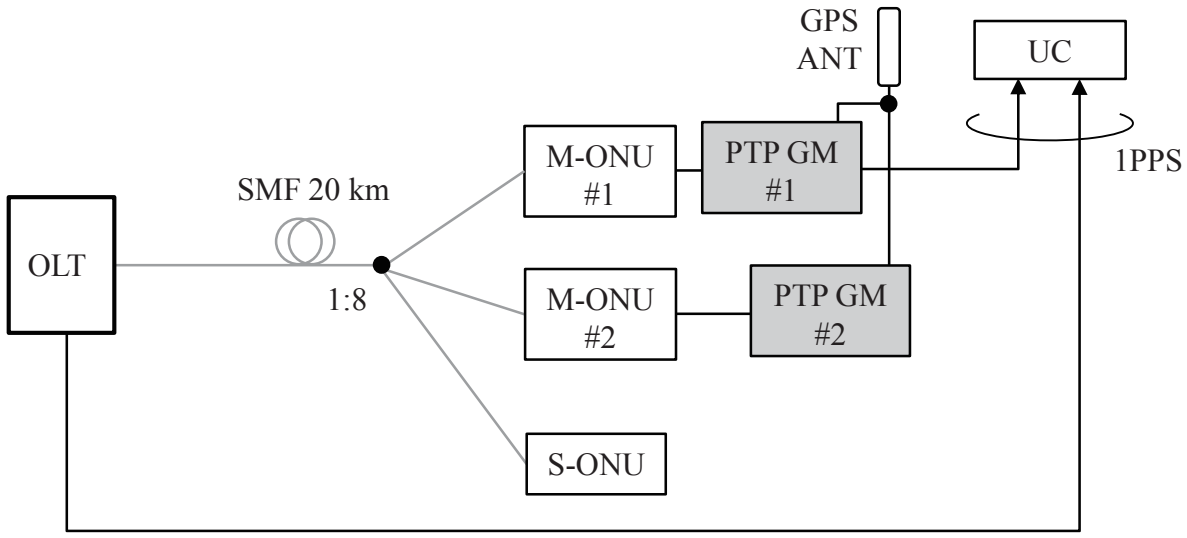

(a)

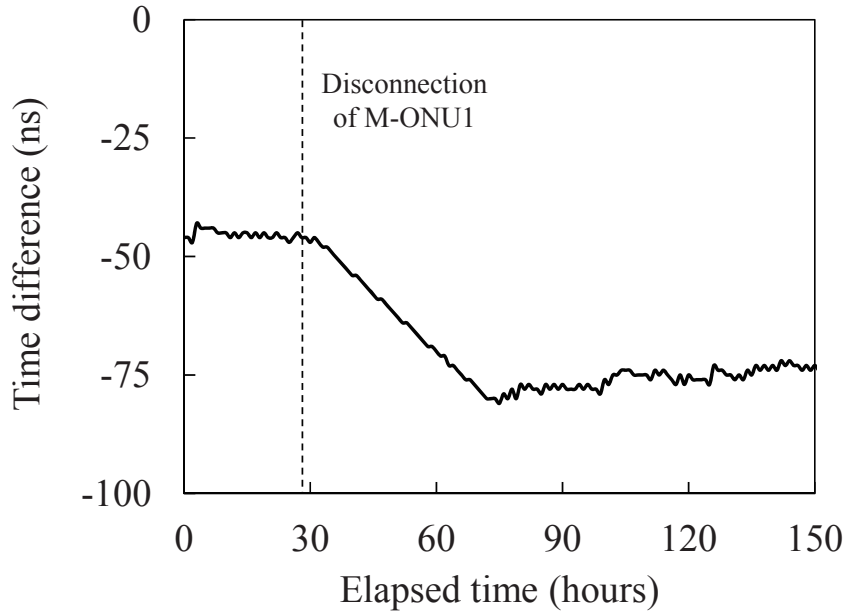

(b)

Fig. 3-17 Performance of a M-ONU redundancy function; (a) experimental setup and (b) experimental result.

3-5.3 Interoperability tests between prototype and mobile base station

In this section, two kinds of interoperability tests for a 10G-EPON prototype that implements the proposed time synchronization scheme are conducted. In the first experiment, the prototype is connected to a commercial PTP slave. Figure 3-18(a) describes the experimental setup. The ODN to connect an M-ONU to an OLT included a 20-km SMF and a 1:8 optical power splitter whereas the other ODN to connect an S-ONU to the OLT consisted of 10-km SMF and 1:8 optical power splitter. A PTP GM and a PTP slave are connected to the M-ONU and the S-ONU, respectively. Figure 3-18(b) depicts the timing difference of 1PPS signals from the PTP GM and the PTP slave for 72 hours. The time difference and fluctuation were 38 ns and 55 ns at maximum, respectively. In comparison with the experimental results from Figure 3-16(b), the values in this experiment are large. The difference is considered to be due to the fluctuations in the regeneration and transmission of PTP packets, in addition to the performance of the PTP slave. However, the obtained values are sufficiently small, compared to the requirement in TD-LTE systems of ±1.5 μs.

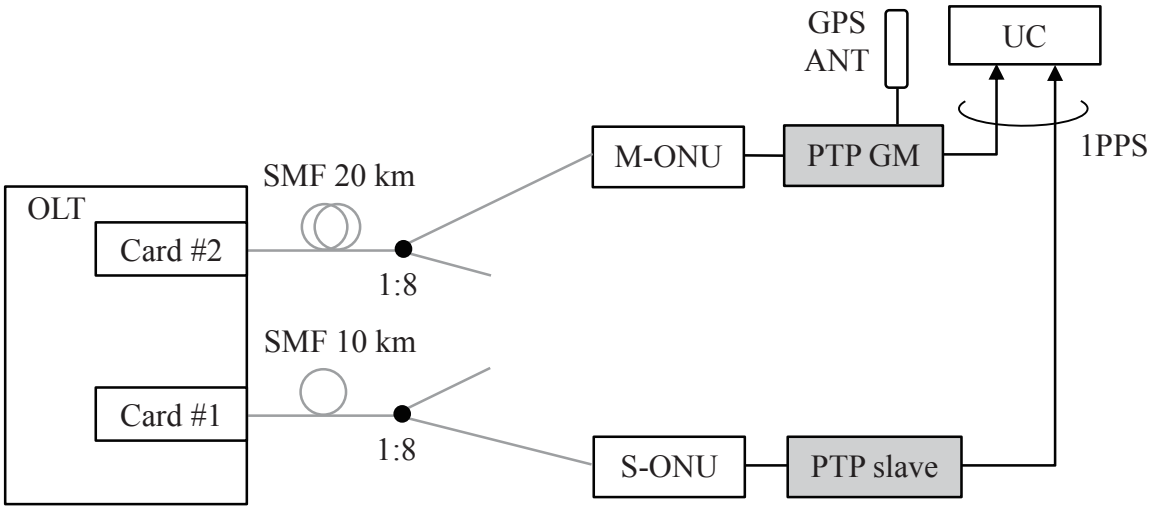

(a)

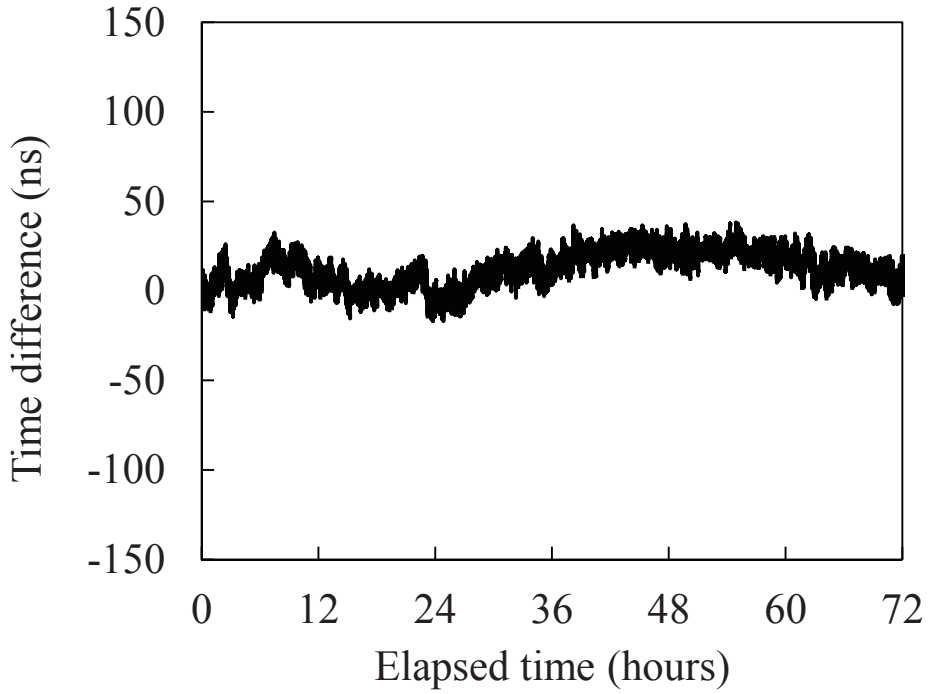

(b)

Fig. 3-18 Time accuracy and stability in a commercial PTP slave; (a) experimental setup and (b) experimental result.

Figure 3-19(a) describes the second experimental setup. In the experiment, an S-ONU and an M-ONU of the 10G-EPON prototype were connected to a commercial TD-LTE BS and a PTP GM, respectively. A 20-km SMF and a 1:8 optical power splitter were included in the PON ODN. Evolved packet core (EPC) for the BS was located on the upper network, and the BS was activated by the communication with the EPC. The BS was able to emit the RF signal only when the internal PTP slave was successfully synchronized with the S-ONU by PTP. UE was used for generating continuous traffic on the system by file transfer protocol (FTP). Figure 3-19(b) shows the timing difference of 1PPS output signals between the PTP GM and the BS for 60 hours. The time difference and fluctuation in the BS were measured to be 119 ns and 230 ns at maximum, respectively. These values are much larger than those from Figure 3-18(b). However, the obtained time accuracy was sufficient for TD-LTE BS, and the BS was continuously emitting the RF signal. It was experimentally confirmed that the internal clock in a commercial BS can be precisely and stably synchronized with that in an S-ONU of the proposed TDM-PON system by PTP. Additionally, from the results of Figures 3-18(b) and 3-19(b), it was clarified that the time accuracy obtained by PTP significantly changes depending on the PTP slave performances.

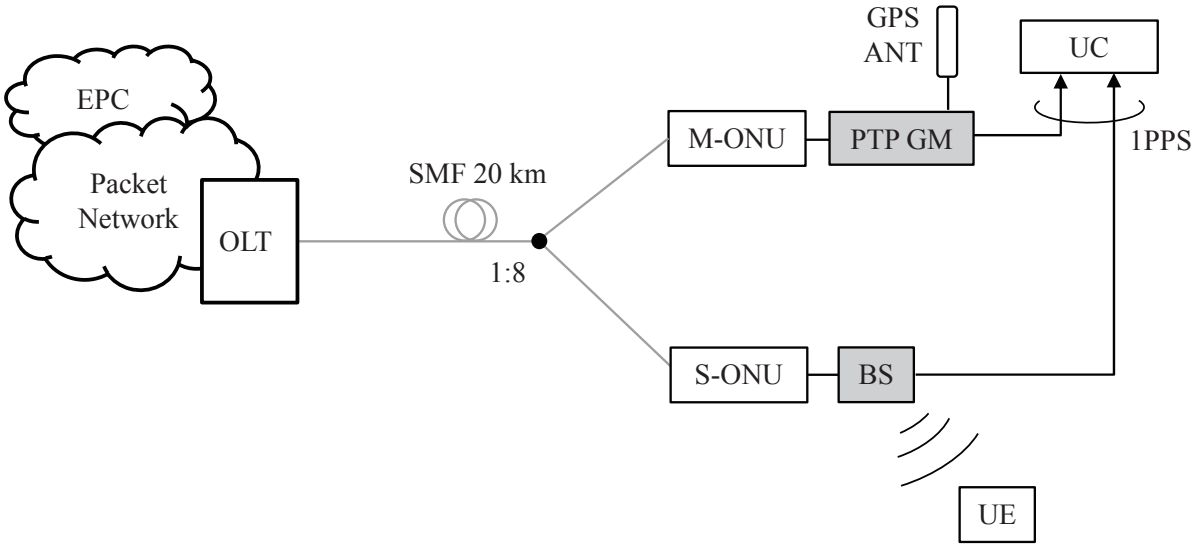

(a)

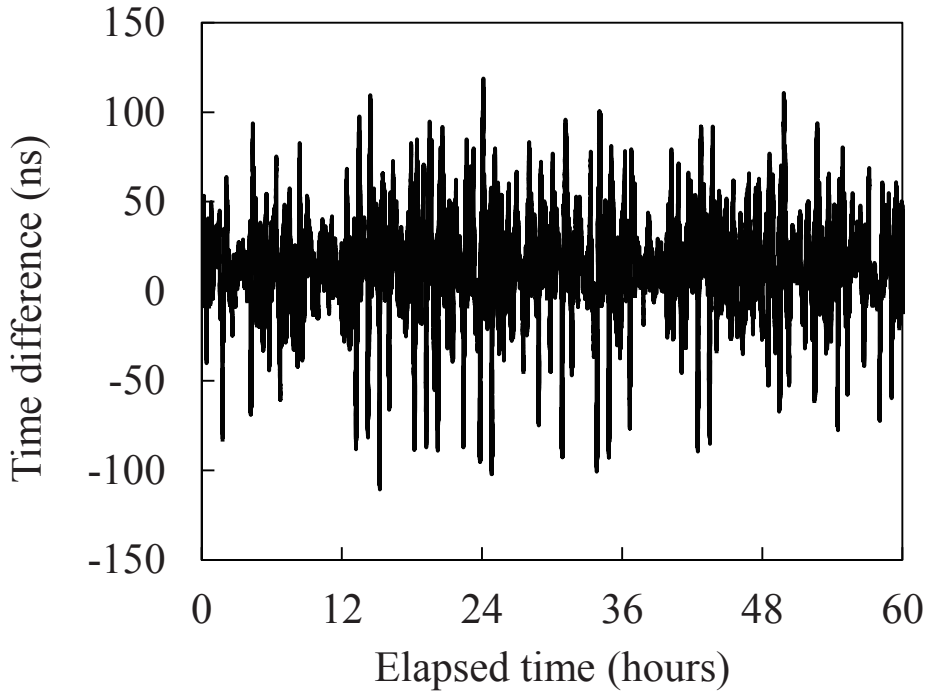

(b)

Fig. 3-19 Time accuracy and stability in a TD-LTE BS; (a) experimental setup and (b) experimental result.

3-6 Conclusion:

A TDM-PON-based MBH system with a time synchronization function for mobile BSs was proposed. In the proposed system, a GPS antenna is located not at the OLT site but at the ONU site to deploy the mobile BSs more promptly and flexibly. The information on the difference between the precise time from the GPS signal and the local time of the ONU is transmitted to the other ONUs over TDM-PON via the OLT. Each ONU generates PTP packets using the time information transmitted over the PON and sends them to BSs. To make the time synchronization function more reliable, the site redundancy of GPS antennas can be implemented.

To verify the effectiveness of the proposed technique, a 10G-EPON prototype was developed and evaluated in the unit tests and interoperability tests with commercially used equipment such as PTP slave and TD-LTE BS. In the unit tests for 72 hours, the absolute time accuracy and the time fluctuation of ONUs were measured to be 13 ns and 17 ns at maximum, respectively, independent of the access fiber length and traffic loads in the PON system. The site redundancy function was also experimentally demonstrated. In the interoperability tests, the absolute time accuracy and time fluctuation of a commercial PTP connected to an ONU for 72 hours were measured to be 38 ns and 55 ns, respectively. Additionally, when a commercial TD-LTE BS with a PTP slave function was connected to an ONU of the prototype for 60 hours, the absolute time accuracy and time fluctuation of the BS were 119 ns and 230 ns, respectively. Compared to a criterion for time accuracy in TD-LTE of ±1.5 μs, the obtained values in these experiments are sufficiently small. It was confirmed from these experimental results that the proposed EPON system with a time synchronization function is effective for 4G MBH and has high potential for the future advanced mobile applications.

References

[1] A. Damnjanovic, J. Montojo, Y. Wei, T. Ji, T. Luo, M. Vajapeyam, T. Yoo, O. Song, and D. Malladi, "A survey on 3GPP heterogeneous networks," *IEEE Wireless Communications*, vol. 18, no. 3, pp. 10-21, 2011.

[2] IEEE Std 802.3ah-2004, "Part 3: Carrier Sense Multiple Access with Collision Detection (CSMA/CD) Access Method and Physical Layer Specifications Amendment: Media Access Control Parameters, Physical Layers, and Management Parameters for Subscriber Access Networks," 2004.

[3] ITU-T Reccommendation ITU-T G.984.1, "Gigabit-capable passive optical networks (GPON): General characteristics," 2008.

[4] H. Zhang and H. Dai, " Cochannel Interference Mitigation and Cooperative Processing in Downlink Multicell Multiuser MIMO Networks," *EURASIP Journal on Wireless Communications and Networking*, pp. 222-235, 2004.

[5] S. Vasudevan, R. N. Pupala and K. Sivanesan, "Dynamic eICIC — A Proactive Strategy for Improving Spectral Efficiencies of Heterogeneous LTE Cellular Networks by Leveraging User Mobility and Traffic Dynamics," *IEEE Trans. on Wireless Communications*, vol. 12, no. 10, pp. 4956-4969, 2013.

[6] IEEE Std 1588-2008, "IEEE Standard for a Precision Clock Synchronization Protocol for Networked Measurement and Control Systems," 2008.

[7] Y. Horiuchi and K. Tanaka, "Precise Time Distribution using Ethernet Passive Optical Network," *in Proc. European Conference on Optical Communication (ECOC)*, We.2.F.7, Brussels, Belgium, Sept. 2008.

[8] K. Tanaka, N. Nishi, R. Inohara, and K. Nishimura, "Time Synchronization Technique for Mobile Base Stations over TDM-PON-Based Mobile Backhaul Using Precision Time Protocol," *IEICE Trans. Commun.*, vol. E101-B, no. 4, pp. 979-986, 2018.

[9] ITU-T Reccommendation ITU-T G.8261/Y.1361, "Timing and synchronization aspects in packet networks," 2019.

[10] ITU-T Reccommendation ITU-T G.8262/Y.1362, "Timing characteristics of synchronous equipment slave clock," 2018.

[11] IEEE Std 802.1AS-2011, "Timing and Synchronization for Time-Sensitive Applications in Bridged Local Area Networks," 2011.

[12] ITU-T Recommendation ITU-T G.8271 “Time and phase synchronization aspects of packet networks,” 2016.

[13] ITU-T Recommendation ITU-T G.8265.1 “Precision time protocol telecom profile for frequency synchronization,” 2014.

[14] ITU-T Recommendation ITU-T G.8275.1 “Precision time protocol telecom profile for phase/time synchronization with full timing support from the network,” 2016.

[15] ITU-T Recommendation ITU-T G.8275.2 “Precision time protocol telecom profile for phase/time synchronization with partial timing support from the network,” 2016.

[16] Y. Luo and F. J. Effenberger, “Time Synchronization over Ethernet Passive Optical Networks,” *IEEE Communications Magazine*, vol. 50, no. 10, pp. 136-142, 2012.

[17] F. Effenberger, D. Cleary, O. Haran, G. Kramer, R. D. Li, M. Oron, and T. Pfeiffer, “An Introduction to PON Technologies,” *IEEE Communications Magazine*, vol. 45, no. 3, pp. S17-S25, 2007.

[18] T. Tashiro, S. Kuwano, J. Terada, T. Kawamura, N. Tanaka, S. Shigematsu, and N. Yoshimoto, “A novel DBA scheme for TDM-PON based mobile fronthaul,” in *Proc. Optical Fiber Communication Conference (OFC)*, Tu3F.3, San Francisco, CA, Mar. 2014.

[19] K. Tanaka, K. Nishimura, A. Agata, and N. Nishi, “PON system and communication method,” Japan patent, P2017-50775A, 2017.

[20] 3GPP TS 23.401 V14.3.0, “General Packet Radio Service (GPRS) enhancements for Evolved Universal Terrestrial Radio Access Network (E-UTRAN) access (Release 14),” 2017.

[21] K. Correll, N. Barendt, and M. Branicky, “Design Considerations for Software Only Implementations of the IEEE 1588 Precision Time Protocol,” IEEE 1588 Standard for a Precision Clock Synchronization Protocol for Networked Measurement and Control Systems, 2006.

Chapter 4

IFoF transmission technologies in mobile fronthaul links

4-1 Introduction

As described in Chapter 2, the data rates of CPRI links for 4G MFH are about sixteen times higher than mobile user data rates [1]. When mobile user data rates increase, expensive high-speed transceivers, WDM transmission, or additional access fibers will be needed in the CPRI links, which results in expensive optical access systems. To date, to reduce the required bandwidths in the optical components, IFoF transmission technologies have been proposed and studied. PtP IFoF transmission systems that assumed to use DSP for IF channel aggregation and deaggregation were successfully demonstrated [2]-[10]. To make the optical transmission systems more cost-effective, IFoF transmission systems using a VCSEL were also experimentally verified [10]. However, the applicability of the IFoF systems to commercial systems such as mobile BSs and deployed fibers had not been studied and verified by transmission experiments using real commercial systems.

In this chapter, the applicability of IFoF transmission technologies to existing 4G mobile systems are studied. Commercial broadcasting systems are firstly introduced as an application of A-RoF technologies, and then the difference between broadcasting systems and mobile systems both using A-RoF technologies is explained. Next, in order to investigate the possibility of IFoF transmission for MFH links, the performance of the IFoF transmission is estimated by numerical calculations in various transmission conditions. Finally, an IFoF-based MFH link, for three sectors, four frequencies, and 2×2 MIMO, is experimentally demonstrated using a commercial LTE BS and deployed fibers.

4-2 Applications of analog RoF technologies

In this section, two kinds of analog RoF applications are described. One is broadcasting systems that have been commercially available. The other one is MFH systems that have been studied a lot as the future technologies. The difference between two systems are also explained [11].

4-2.1 Broadcasting systems

An A-RoF technology has been widely used for retransmission of terrestrial and satellite broadcasting in CATV services [12]. In the retransmission, two transmission technologies have been utilized. One is a trans-modulation scheme where the broadcasting signals are converted to 64-QAM signals, and the converted signals are transmitted to the subscriber's home. The other is a pass-through scheme where the broadcasting signals are transmitted to the subscriber's home without any changes in the signal format. Figure 4-1 shows an example of an optical access system for terrestrial and satellite broadcasting retransmission services that uses a typical pass-through scheme. In a head end (HE) building, satellite broadcasting signals are received by an antenna and down-converted to IF signals by a down-converter. After the down conversion, the IF signals are led to the inside by RF cables. The power of the IF signals are properly adjusted by RF amplifiers, and the IF signals are additionally converted to the lower frequencies depending on the system design. Terrestrial broadcasting signals are also received by the other antenna, and the power of the RF signals are adjusted by amplifiers. Then, the RF signals of terrestrial broadcasting and the IF signals of satellite broadcasting are multiplexed in a frequency domain. The SCM signals are input to an E/O such as directly modulated laser (DML). The analog signal waveform is directly converted to an optical intensity signal and then transmitted over a PON ODN to subscriber's home. After the transmission, the optical signal is converted to the original SCM signals by direct detection in an O/E such as PIN photodiode (PIN-PD). The terrestrial and satellite broadcasting signals are separated with each other by a demultiplexer (Demux). When the second down conversion is applied to the satellite broadcasting signals in the HE, the satellite signals should be up-converted in the subscriber home. Finally, both broadcasting signals are input to a television receiver.

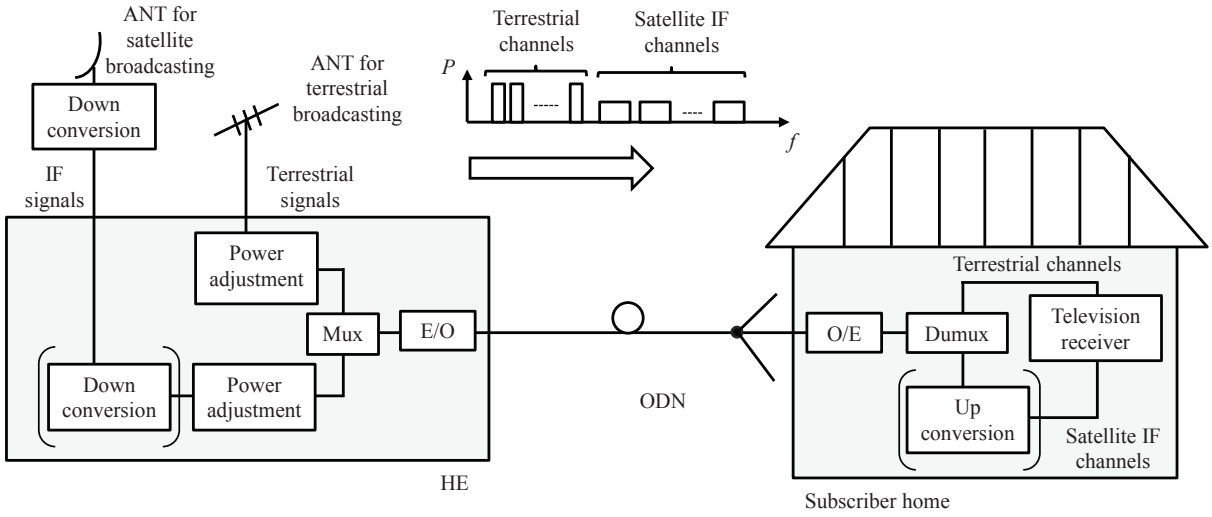

Fig. 4-1 An optical access system for broadcasting services.

4-2.2 Mobile communication systems

Recently, A-RoF has also attracted attention as a technology for accommodating mobile wireless BSs with a C-RAN configuration. A supplement document of ITU-T G. suppl. 55 [13] on summarized RoF technologies and their applications has been released. Additionally, in a standardization document of ITU-T G. 9803 [14], A-RoF-based MFH systems that mainly support 4G mobile systems have been described. Figure 4-2 depicts an example of an optical access system for C-RAN-based MFH. A-RoF technologies that have been widely used for CATV services are effectively applied to the optical transmission. In mobile applications, uplink transmission from an antenna site to a CO is also required. However, the uplink transmission basically takes the reverse process of the downlink, except for the RF power adjustment for obtaining better transmission performances. Therefore, in this chapter, only downlink transmission is described. In a conventional broadcasting system, the frequency of each RF signal is different from the others whereas, in a MFH system, the frequency of an RF signal will be the same as all of or some of the other signals for advanced wireless technologies such as MIMO and

beamforming [15]. Therefore, in a CO, the frequencies of the RF signals from a BBU should be converted to the others and multiplexed in a frequency domain. Depending on the system design, the functions will be included in the BBU equipment. The FDM signals drive an E/O, and the optical signal is transmitted over an IFoF link to an antenna site. In the antenna site, each of the IF signals that are output from an O/E is extracted and converted to the RF signal. Finally, the RF signals are emitted from antennas. The functions of frequency conversions, multiplexing, and demultiplexing that are needed in IFoF transmission can be implemented in digital signal processing. Additionally, the digital signal processing before and/or after optical transmission is expected to compensate the performance deteriorations due to chromatic dispersions and non-linearity from the optical transmission. These kinds of A-RoF technologies with DSP are also called DSP-assisted A-RoF [13]. It is noted that IFoF technologies are part of A-RoF technologies, and the difference is the frequencies of electric signals transmitted over a fiber, IF or RF.

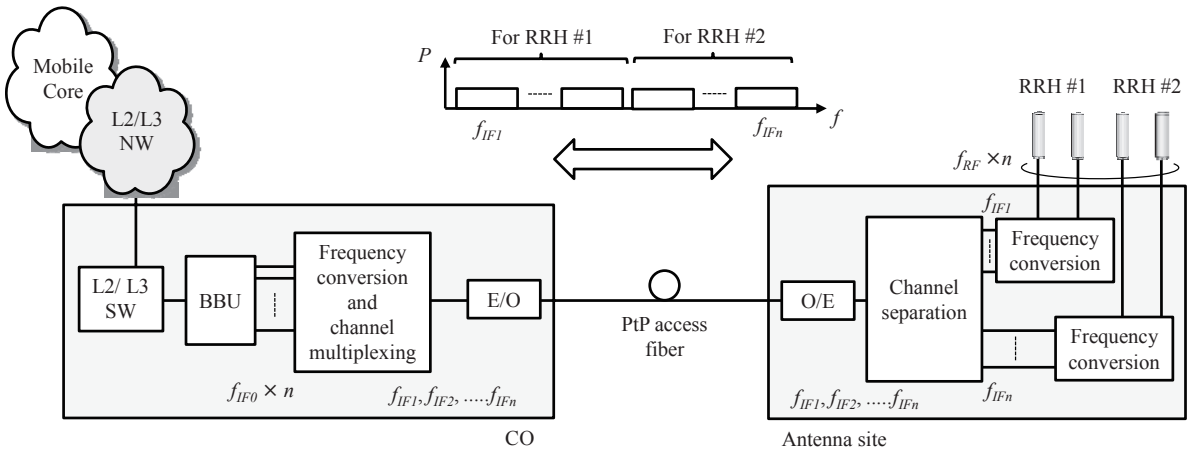

Fig. 4-2 Optical access system for mobile communication services.

As mentioned above, A-RoF transmission systems that have high spectral efficiencies are useful for C-RAN applications, in terms of reducing the required bandwidths in the optical components. However, in comparison with digital transmission technologies that have been widely used in commercial systems, A-ROF systems have some disadvantages. The first one is low optical power budget. In A-RoF transmission, analog RF signal waveforms are transmitted as it is. When an E/O device have a nonlinear characteristic, the transmitted electrical signal suffers some distortions. Therefore, in general, only a high-linearity region of optical devices can be used in analog transmission. In other word, the optical modulation index (OMI) becomes small. To achieve high optical transmission performances, the received optical power at an O/E device should be high. An erbium-doped fiber amplifier (EDFA) can be used for the purpose. However, it is obvious that the EDFA causes higher transmission costs. Optical access networks severely require cost-effective technologies, and the use of an EDFA for each optical link will not be desirable. The second disadvantage is a concern about signal deteriorations due to the beat noises caused by optical multiple reflections. In analog transmission, high signal-to-noise ratio (SNR) is required, in comparison with digital transmission schemes such as non-return to zero (NRZ) that is widely used in currently available PON systems. Therefore, the beat noise may not be negligible in analog transmission systems. When optical reflectivity on each link is strictly managed using optical connectors with low reflectivity such as angled physical contact (APC) connectors, the concern will be addressed. However, deployment and operation costs will increase.

In A-RoF systems for both terrestrial digital broadcasting signals by the pass-through scheme and mobile wireless signals, OFDM signals should be transmitted over a fiber. OFDM channel bandwidths of a broadcasting signal, a 4G wireless signal, a 5G wireless signal are 5.6 MHz, 20 MHz, and 100 MHz and more, respectively. There is large difference in a channel bandwidth between broadcasting systems and mobile systems. Therefore, larger performance deteriorations may be caused in the mobile applications. The concern should be investigated experimentally using commercial optical transmission lines.

4-3 Numerical calculations of IFoF-based mobile fronthaul links

In this section, the influence of optical transmission losses and multiple reflections on IFoF transmission performances is evaluated by numerical calculations, and the optical transmission conditions where IFoF technologies will be successfully applied are investigated. Additionally, in a specific MHF use case, the performances of some IFoF links are estimated [11].

4-3.1 Calculation conditions

Carrier-to-noise ratio (CNR) has been widely and commonly used in designing analog transmission systems such as commercially available terrestrial digital broadcasting. The value is an important factor that expresses the signal quality over analog optical links. In general, the CNR of an IF signal transmitted over an optical transmission line can be expressed as follows:

$$CNR = 10 \log_{10} \left[\frac{1}{B_N} \cdot \frac{\frac{1}{2} \cdot \left(m_k \cdot R \cdot P_r \right)^2}{RIN \times \left(R \cdot P_r \right)^2 + 2 \cdot e \cdot \left(I_{d0} + R \cdot P_r \right) + I_{eq}{}^2} \right] , \quad (4.1)$$

$$M = \sqrt{\sum_k m_k{}^2} . \quad (4.2)$$

Here, B_N is the noise bandwidth of an IF signal, m_k is the OMI for the k-th IF signal, M is the total OMI from all IF signals, R is the optical to electric conversion efficiency in an optical receiver element, P_r is the received optical power, and RIN is the relative intensity noise input to an optical receiver, e is the elementary charge, I_{d0} is the dark current in an optical receiver element, and I_{eq} is the input referred noise in an optical receiver. When long transmission and relay transmission with EDFAs are not assumed, RIN can be expressed as follows:

$$RIN = 10 \log_{10} \left\{ 10^{\frac{RIN_{LD}}{10}} + 10^{\frac{RIN_f}{10}} \right\} . \quad (4.3)$$

Here, RIN_{LD} is the relative intensity noise of a laser light source, and RIN_f is the relative intensity noise of the optical fiber transmission. For RIN_f, in this study, the following things are assumed: Two large optical reflection points exist, the influence of Rayleigh scattering is sufficiently small in comparison with optical multiple reflections, the relationship in polarization states between direct signal and multiple-reflection signal is same with each other where the beat noise level in the optical receiver becomes maximum. Additionally, the loss factor of an optical fiber is expressed by α. Considering this situation, RIN_f is expressed by

$$RIN_f(f) = \frac{4r^2}{\pi}\left[\frac{\Delta\nu}{f^2 + (\Delta\nu)^2}\right] \times \left\{\sin^2(\omega_0\tau)\cdot\left[1 + \exp(-4\pi\Delta\nu\tau) - 2\exp(-2\pi\Delta\nu\tau)\cdot\cos(2\pi f\tau)\right] + \cos^2(\omega_0\tau)\left[1 - \exp(-4\pi\Delta\nu\tau) - 2\exp(-2\pi\Delta\nu\tau)\cdot(\Delta\nu / f)\cdot\sin(2\pi f\tau)\right]\right\} \quad , (4.4)$$

$$r = \alpha\sqrt{r_1 r_2} \quad . \quad (4.3)$$

Here, r is the effective reflectance coefficient, Δv is the full width at half maximum (FWHM) of an LD, f is the frequency of a signal, and ω_0 is the center angular frequency of the light. τ is the delay difference between direct optical signal and multiple-reflection optical signal as shown in Figure 4-3. Actually, only one optical reflection point is not a serious issue because optical isolator can successfully suppress the reflected signal to a transmitter (Tx). However, the signals from multiple reflection points can not be suppressed in an Rx because the reflected signal has the same wavelength as the direct signal. τ is expressed by $2dn/c$ where d is the distance between two optical reflection points, n is the refractive index of an optical fiber, and c is the speed of light.

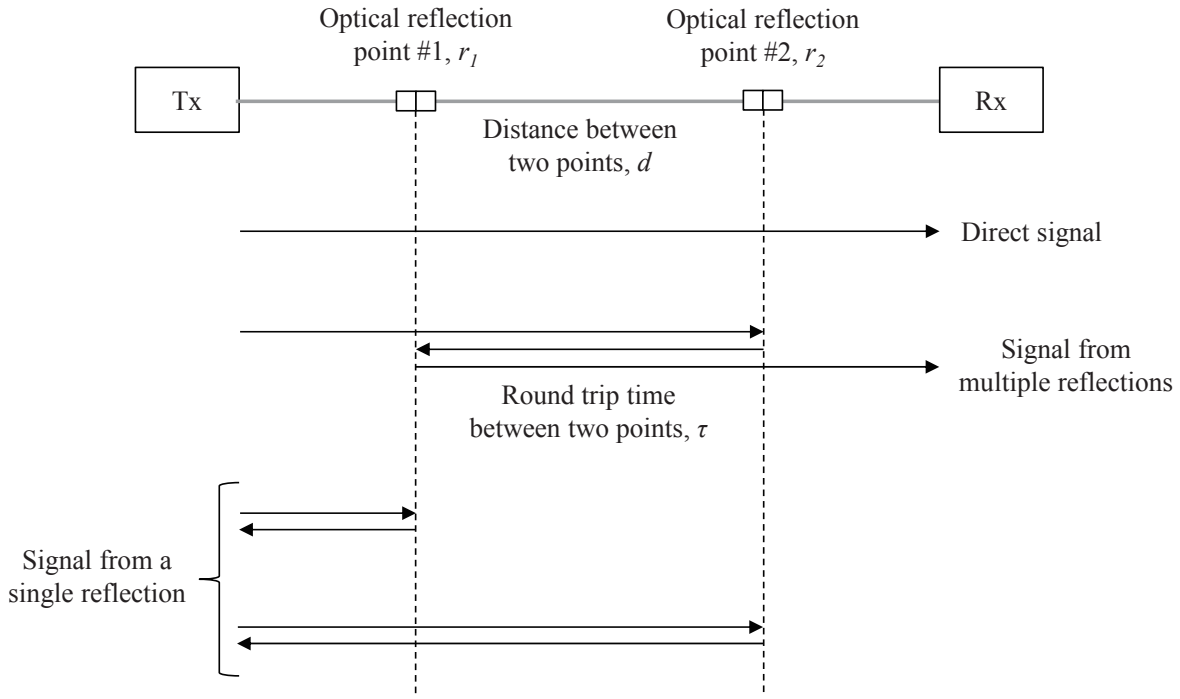

Fig. 4-3 Schematic diagram of multiple reflections on an optical link.

As indicated in Section 4-2.2, the bandwidth of each channel for mobile applications is wider than that for broadcasting applications. Therefore, using each parameter value shown in Table 4-1, CNR values of optical transmission are firstly calculated when noise bandwidth of B_N and signal bandwidth are changed to 5.6 MHz, 20 MHz and 100 MHz. The number of transmitted IF channels is 54. That is because when a 100-MHz channel bandwidth for 5G mobile systems and a 3.75-bit/s/Hz spectral efficiency that is equivalent to available LTE systems are assumed, the 20-Gbit/s user data rate that is one of the requirements in 5G systems can be achieved by 54 channels. The OMI of the f-th IF signal, m_k, is set to 3%/Ch where the total OMI, M, becomes 22%.

Table 4-1 Parameters and the values in CNR performance calculations.

Parameter	Value	Paremeter	Value
B_N	5.6 to 100.0 $\times 10^6$ Hz	α	0.3 dB/km
m_k	3 %/Ch	r_1, r_2	-25, -15 dB
e	1.602×10^{-19} C	Δv	5 MHz
R	0.8 A/W	f	0 to 1000 MHz
P_r	-20 to 0 dBm	d	200 m
I_{d0}	1 nA	n	1.465
I_{eq}	15 pA/√ Hz	c	299792458 m/s
RIN_{LD}	-155 dB/Hz	-	-

Next, CNR values of optical transmission are calculated when two large optical reflection points exist on an optical transmission line and also noise bandwidth of B_N and signal bandwidth are changed to 5.6 MHz, 20 MHz and 100 MHz. The OMI of the k-th IF signal, m_k, is set to 3%/Ch where the total OMI, M, becomes 22%. The received optical power of P_r is set to 0 dBm in order to reduce the influence of the noise from the small received power. The distance between two optical reflection points of d are set to 200 m that is longer than the coherence length. Additionally, the polarization of a direct signal is the same as that of the multiple-reflection signal.

Finally, CNR values of optical transmission are calculated in a specific use case where 24 IF channels are transmitted over a fiber which corresponds to three sectors, 2×2 MIMO, four frequencies in an antenna site. Table 4-2 shows parameters and the values used in the calculations. In conventional analog transmission, the total OMI of M is commonly set to less than 30% to avoid optical modulation distortions due to the high RF power to an E/O. Therefore, in this calculation, the OMI of the k-th IF signal of m_k is set to 3 to 6 %/Ch and, as a result, the total OMI of M becomes 15 to 30%.

Table 4-2 Parameters and the values in CNR performance calculations in a specific use case.

Parameter	Value	Paremeter	Value
B_N	20×10^6 Hz	α	0.3 dB/km
m_k	3 to 6 %/Ch	r_1, r_2	-25, -15 dB
e	1.602×10^{-19} C	Δv	5 MHz
R	0.8 A/W	f	0 to 1000 MHz
P_r	-20 to 0 dBm	d	200 m
I_{d0}	1 nA	n	1.465
I_{eq}	15 pA/√ Hz	c	299792458 m/s
RIN_{LD}	-155 dB/Hz	-	-

4-3.2 Results and Discussion

Figure 4-4 shows calculated CNR values as a function of the received optical power when the noise bandwidth is changed. In this calculation, the influence of multiple optical reflections on CNR values is ignored. The CNR deteriorates due to the increase of the signal bandwidth. When a channel bandwidth is set to 5.6 MHz, 20 MHz, and 100 MHz, the received optical power of more than -15.7 dBm, -12.9 dBm, and -9.2 dBm are required, respectively, in order to achieve a CNR value of 22 dB that is a requirement in 64-QAM LTE signals [16]. It is confirmed that the CNR criterion can be achieved when the optical received power is properly adjusted for each application. Successful IFoF transmission for 5G and beyond 5G mobile systems are also expected.

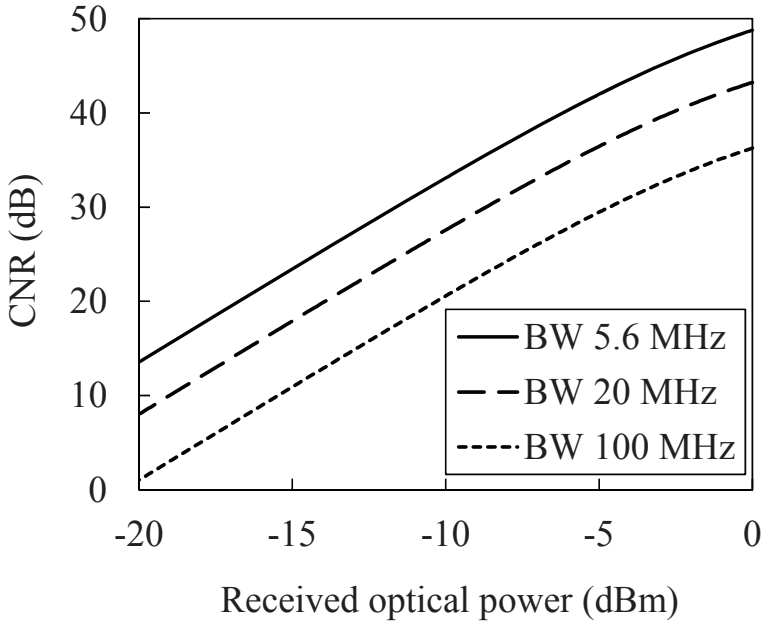

Fig. 4-4 CNR performances as a function of the received optical power after optical transmission.

Figures 4-5(a) and 4-5(b) show the CNR characteristics when the optical reflectivity is set to -25 dB and -15 dB, respectively. The reflectivity of r_1 is the same as that of r_2. In the numerical calculations, the center frequency of the evaluated IF signal is changed from 50 to 950 MHz. From Figure 4-5(a), it is found that all of the IFs can satisfy a CNR criterion of 22 dB when IF channel bandwidth becomes 5.6 MHz and 20 MHz. Additionally, IFs of more than 69 MHz can meet the CNR criterion even when IF channel bandwidth is set to 100 MHz. Common PC-polished optical connecters with a reflectivity of about -25 dB, that have been used for digital transmission systems, are also expected to be used in the IFoF transmission. From Figure 4-5(b), it is confirmed that, in all of the channel bandwidths, the CNR criterion can not be satisfied when IF signals are allocated to lower frequency ranges. However, in channel bandwidths of 5.6 MHz, 20 MHz, and 100 MHz, the CNR criterion can be satisfied when center frequencies of IF signals are assigned to more than 111 MHz, 210 MHz, and 479 MHz, respectively. Also in 5G and beyond 5G mobile communication systems, when the frequencies of IF signals are properly

allocated, the CNR criterion is expected to be satisfied. From the calculation results in Figures 4-4 and 4-5, IFoF technologies are expected to be applicable to 5G and future mobile systems, when IF frequencies and optical transmission lengths are selected in the condition where the influence of chromatic dispersion from optical transmission is negligible.

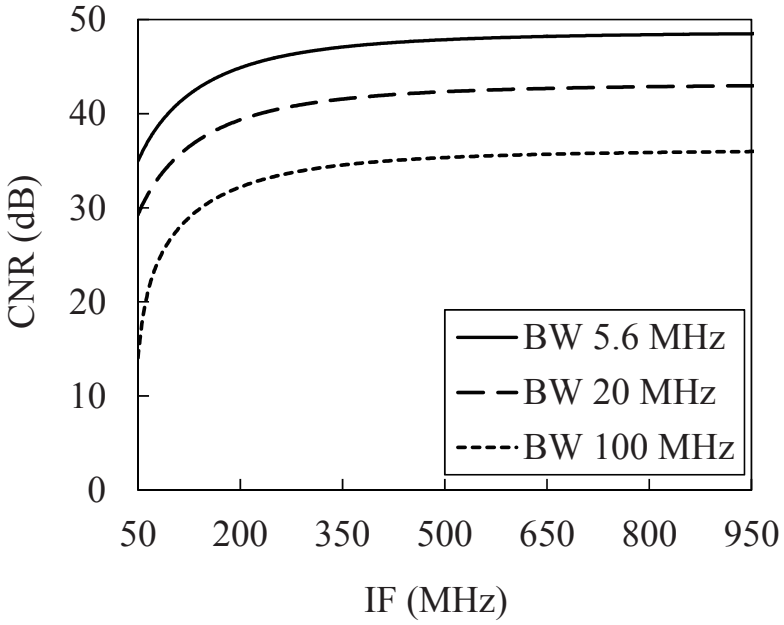

(a)

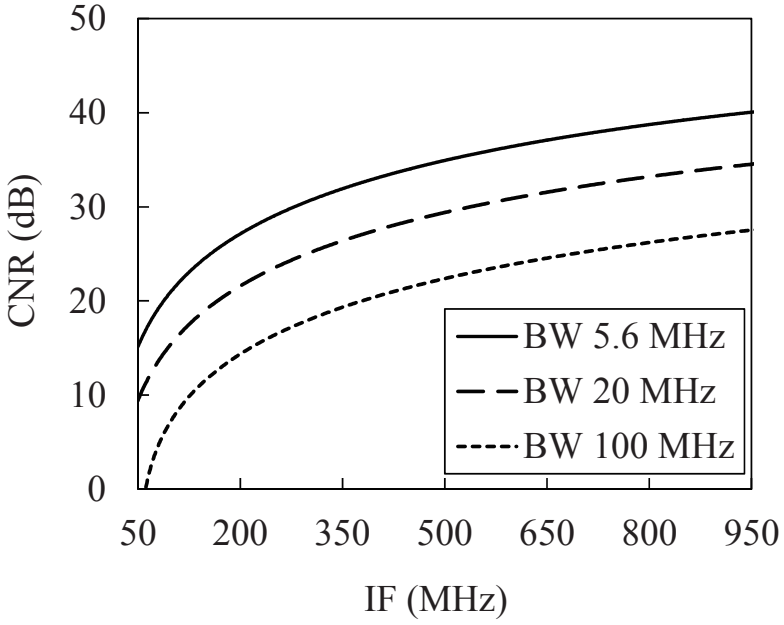

(b)

Fig. 4-5 CNR performance deterioration due to optical multiple reflections (a) with reflectivity of -25 dB and (b) with reflectivity of -15 dB.

Figure 4-6 depicts CNR characteristics as a function of received optical power when a specific use case shown in Section 4-3.1 is assumed. In the RIN_f, the element of optical multiple reflections is ignored, to confirm the influence of the almost pure received optical power. In each OMI case, the degradation of the CNR can be found when the received optical power decreases. However, the CNR criterion of 22 dB from 64-QAM LTE signals can be met when the OMI of m_k and the received optical power of P_r are set to 4%/Ch and -14.1 dBm, respectively. Regarding the estimation on the influence of optical multiple reflections, it is assumed that the reflectivity of r_1 is the same as that of r_2, and the polarization state between direct signal and multiple-reflection signal is same with each other. In addition, in Table 4-2, m_k of 4%/Ch, P_r of -7.0 dBm, and a center frequency of an IF channel of 50 MHz are assumed. In such conditions, the CNR values become 30.3 dB, 21.7 dB, and 11.9 dB when the optical reflectivity is set to -25 dB, -20 dB, and

-15 dB, respectively. From these calculation results, even when there exist two optical reflection points with -25-dB reflectivity, it is expected that 24 64-QAM LTE signals can be transmitted over an IFoF link. Actual transmission experiments based on this study are presented in Section 4-4. Though, EVM performance is discussed in Section 4-4, EVM can be translated into CNR by an equation [17] of

$$EVM = \frac{1}{\sqrt{CNR}} \quad . \tag{4.4}$$

Therefore, the CNR criterion of 22 dB for 64-QAM signals corresponds to EVM of 8%. The equation above will work well when the total OMI of *M* is less than 30%.

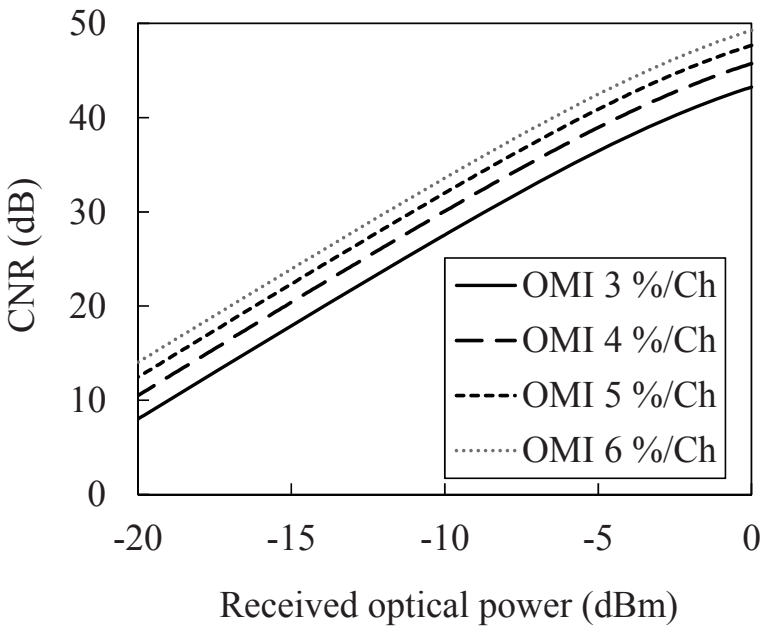

Fig. 4-6 CNR performances as a function of received optical power when 24 IF channels are transmitted over a fiber.

4-4 Transmission experiment of LTE signal over deployed fiber

In this section, IFoF transmission experiments for multiple LTE signals using commercial LTE BS and deployed fibers are conducted. As a result, the applicability of A-RoF technologies to commercially available systems are shown [11].

4-4.1 Experimental setup

Figure 4-7 shows an experimental setup for IFoF transmission using commercial LTE BS and deployed fibers. To generate an LTE signal with a 20-MHz channel bandwidth that is specified in the 3rd generation partnership project (3GPP), BBU and RRH of a commercial LTE BS were directly connected with each other. A smartphone was used for UE, and the RF signal ware transmitted between the RRH and the UE through the air. Files were continuously downloaded between the EPC and the smartphone by FTP, and, during this experiments, the LTE RF signal was continuously output by the RRH. The modulation format of the LTE signal depends on the transmission condition. In the experiment, thanks to the short air transmission, a 64-QAM LTE signal with a 20-MHz channel bandwidth was able to be output from the RRH. The RRH had two antenna ports for the dual polarization. One was directly connected to an antenna. The other output was split into two signals, and one of the split signal was used for the IFoF transmission whereas the other split signal was connected to another antenna. The LTE RF signal was converted to the required IF signal by a mixer and a local oscillator (LO). To emulate multiple LTE signals, 23 dummy 64-QAM LTE signals with a 20-MHz channel bandwidth were generated by an arbitrary waveform generator (AWG). The LTE IF signal and these dummy signals were multiplexed in a frequency domain, and the frequency division multiplexing (FDM) signals were input to a distributed feedback laser diode (DFB-LD) for the direct modulation. The center frequency of the LTE IF signal was set to the lowest frequency of 50 MHz, the middle frequency of 380 MHz, or the highest frequency of 740 MHz in turn. The center frequency intervals between adjacent IF channels were set to 30 MHz. The total bandwidth of the FDM signals corresponded to the bandwidth that is required from the BS configuration where three

sectors, four frequencies, and 2×2 MIMO are assumed. The wavelength and output power of the DFB-LD were 1552 nm and +5.1 dBm, respectively. The total OMI to the directly modulated DFB-LD was about 19% with 24 IF channels where each OMI by an IF channel was about 4%/Ch. The optical link consisted of deployed access fibers with a 7.4-km length in total and indoor fibers with a 0.4-km length in total. A kind of a loop-back access fiber via a CO was configured by connecting two deployed access fibers. In the CO, multiple optical connectors seemed to exist. After transmission, the optical signal was converted to the electric FDM signals by a PIN-PD. Then, the analog electric signal was digitized by a spectrum analyzer (SA), and the constellation and EVM performances for the real LTE signal were measured by a vector signal analyzer (VSA).

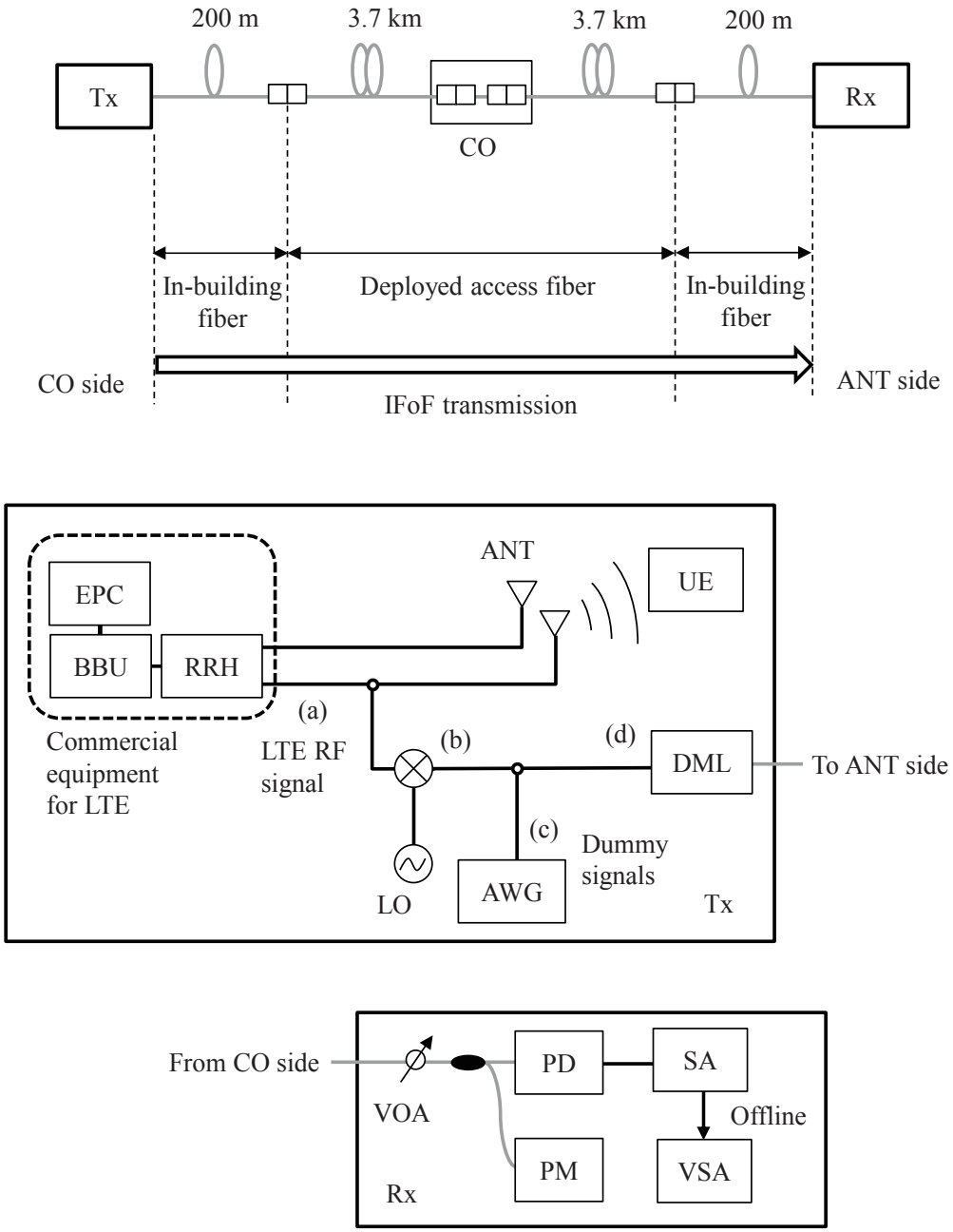

Fig. 4-7 Experimental setup for a field trial of an IFoF transmission system.

4-4.2 Results and Discussion

Figure 4-8(a) shows the RF spectrum of the LTE signal that was output from the RRH. The frequency and bandwidth were measured to be 2.12 GHz and 20 MHz, respectively. The CNR performance is found to be more than 40 dB from the RF spectrum. Figure 4-8(b) presents the RF spectrum of the LTE signal from the RRH that was down-converted to 380 MHz. From the spectrum, the CNR are still more than 40 dB. Figure 4-8(c) depicts the RF spectrum of 23 dummy IF signals that were generated by an AWG. In this figure, the center frequencies of the dummy signals were adjusted to 50 MHz to 740 MHz at 30-MHz intervals between adjacent IF channels, except for the center frequency of 380 MHz that was reserved for the LTE signal. The RF power for the LTE band was successfully suppressed. Finally, Figure 4-8(d) describes the RF spectrum of the FDM signals that consisted of the real LTE signal and 23 dummy signals before being input to the directly modulated DFB-LD. The real LTE signal was found to be successfully multiplexed to the dummy signals in a frequency domain.

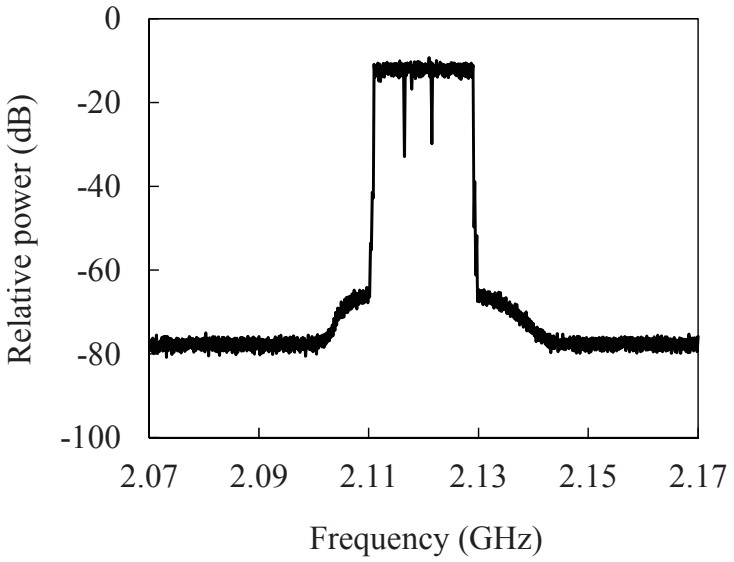

(a)

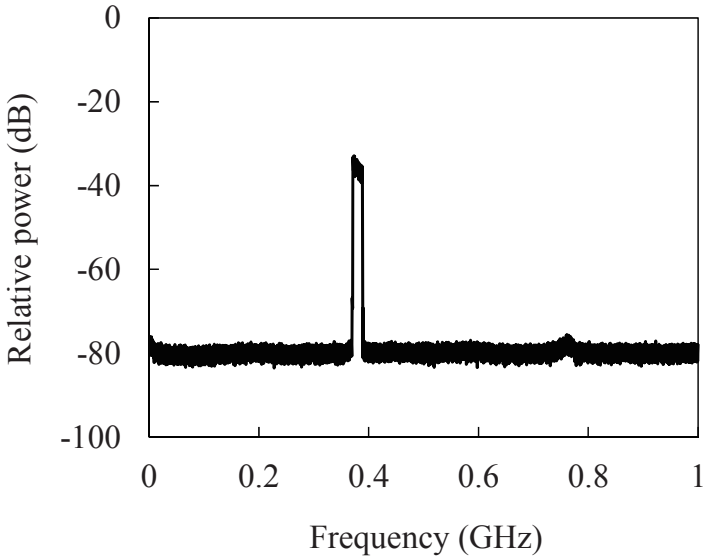
0
-20
-40
-60
-80
-100
Relative power (dB)
0
0.2
0.4
0.6
0.8
1
Frequency (GHz)

(b)

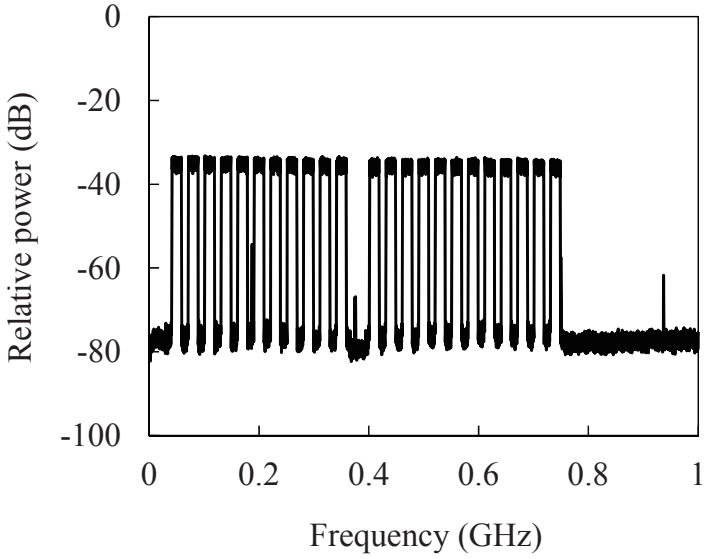
0
-20
-40
-60
-80
-100
Relative power (dB)
0
0.2
0.4
0.6
0.8
1
Frequency (GHz)

(c)

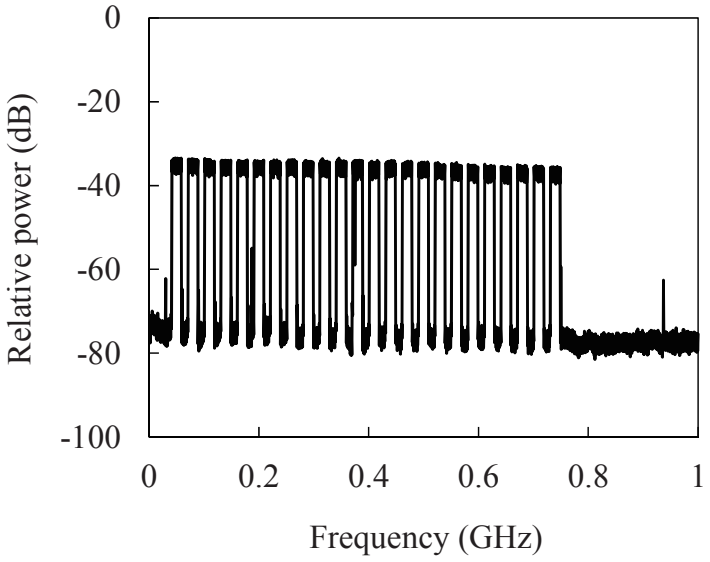

(d)

Fig. 4-8　Measured RF spectra (a) after the RRH output, (b) after the frequency conversion, (c) after the AWG output, and (d) before the input to the DFB-LD.

Figure 4-9 shows measured transmission fiber characteristics by an optical time-domain reflector (OTDR), for both the deployed fibers in this field trial and 10-km experimental SMF as a reference. In the deployed fibers, optical reflection points with large reflectivity of -27.9dB and -21.5 dB were found at the transmission distance of 3.68 km and 3.91 km, respectively. Such high reflectivity is considered due to the optical connection points in the CO. The total optical transmission losses from the 7.8-km deployed fibers were measured to be 10.3 dB. This loss value is too large, in comparison with the estimated loss by the propagation loss of a common experimental SMF of 0.2 dB/km. On the other hand, in the experimental 10-km SMF, no reflection points with large reflectivity were found, and the optical transmission loss was only 1.8 dB which was good as expected.

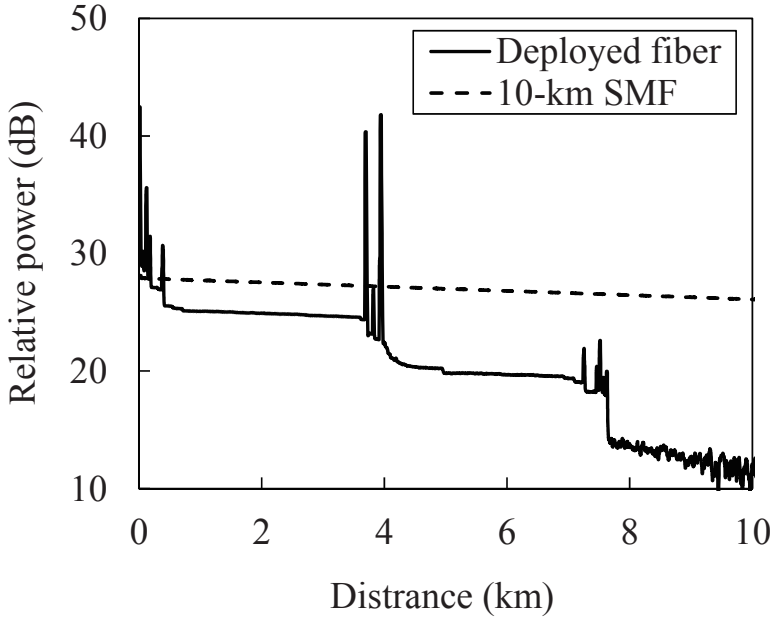

Fig. 4-9 An OTDR measurement result for a field fiber.

Figures 4-10(a) and 4-10(b) describe the RF spectra of 24 LTE signals when the received optical power at the PIN-PD after the IFoF transmission was set to -7 dBm and -15 dBm, respectively. When the received optical power became low, it is obvious that the carrier power decreased and the CNR was limited by the influence of the thermal noise of the receiver. However, when the received optical power was increased to -7 dBm, the carrier power was clearly increased and the shot noise also seemed to affect the CNR performances.

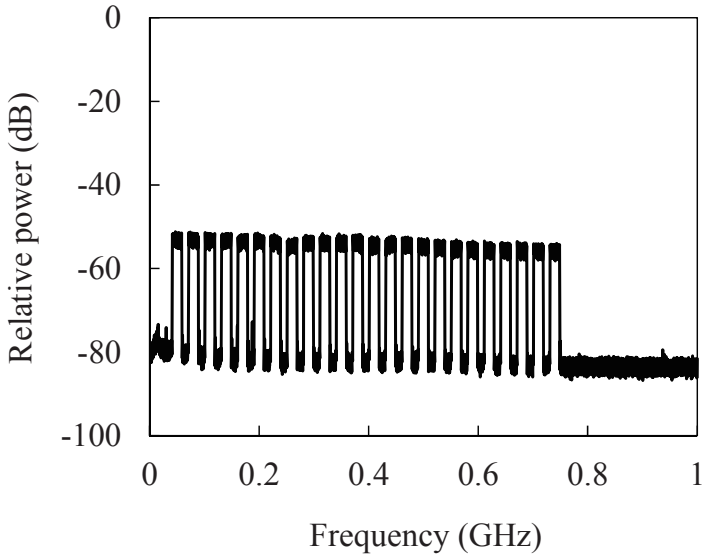

(a)

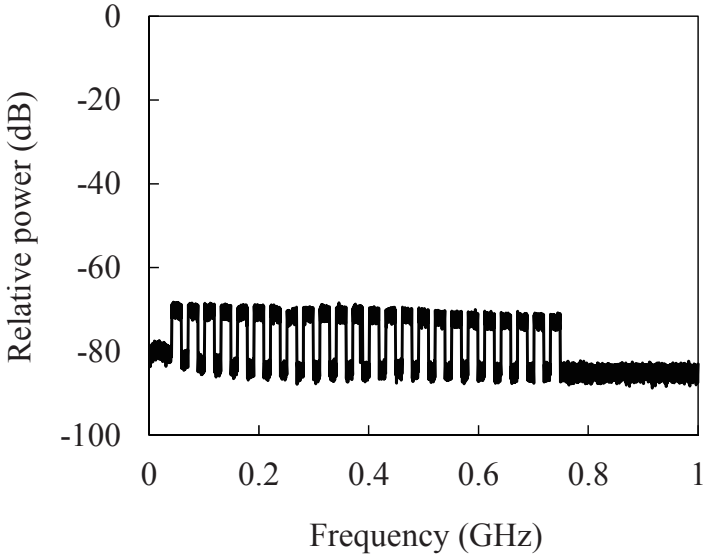

(b)

Fig. 4-10 Measured RF spectra after the IFoF transmission when the received optical power at the PD of (a) -7 dBm and (b) -15 dBm.

Figure 4-11(a) plots the measured EVM performances of a real LTE signal as a function of the received optical power after the IFoF transmission. The center frequency of the LTE IF signal was set to 50 MHz, 380 MHz and 740 MHz in turn. The EVM performances were improved independent of the center frequency of the LTE signal when the received optical power was increased. Additionally, the EVM values for the center IF of 50 MHz were worse than those for the other center IFs. For example, when the received optical power was set to -11 dBm, the EVM performance was 8.6% for the center IF of 740 MHz whereas the EVM value was 11.2% for the center IF of 50 MHz. A relatively high thermal noise was observed in the lower frequency range when the noise spectrum of the receiver was measured. Therefore, this is one of the reason why high EVM values were found in the center IF of 50 MHz. From the numerical calculations in Section 4-3.2, CNR values of more than 30 dB which is equivalent to EVM values of less than 3% were expected in the received optical power of -7 dBm, even when there existed two optical reflection points with reflectivity of -25 dB. However, the measured EVM values were worse than the calculated values. This situation was mainly due to the large EVM performance of the original LTE signal from the RRH in which EVM was specified to be less than 8%.

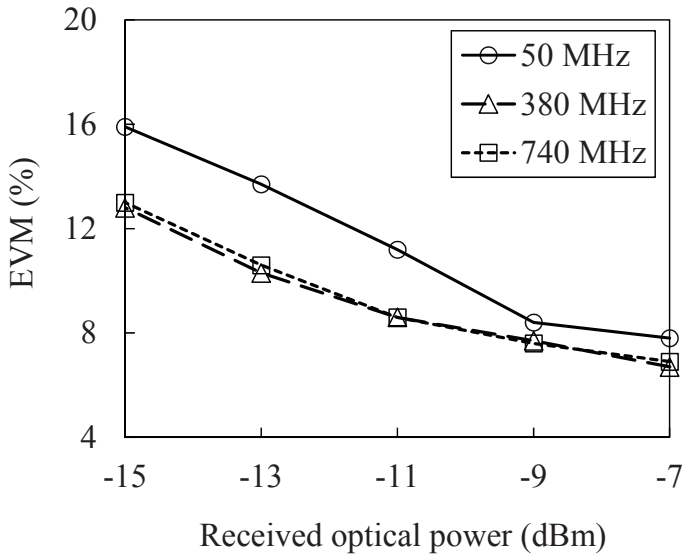

(a)

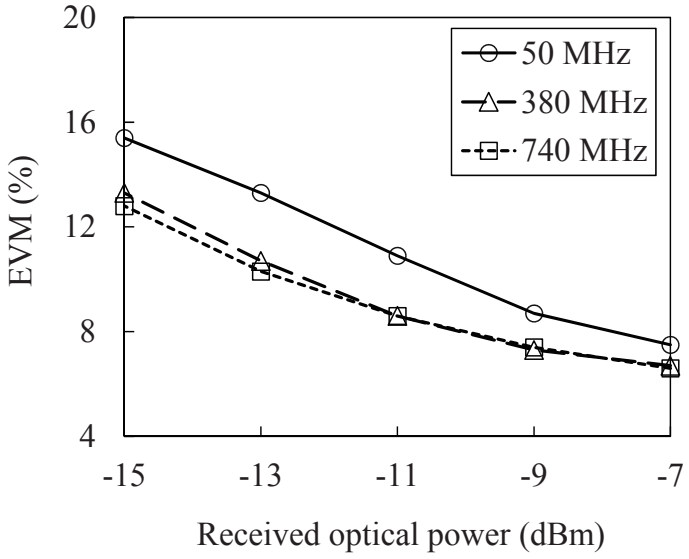

(b)

Fig. 4-11 Measured EVM performances of the LTE signal as a function of received optical power (a) using a 7.8-km deployed fiber and (b) using a 10-km SMF.

Figure 4-12 presents the constellation maps of the LTE signal after the IFoF transmission for various conditions: (a) IF of 50 MHz, (b) IF of 380 MHz, (c) IF of 740 MHz, and received optical power at the PIN-PD of -7 dBm for each case, and (d) IF of 740 MHz and received optical power of -15 dBm. Also from these results, when the center frequency of the IF signal was set to 50 MHz, larger influence of the noise was found than in the higher frequencies.

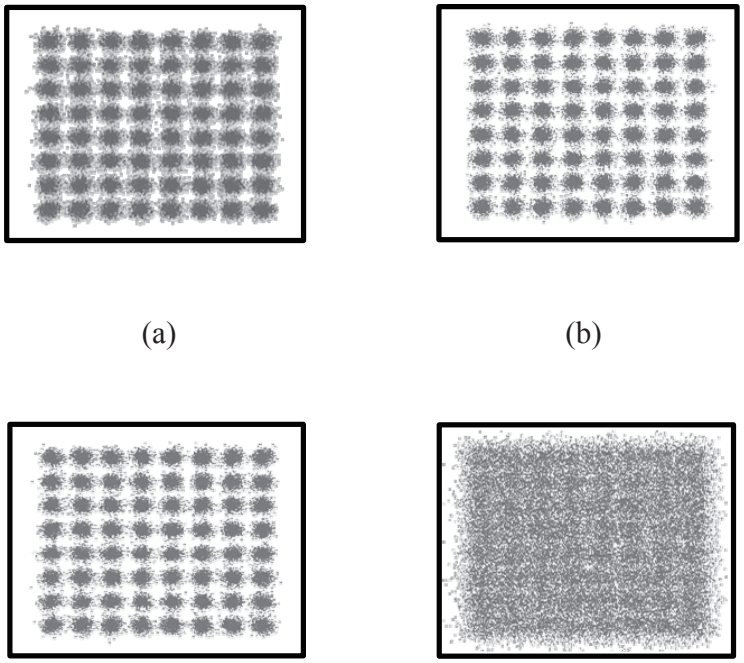

Fig. 4-12 Measured constellation diagrams after the IFoF transmission (a) for the center frequency of the LTE signal of 50 MHz and the received optical power of -7 dBm, (b) for the center frequency of the LTE signal of 380 MHz and the received optical power of -7 dBm, (c) for the center frequency of the LTE signal of 740 MHz and the received optical power of -7 dBm, and (d) for the center frequency of the LTE signal of 740 MHz and the received optical power of -15 dBm.

A relatively high EVM deterioration was observed in the lowest frequency in Figure 4-11(a). However, the EVM criterion for 64-QAM signals of 8% [18] was satisfied independent of the center frequency of the LTE signal when the received optical power was set to -7dBm. It was also confirmed, in the comparison of Figure 4-11(a) and Figure 4-11(b), that there was no significant difference in EVM values between after the deployed fiber transmission and after the experimental 10-km SMF transmission. From all of the experimental results in this section, it was clarified that the A-RoF technologies for C-RAN MFH applications can be actually applied to 4G commercial systems when the transmission conditions such as transmission loss are properly adjusted. Additionally, the A-RoF technologies are expected to be enhanced for the future MFH applications.

4-5 Conclusion

A-RoF technologies for MFH systems were explained, in comparison with commercial broadcasting systems for CATV services. In the mobile applications of A-RoF technologies, multiple filters and frequency converters were shown to be needed in a remote site to support MIMO and/or multiple RRHs. In addition, the channel bandwidth of an analog signal was described to be 20 MHz for 4G LTE services and 100 MHz and more for 5G services whereas that was 5.6 MHz for terrestrial broadcasting services.

CNR performances of IFoF transmission systems were also studied by numerical calculations in various signal and transmission conditions. When OMI per channel and the number of IF channels transmitted over an IFoF link were set to 3% and 54, respectively, allowable received optical powers were -15.7 dBm, -12.9 dBm, and -9.2 dBm for channel bandwidths of 5.6 MHz, 20 MHz, and 100 MHz, respectively. This result showed that wideband IF signals for 5G and future mobile systems can be also transmitted over an IFoF link by adjusting the received optical power optimally. Additionally, the influence of multiple optical reflections on the CNR performances were calculated. When two optical reflection points with reflectivity of -15dB per point existed, minimum allowable center frequencies were 111 MHz, 210 MHz, and 479 MHz for channel bandwidths of 5.6 MHz, 20 MHz, and 100 MHz,

respectively. From this result, CNR criteria not only for 4G mobile applications but also for 5G are expected to be achieved by adjusting the IF channel allocation properly.

IFoF transmission experiments were conducted using a commercial LTE BS and deployed fibers. A 64-QAM LTE signal with a 20-MHz channel bandwidth from an LTE BS and 23 dummy IF signals with 20-MHz channel bandwidths from an AWG were subcarrier multiplexed and then converted to the optical signal by a DML The optical signal was transmitted over an optical fiber link that consisted of 0.4-km in-building fiber and 7.4-km access fiber with two large optical reflection points of -27.9 dB and -21.5 dB. After the IFoF transmission, the EVM values for the LTE signal allocated to the lowest, middle, or highest frequency among IF channels were measured to be less than 8%, a criterion for 64-QAM signal, by setting the transmission conditions properly. The applicability of IFoF technologies to 4G LTE systems were experimentally demonstrated for the first time.

References

[1] K. Tanaka and A. Agata, "Next-Generation Optical Access Networks for C-RAN," in *Proc. Optical Fiber Communication Conference (OFC)*, Tu2E.1, Los Angeles, CA, Mar. 2015.

[2] X. Liu, F. Effenberger, N. Chand, L. Zhou, and H. Lin, "Demonstration of Bandwidth-Efficient Mobile Fronthaul Enabling Seamless Aggregation of 36 E-UTRA-Like Wireless Signals in a Single 1.1-GHz Wavelength Channel," in *Proc. Optical Fiber Communication Conference (OFC)*, M2J.2, Los Angeles, CA, Mar. 2015.

[3] C. Ye, K. Zhang, Q. Chang, Z. Gao, X. Hu, X. Huang, and X. Sun, "A DSP-assisted symbol-cascade mobile fronthaul solution with large capacity and neat RRHs," in *Proc. European Conference on Optical Communication (ECOC)*, We.4.4.2, Valencia, Spain, Sept. 2015.

[4] X. Liu, H. Zeng, N. Chand, and F. Effenberger, "Experimental Demonstration of High-Throughput Low-Latency Mobile Fronthaul Supporting 48 20-MHz LTE Signals with 59-Gb/s CPRI-Equivalent Rate and 2-ms Processing Latency," in *Proc. European Conference on Optical Communication (ECOC)*, We.4.4.3, Valencia, Spain, Sept. 2015.

[5] C. Han, S. H. Cho, H. S. Chung, and J. H. Lee, "Linearity improvement of directly-modulated multi-IF-over-fibre LTE-A mobile fronthaul link using shunt diode predistorter," in *Proc. European Conference on Optical Communication (ECOC)*, We.4.4.4, Valencia, Spain, Sept. 2015.

[6] C. Han, M. Sung, S. H. Cho, H. S. Chung, S. M. Kim, and J. H. Lee, "Impact of Dispersion-Induced Second-Order Distortion in Multi-IFoF-based Mobile Fronthaul Link for C-RAN," in *Proc. Optical Fiber Communication Conference (OFC)*, TU2B.4, Anaheim, CA, Mar. 2016.

[7] M. Befekadu, S. Straullu, S. Abrate, and R. Gaudino, "Experimental Optimization of DSP-Aggregated Front-hauling Transmission for up to 4x96 LTE radio waveforms," in *Proc. European Conference on Optical Communication (ECOC)*, W.4.P1.SC7.73, Düsseldorf, Germany, Sept. 2016.

[8] F. Lu, M. Xu. L. Cheng, J. Wang, S. Shen, J. Zhang, and G. K. Chang, "Sub-Band Pre-Distortion for PAPR Reduction in Spectral Efficient 5G Mobile Fronthaul," *IEEE*

Photon. Technol. Lett., vol. 29, no. 1, pp. 122-125, 2017.

[9] B. G. Kim, S. H. Bae, H. Kim, and Y. C. Chung, "DSP-based CSO cancellation technique for RoF transmission system implemented by using directly modulated laser," *Optics Express*, vol. 25, no. 11, pp. 12152-12160, 2017.

[10] B. G. Kim, S. R. Bae, R. Kim, and Y. C. Chung, "Mobile fronthaul optical link for LTE-A system using directly-modulated 1.5-μm VCSEL," in *Proc. Optoelectronics and Communications Conference (OECC)*, TuA2-3, Niigata, Japan, July 2016.

[11] K. Tanaka, B. G. Kim, T. Kobayashi, A. Bekkali, S. Nanba, K. Nishimura, H. Kim, Y. C. Chung, and M. Suzuki, "Transmission of Multiple Mobile Wireless Signals by IF-over-Fiber Technique," *IEICE Trans. Electron.*, vol. J101-C, no. 2, pp. 107-118, 2018.

[12] T. Kuri, Y. Horiuchi, T. Nakatogawa, and K. Tsukamoto, "Communication and Broadcasting Systems with Microwave and Millimeter-Wave Photonics Technologies," *IEICE Trans. Electron.*, vol. J91-C, no. 1, pp. 11-27, 2008.

[13] ITU-T G-series Reccommendations - Supplement 55, "Radio-over-fibre (RoF) technologies and their applications," 2015.

[14] ITU-T Reccomendation ITU-T G.9803 (2018) - Amendment 1, "Radio over fibre systems Amendment 1," 2019.

[15] M. Agiwal, A. Roy, and N. Saxena, "Next generation 5G wireless networks: A comprehensive survey," *IEEE Communications Surveys and Tutorials*, vol. 18, no. 3, pp. 1617–1655, 2016.

[16] B. G. Kim, H. Kim, and Y. C. Chung, "Impact of Multipath Interference on the Performance of RoF-Based Mobile Fronthaul Network Implemented by Using DML," *IEEE J. Lightwave Technol.*, vol. 35, no. 2, pp. 145-151, 2017.

[17] R. Shafix, S. Rahman, and R. Islam, "On the extended relationship among EVM, BER and SNR as performance metrics," in *Proc. Int. Conf. Electr. Comput. Eng.*, pp. 408-411, Dhaka, Bangladesh, Dec. 2006.

[18] 3GPP TS 36.104 v12.5.0 Release 12, "Technical Specification Group Radio Access Network; Evolved Universal Terrestrial Radio Access (E-UTRA); Base Station (BS) radio transmission and reception," 2014.

Chapter 5

Cascaded IFoF systems with hybrid signal processing

5-1 Introduction

As mentioned in Chapter 2 and Chapter 4, IFoF technologies to address the CPRI large-capacity issue have been actively studied. The technologies to solve the influence of RF power fading [1]-[3], distortions from optical transmission and transmission components [3]-[5], and optical multiple reflections [6] have been studied. Regarding the IF channel filters and frequency converters in antenna sites, experimental demonstrations by analog signal processing [7] and digital signal processing [8], [9] have been reported. However, real-time DSP that can sufficiently supports 5G MFH applications have not been experimentally demonstrated. In such applications, a channel bandwidth of 400 MHz and more, multi-user MIMO, and CA signals should be considered. Additionally, to address the restrictions of deployment space and power in antenna sites and the shortage of available access fibers, technologies to simplify the equipment placed in antenna sites and to reduce the number of the used fibers have been studied. The use of DSP will simplify the equipment placed in antenna sites in the future. Various systems based on PtMP architectures such as WDM ring [10], WDM-PON [11], and SCM-PON [12] have been also proposed for reducing access fibers. However, in each system, one or several disadvantages exist, as described in Chapter 1. Therefore, cascaded IFoF systems with analog and digital hybrid signal processing was proposed as a new kind of analog transmission system that is suitable for mobile applications [13].

In this chapter, the potential of cascaded IFoF systems with hybrid signal processing for future MFH is studied and confirmed. Firstly, the concept of the cascaded IFoF system targeting 5G mobile systems is presented in detail. An SCM-PON-based MFH system is also introduced as another PtMP MFH architecture. Then, the cascaded IFoF system is compared with SCM-PON system from the viewpoints of the bandwidths required in optical components, focusing on the

downlink transmission. Next, two kinds of real-time FPGA that are newly developed for digital filtering and frequency conversion in antenna sites of the cascaded IFoF system are described in detail: One is for an output of a single RF stream, whereas the other is for simultaneous outputs of plural RF streams. Finally, the cascaded IFoF systems with over 20-Gbit/s user data rates that use the first FPGA and the second FPGA are experimentally demonstrated for MFH with high spectral efficiency and MFH that is suitable for 5G, respectively.

5-2 Concept of cascaded IFoF systems with analog and digital signal processing

In this section, a cascaded IFoF systems with analog and digital hybrid signal processing is explained in detail [14]. In the future mobile systems that use higher frequencies, much more antennas will be required because higher frequencies have high directivity. To expand the service areas smoothly, simplifying the equipment placed in antenna sites and reducing the number of required access fibers will be important. Figure 5-1(a) shows a proposed MFH system for such a purpose. The system is introduced focusing on the downlink because the uplink process can be the almost reverse process of the downlink. Almost all of the functions of a BS are placed and centralized in a CO. Multiple IF signals for plural antenna sites are generated and subcarrier multiplexed. Figure 5-1(b) describes an example of the IF signal allocation. In the figure, the number of RF streams for each antenna site and that of antenna sites are expressed by M and N, respectively. A set of M IF signals for each antenna site is assigned to a continuous band. The SCM signals are converted to the optical signal by a broadband E/O, and the optical signal is transmitted over a broadband IFoF link to a relay site.

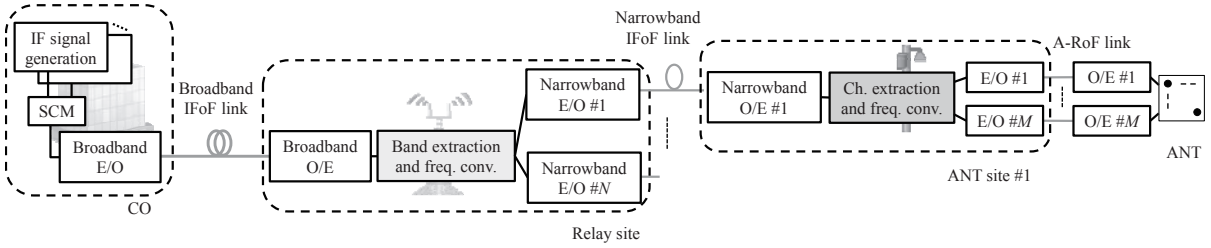

(a)

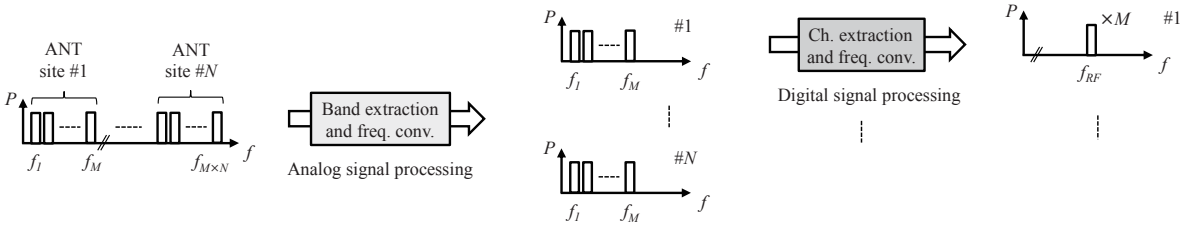

(b)

Fig. 5-1 Cascaded IFoF links for a MFH system: (a) network architecture and main functional blocks and (b) IF channel allocations and frequency conversions applied in relay and antenna sites.

Figure 5-2(a) illustrates the total bandwidth of $M\times N$ IF signals. The start frequency, the bandwidth of an IF channel, the band gap between IF channels in an antenna site, the band gap between IF channels for two antenna sites are expressed by B_0, B_{IF}, B_{GC}, and B_{GB}, respectively. When the total bandwidth is sufficiently narrow, a DML will be used for the broadband E/O. If a DML is difficult to be used, an external modulator will be required. The maximum transmission length of the broadband IFoF link will be 20 km, following conventional optical access systems and CPRI-based MFH links.

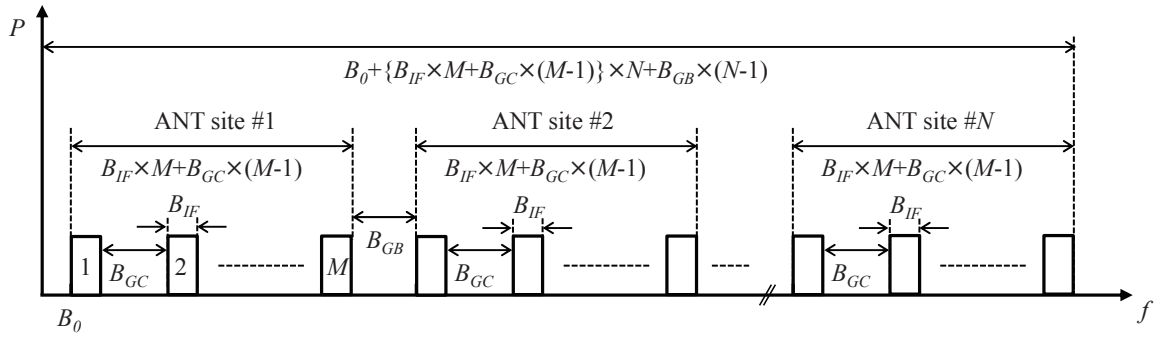

(a)

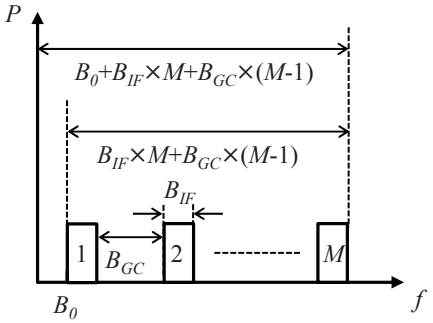

(b)

Fig. 5-2 Detailed IF channel allocations and required bandwidths (a) on a broadband IFoF link and (b) on a narrowband IFoF link.

In a relay site, the transmitted signal is converted to the electric SCM signals by a broadband O/E. When commercially used 4G macro-cell sites are available, the sites should also be the relay site, to reduce the construction time and cost. A continuous band for each antenna site is extracted from the others by an electric filter and then converted to the lowest frequency range by LO and mixer. Each of the M IF signals is transmitted on a narrowband IFoF link from the relay site to an specific antenna site using a narrowband E/O. Figure 5-2(b) shows the bandwidth for the M IF signals transmitted to an antenna site. The fiber length will be several kilometers at maximum,

and a cost-effective DML will be used for the narrowband E/O. In the relay site, analog signal processing will be used because the signal bandwidth may be too wide to be processed by reasonable DSP technologies. Figures 5-3 presents calculation results of contour plots for various total bandwidths of 5, 6, and 7 GHz when B_{GB} and B_{GC} in Figure 5-2(a) were changed: Figures 5-3(a), (b), and (c) show the results when B_{IF} becomes 0.1 GHz, 0.2 GHz, and 0.4 GHz, respectively. Parameters used for the calculations are shown in Table 5-1. The total bandwidth can be less than 6 GHz in Figures 5-3(a) and (b). On the other hand, from Figure 5-3(c), the 6-GHz total bandwidth can not be achieved. In the 5G mobile systems, DSP technologies for less than 6 GHz will be reasonable because more and more BSs that use sub 6-GHz bands are deployed. Therefore, 6 GHz can be a criterion when either analog or digital signal processing is chosen. From this study, analog signal processing is considered to be a better choice. It is obvious that, in the analog signal processing, various kinds of RF components are required. However, the advantage of the reduction of the number of access fibers can prevail the negative point.

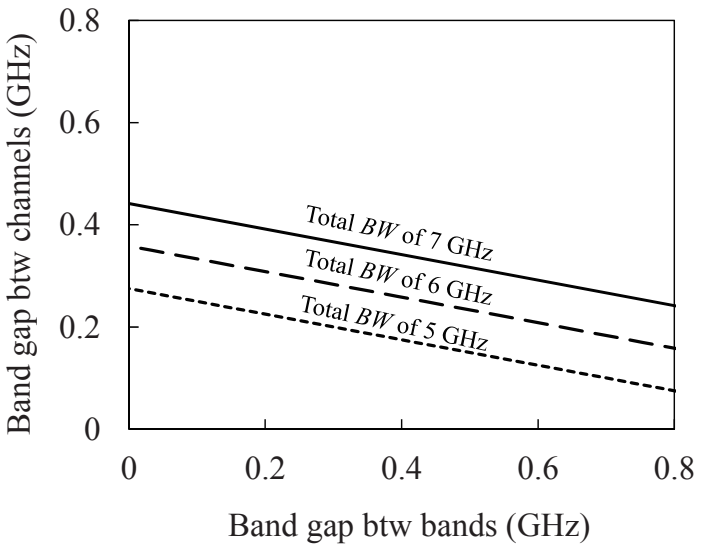

(a)

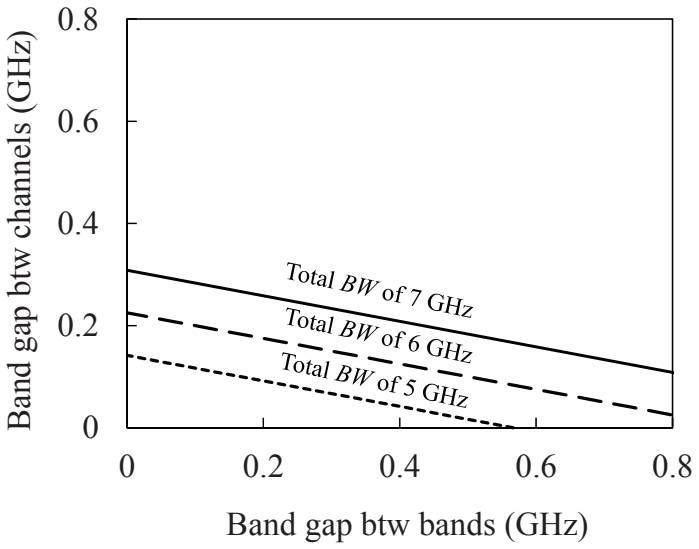

(b)

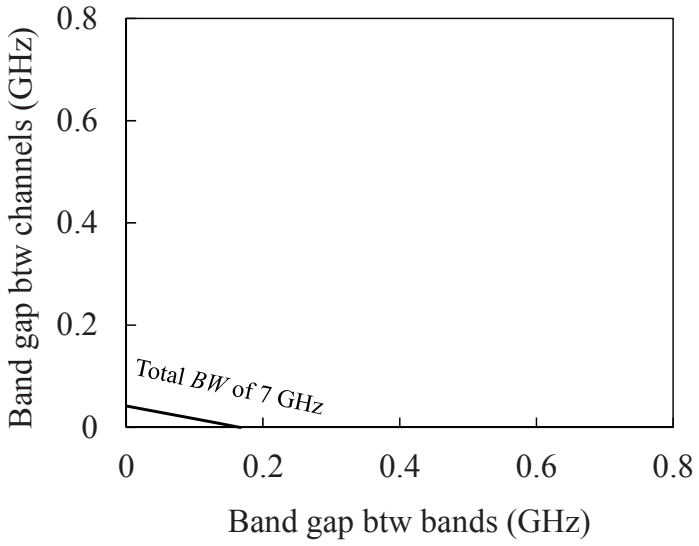

(c)

Fig. 5-3 Calculated contour plots for various total bandwidths of 5 GHz, 6 GHz and 7 GHz when the bandwidth of an IF channel becomes (a) 0.1 GHz, (b) 0.2 GHz, and (c) 0.4 GHz.

Table 5-1 Parameters in the first numerical calculations.

Parameter	Value
Number of RF streams for an antenna site, M	4
Number of antenna sites, N	4
IF channel bandwidth, B_{IF}	0.1, 0.2, 0.4 GHz
Start frequency of the first IF channel, B_0	0.1 GHz
Band gap between channels, B_{GC}	0 to 0.8 GHz
Band gap between bands, B_{GB}	0 to 0.8 GHz

The optical signal transmitted from the relay site to an antenna is converted to the electric IF signals by a narrowband O/E. Each of the IF signals is separated from the others, and the obtained signal is converted to the RF signal. Then, the power for each of the M RF signals is properly adjusted, and the signals are emitted from antenna equipment. When the space and power in an antenna site are not enough, RoF links will be useful for remote antenna configurations.

The process in an antenna site will be conducted by DSP technologies because the bandwidth of the M IF signals becomes less than 6 GHz. Actually, Figure 5-4 shows the calculation results of the bandwidth that is shown in Figure 5-2(b), when the parameter of B_{IF} becomes 0.1, 0.2, and 0.4 GHz. The parameters used for the calculations are shown in Table 5-1. Even when the parameter of B_{IF} becomes 0.4 GHz, in dependent of the band gap between IF channels of B_{GB}, the bandwidth becomes less than 6 GHz. Therefore, DSP technologies will be available for the filters and frequency converters needed in an antenna site. Figures 5-5(a) and (b) depict electric components in an antenna site by analog and digital signal processing, respectively. In an analog approach, a 1:M RF splitter, M kinds of a set of BPF, mixer, and LO, and M BPFs for suppressing unwanted elements will be used, which may complicate the antenna site. On the other hand, in a digital approach, simple DSP equipment that implements an ADC, signal processing circuits, M

DACs, and *M* BPFs for removing undesired elements will be needed. When high radio frequencies such as millimeter waves are required, *M* analog upconverters will be also used because high frequencies can not be easily output from the DACs. In such cases, the outputs from *M* DACs should be set to a specific IF, in order to use a common LO in *M* upconverters. The DSP technologies are expected to simplify the antenna site, and also to enhance the spectral efficiency by digital steep filters. Additionally, the system can be more flexible.

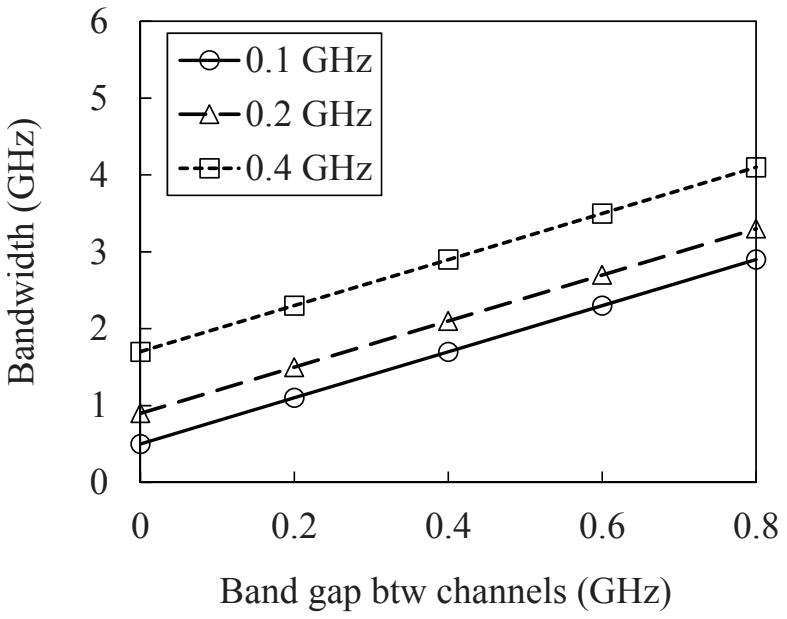

Fig. 5-4 Calculated bandwidths in a narrowband IFoF transmission when various IF channel bandwidths of 0.1 GHz, 0.2 GHz, and 0.4 GHz are assumed.

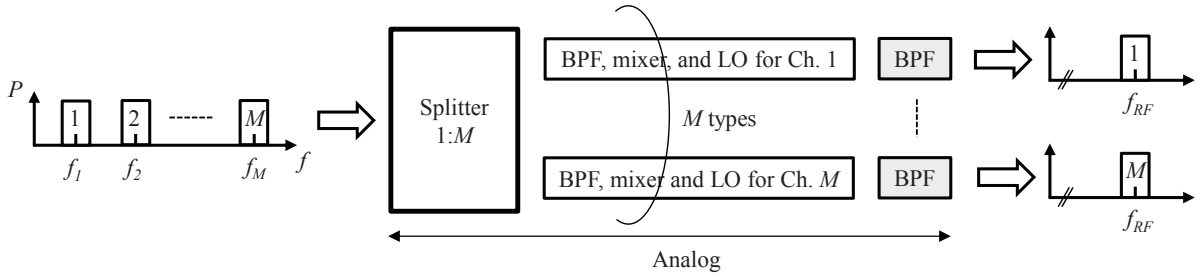

(a)

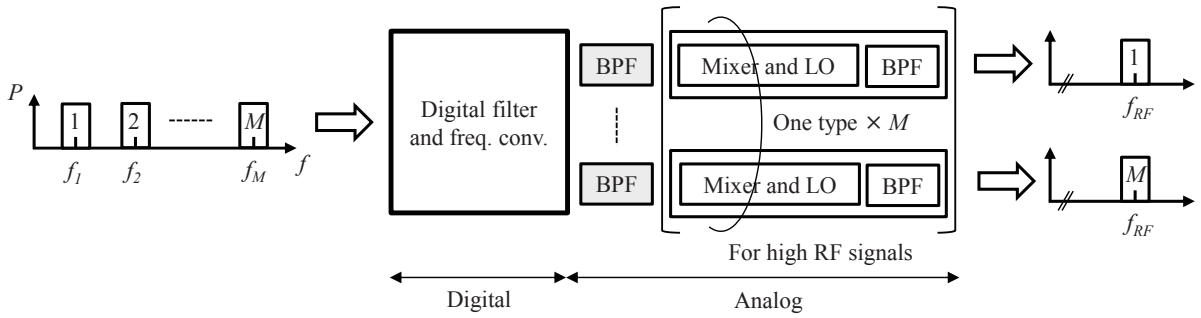

(b)

Fig. 5-5 Channel extractions and frequency conversions in an antenna site: (a) by analog signal processing and (b) digital signal processing.

5-3 Comparison of cascaded IFoF systems with SCM-PON systems

In this section, firstly, a SCM-PON system for MFH applications that can also use existing deployed access fibers is described. Then, a cascaded IFoF system is compared to a SCM-PON system from the perspective of the bandwidth required for downlink transmission [14].

5-3.1 SCM-PON-based mobile fronthaul systems

Figures 5-6(a) and (b) illustrate a SCM-PON system for MFH applications and IF or RF signals transmitted over each optical link, respectively. A frequency band is assigned to signals for each antenna site. This idea is almost the same as Figure 5-1(b). However, when the use of digital signal processing in each antenna site is assumed, the band gap between IF channels for two antenna sites, B_{GB}, can be smaller by steep digital filters. Though the use of analog and hybrid signal processing can be also considered, this study focuses on the use of digital signal processing. In Figure 5-6(a), IF signals for N antennas sites are multiplexed in a frequency domain, and the SCM signals are transmitted to all antenna sites via a 1:N optical power splitter. In an antenna site, each IF signal for its site is separated from the others and converted to the RF signal.

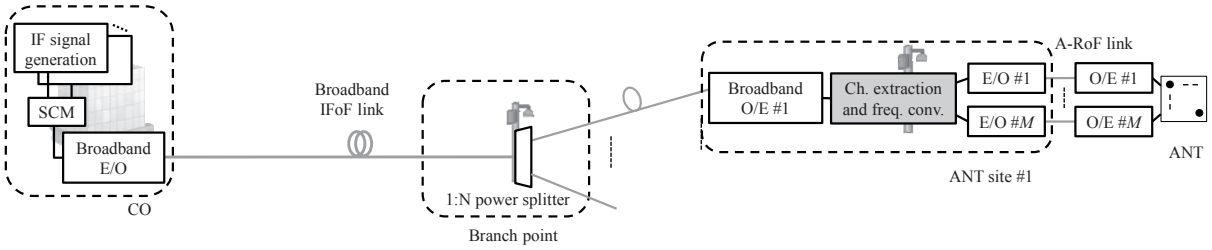

(a)

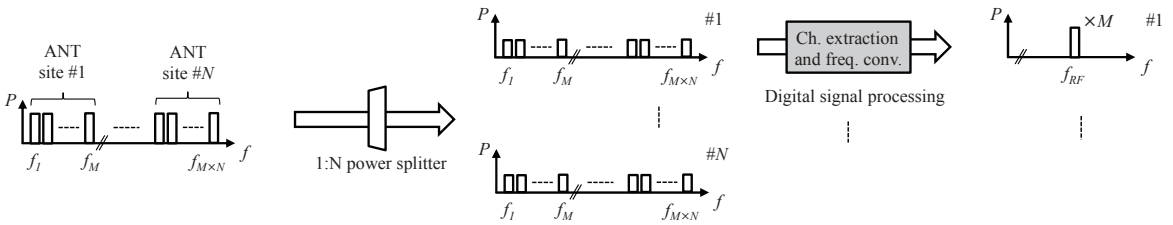

(b)

Fig. 5-6 MFH system based on SCM-PON: (a) network architecture and main functional blocks, and (b) IF channel allocations and frequency conversions applied in antenna sites.

5-3.2 Calculation of required bandwidth

The parameters that are used in this comparison study are presented in Table 5-2. In the table, a band gap between channels and a band gap between bands are described as B_{GC} and B_{GB}, respectively. There is no difference in meaning of the definition between this section and Section 5-2. The band gap between bands, B_{GB}, is assumed to be one and half as wide as the bandwidth of an IF channel, B_{IF}. Figure 5-7(a) plots the calculation results of the sum of the bandwidths for E/Os and that for O/Es in whole systems. The IF channel bandwidth, B_{IF}, is 0.4 GHz. In the cascaded IFoF MFH system, the sum of the bandwidths for E/Os is the same as that for O/Es. The total bandwidths become wider almost proportionally when the number of antenna sites increases. In comparison with the SCM-PON, the sum of the bandwidths for E/Os becomes wider, independent of the number of antenna sites. On the other hand, the total bandwidth for all of the optical components, in addition to the sum of the bandwidths for OEs, becomes narrower when four and more antenna sites are assumed. Actually, four and more antenna sites will be reasonable because most of the conventional PON systems use 1:4 and/or 1:8 power splitters. The calculation results for the O/E bandwidth in each antenna site is depicted in Figure 5-7(b). The cascaded IFoF system has a constant value, and the value is narrower than the SCM-PON system. As the number of antenna sites increases, the value difference becomes larger.

Table 5-2 Parameters in the second numerical calculations.

Parameter	Value
Number of RF streams for an antenna site, M	4
Number of antenna sites, N	2, 4, 8, 16
IF channel bandwidth, B_{IF}	0.1 to 0.8 GHz
Start frequency of the first IF channel, B_0	0.1 GHz
Band gap between channels, B_{GC}	0 GHz
Band gap between bands, B_{GB}	0.15 to 1.2 GHz

Figure 5-7(c) shows the calculation results for the total bandwidth of E/Os and that of O/Es in each of the whole systems. Eight antenna sites are assumed in the calculations. The total bandwidth of E/Os and that of O/Es in the cascaded IFoF MFH system are wider and narrower than those in the SCM-PON-based MFH system, independent of the bandwidth of an IF channel. In addition, the cascaded IFoF system has smaller values in the sum of the total bandwidths than the SCM-PON system. Figure 5-7(d) plots the bandwidth of an O/E placed in an antenna site when eight antenna sites are assumed. The cascaded IFoF system has narrower bandwidths than the SCM-PON in any IF channel bandwidth conditions. The difference is proportionally larger when the IF channel bandwidth becomes wider. From the calculation results in this section, a cascaded IFoF system is confirmed to be more effective for reducing the bandwidth of an O/E in an antenna site and the sum of the total bandwidths of E/Os and O/Es in a whole system.

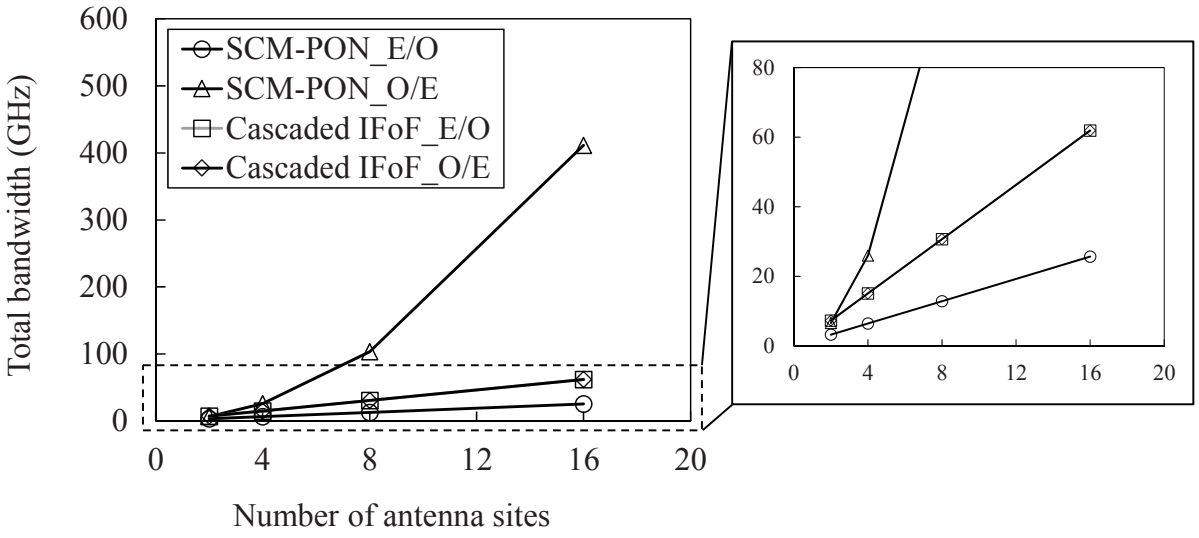
Total bandwidth (GHz)
600
500
400
300
200
100
0
SCM-PON_E/O
SCM-PON_O/E
Cascaded IFoF_E/O
Cascaded IFoF_O/E
0
4
8
12
16
20
Number of antenna sites
80
60
40
20
0
0
4
8
12
16
20

(a)

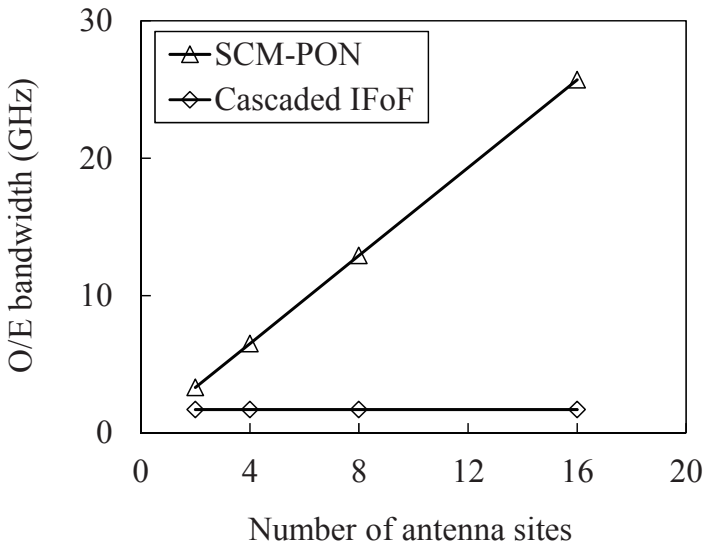
O/E bandwidth (GHz)
30
20
10
0
SCM-PON
Cascaded IFoF
0
4
8
12
16
20
Number of antenna sites

(b)

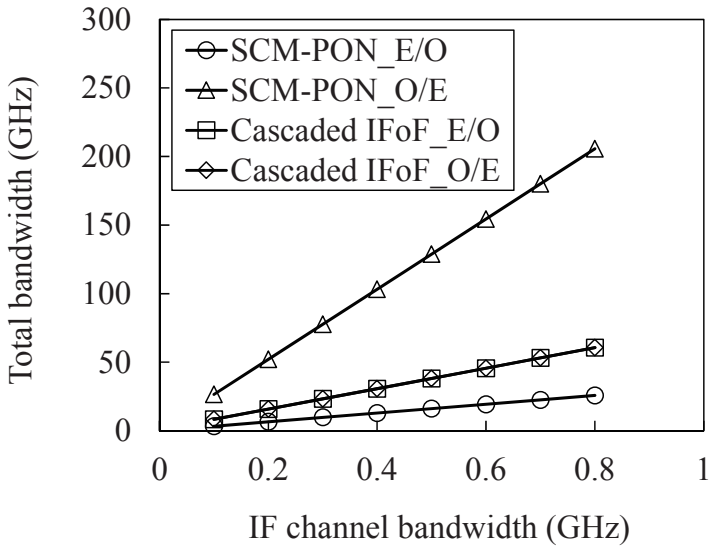

(c)

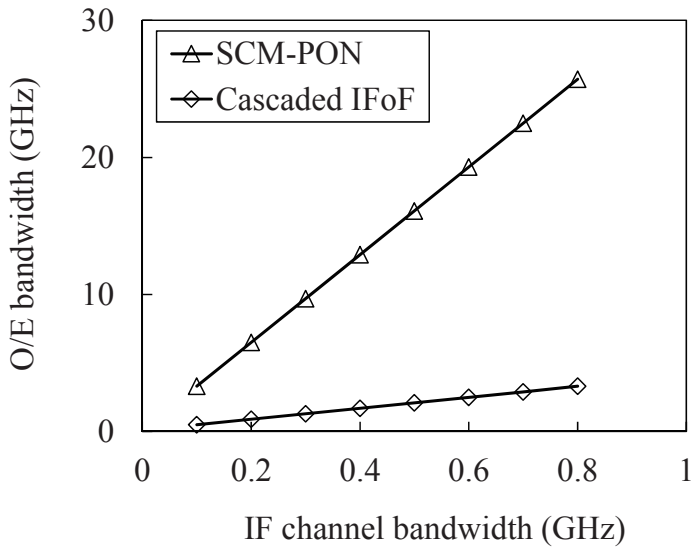

(d)

Fig. 5-7 Calculated bandwidths in a SCM-PON system and a cascaded IFoF system (a) for the whole system with B_{IF} of 0.4 GHz, (b) for an antenna site with B_{IF} of 0.4 GHz, (c) for the total system with N of 8, and (d) for an antenna site with N of 8.

5-4 Developed real-time digital signal processors

In this section, two kinds of FPGA-based real-time digital signal processors for each antenna site of the cascaded IFoF systems are described. One is for an output of an IF signal and the other is for multiple outputs of plural IF signals. Both of the DSP equipment can work using a precise 10-MHz reference clock and have a FPGA clock rate of 400 MHz [14].

5-4.1 FPGA for single RF stream output

Figure 5-8 shows the functional blocks of the firstly developed DSP equipment. The equipment is designed by the concept where six filtered OFDM (f-OFDM) signals are input from an input port, arbitrary one of the six signals is separated from the others and then converted to a specific frequency without any large deteriorations, and then the obtained IF signal is output from an output port. Regarding the IFoF channel allocation, the start frequency of the first channel of 100 MHz, the signal bandwidth per channel of 360 MHz, the guard band between IF signals of 3.6 MHz are targeted by a steep digital filter. In the equipment, firstly, six SCM f-OFDM signals are digitized by an ADC with a sampling rate of 6.4 GHz, an amplitude resolution of 12 bit, and an analog bandwidth of 8 GHz. The digitized signal is processed by a real-time FPGA with 1608 multipliers. One of the selected IF signals is converted to the baseband signal by multiplying the inverted carrier frequency from a numerically controlled oscillator (NCO) that has a resolution of 12 bit. For reducing the sampling rate to 0.8 GSa/s, an anti-aliasing finite impulse response (FIR) filter is used. The cut-off frequency, number of taps, coefficient resolution are set to 272 MHz, 81 taps, and 10 bit, respectively. Then, a steep band pass filter is used to extract only the desired signal. The filter has 181.8-MHz cut-off frequency, 769 taps, and 10-bit coefficient resolution. Next, the sampling rate of the filtered signal is converted to 3.2 GSa/s, and an anti-aliasing filter is applied to the signal. The filter has 200-MHz cutoff frequency, 81 taps, and 10-bit coefficient resolution. After the upsampling, the signal is converted to a specific frequency up to 1.6 GHz by multiplying the carrier frequency from an NCO with a 12-bit resolution. Finally, the digital signal is converted to the analog signal by a DAC that has 3.2-GHz sampling rate, 16-bit resolution, and 2.5-GHz analog bandwidth.

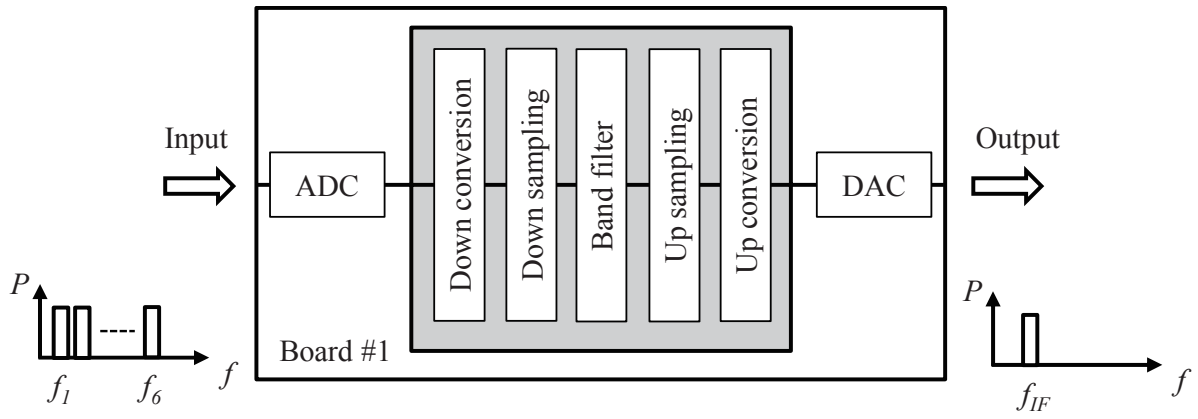

Fig. 5-8 Funcitional blocks of FPGA-based DSP equipment with one output.

5-4.2 FPGA for simultaneous and multiple RF stream outputs

Enhancing the firstly developed DSP equipment, the second DSP equipment was developed. Figure 5-9 illustrates the functional blocks. In comparison with the first DSP equipment, the numbers of the signal processing lines and DACs increase. The equipment is designed by the concept where six OFDM signals are input from an input port, arbitrary one or two of the six signals are extracted from the others and converted to specific frequencies without any large deteriorations, and then the obtained one or two IF signals are simultaneously output from one of the four output ports. Regarding the IFoF channel allocation, the start frequency of the first channel of 109.92 MHz, the signal bandwidth per channel of 380.16 MHz, the guard band between IF signals of 19.84 MHz are targeted. In the equipment, firstly, six SCM OFDM signals are digitized by an ADC that was also used in the first DSP equipment. The digitized signal is simultaneously processed in six parallel lanes. One FPGA board that has 2042 multipliers takes the first to the fourth processing lanes, and the other FPGA that has 1021 multipliers processes the fifth and the sixth lanes. DAC #1 generates two carrier aggregated IF signals from the first and the second signal processing lanes. DAC #2 also generates two IF signals from the third and the fourth lanes. On the other hand, DAC #3 and DAC #4 output the signals from the fifth and the

sixth processing lanes, respectively. Each signal processing lane takes almost the same processing as the first DSP equipment. Therefore, different points with each other are mainly described. The anti-aliasing FIR filter after the down conversion is changed to one with 296 MHz cut-off frequency, 111 taps, and 12 bit. The steep digital filter is also redesigned by 200-MHz cutoff frequency, 155 taps, and 12-bit resolution. The sampling rates of the signals for DAC#1 and DAC #2 are converted to 3.2 GSa/s after the band filters, whereas those for DAC #3 and DAC #4 are converted to 1.2 GSa/s. The anti-aliasing filter for each processing lane has a 400-MHz cutoff frequency, 31 taps, and 12-bit resolution for DAC #1 and DAC #2. The cutoff frequencies are set to 200 MHz for DAC #3 and DAC #4. After the upsampling, each signal is converted to a specific frequency. Finally, two carrier aggregated IF signals are generated by DAC #1 that have a sampling rates of 3.2 GSa/s, an amplitude resolutions of 16 bit, and an analog bandwidth of 2.5 GHz. DAC #2 also generates two IF signals. On the other hand, only one IF signal is generated, via the fifth processing lane, by DAC #5 that has a sampling rate of 1.2 GSa/s, a function of resampling to 2.4 GSa/s including an anti-aliasing filter, a resolution of 16-bit, and an analog bandwidth of over 0.6 GHz. DAC #6 also has the same function as DAC #5. It is noted that, in two kinds of the developed DSP equipment, no modulation and demodulation of baseband signals are included. Such functions are considered to cause a heavy load in the signal processing.

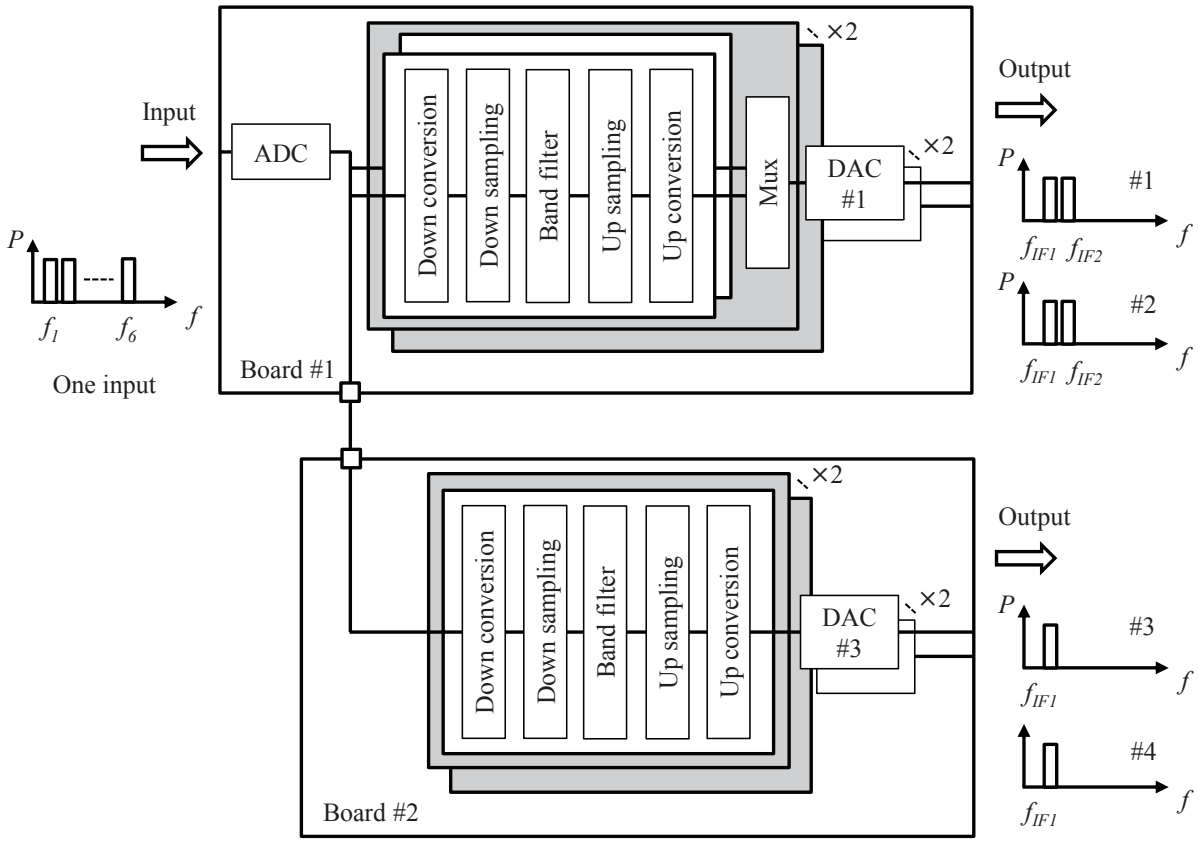

Fig. 5-9 Functional blocks of FPGA-based DSP equipment with four outputs.

5-5 Cascaded IFoF mobile fronthaul systems with high spectral efficiency

In this section, downlink IFoF transmission experiments are conducted using the firstly developed DSP equipment. Cascaded IFoF systems with analog and digital signal processing for the future MFH systems are experimentally verified [14].

5-5.1 Experimental setup

To confirm the potential of a cascaded IFoF system with analog and digital hybrid signal processing for the future MFH applications, the system using the firstly developed DSP

equipment is quantitatively evaluated. Figure 5-10 shows the experimental setup. SCM IF signals were generated by an offline process and sent to an AWG. The AWG that ran at 50 GSa/s output the SCM signals for this transmission experiment. Figure 5-11 illustrates the schematic diagram of IF signals from the AWG. In this experiment, three antenna sites were considered, and the signals for each antenna site were allocated in a continuous frequency band. The start frequency and the band gaps between adjacent bands were set to 100 MHz and 822 MHz, respectively. Each band included six 360-MHz-bandwidth f-OFDM signals. The band gap between adjacent IF signals were set to 3.6 MHz. This value is only 1% of the bandwidth of an IF signal. Each f-OFDM signal had a signal bandwidth of 360 MHz and a modulation format of 64 QAM. The total user data rate corresponds to 24.3 Gbit/s when a spectral efficiency of 3.75 bit/s/Hz is assumed. In more detailed explanation on the f-OFDM signal, the inverse fast Fourier transform (IFFT) size for an OFDM signal was set to 2048 points. The OFDM signal consisted of 1000 64-QAM data subcarriers and 200 binary phase shift keying (BPSK) pilot subcarriers, and the subcarriers had a 300-kHz spacing between adjacent carriers. There existed a pilot subcarrier every 5 data subcarriers. As a result, 360-MHz signal bandwidth was obtained. Cyclic prefix (CP) of 7% was added to the signal after the IFFT process. An FIR filter was applied to the OFDM signal to generate an f-OFDM signal. Hamming window function with 1023 taps and 367.2-MHz bandwidth was used for the FIR filter. This f-OFDM signal was converted to a specific frequency. The other seventeen f-OFDM signals ware generated by the same process, and all of the eighteen IF signals were subcarrier multiplexed. These eighteen f-OFDM signals from an AWG were input to an RF amplifier and a variable ATT to adjust the RF power before being injected to an E/O device. As an E/O for a broadband IFoF link, a DFB-LD operating at 1567.5 nm and a lithium niobate Mach-Zehnder modulator (LN-MZM) were used. The optical input power to a 20-km SMF was adjusted to +6.0 dBm, and the received optical power at O/E equipment was controlled by a variable optical attenuator (VOA). The O/E equipment included a PIN-PD and an RF amplifier.

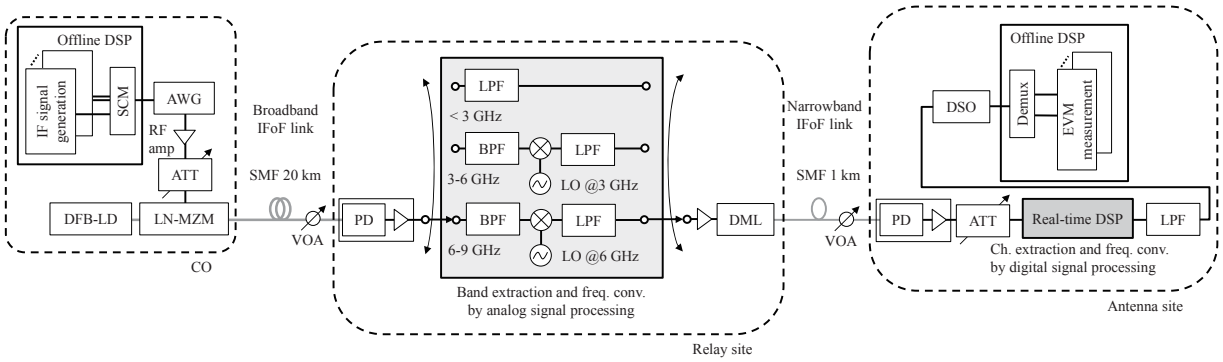

Fig. 5-10 Experimental setup for a cascaded IFoF-based MFH links.

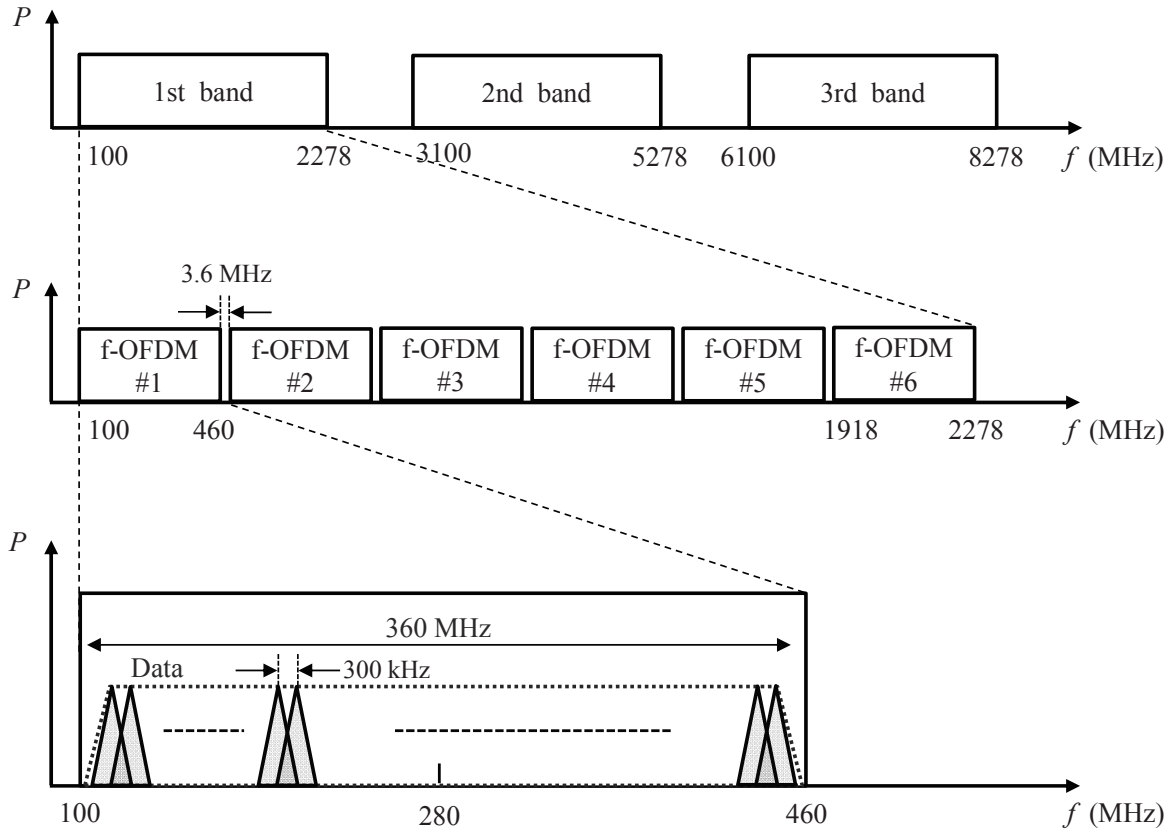

Fig. 5-11 Schematic diagram of IF signals transmitted over a broadband IFoF link in the first transmission experiment.

After the O/E, six IF signals for each antenna site were extracted from the others by an RF filter. A low pass filter (LPF) for less than 3 GHz, a BPF for 3 to 6 GHz and a BPF for 6 to 9 GHz were used for the first band, the second band, and the third band, respectively. The second band and the third band were converted to the lowest frequency range for the first band by LOs and mixers. Six IF signals for each antenna site with a fixed input power of -0.6dBm drove a DML that operated at 1549.8 nm and with a 35-mA bias current. The input optical power to a 1-km SMF was measured to be +5.3 dBm. The received optical power, after the transmission, at an O/E was adjusted by a VOA. The O/E also included a PIN-PD and an RF amplifier. Then, the RF power of the six IF signals was adjusted by a variable ATT just before the DSP equipment shown in Figure 5-8. One IF signal was extracted from the others and converted to 400 MHz as a center frequency. An LPF after the DSP equipment was used to remove undesired components from the signal. The signal after the LPF was input to a digital sampling oscilloscope (DSO) and digitized at 100 GSa/s. Using offline DSP, the EVM performances for all IF signals were measured in turn.

5-5.2 Results and discussion

Figure 5-12 depicts RF spectra of electric BtB, optical BtB, and after 20-km SMF without and with a pre-emphasis for the broadband IFoF link. In the measurement, received optical power at the O/E for optical BtB and 20-km SMF transmission were +5.0 dBm and +2.0 dBm, respectively. From the comparison between electric BtB and optical BtB, RF power reduction in higher frequencies is confirmed in optical BtB, mainly due to the frequency response of the O/E equipment. The influence of the power fading from the fiber chromatic dispersion is small and negligible even when the signals were transmitted over a 20-km SMF. Using a simple pre-emphasis, the RF response after the transmission can be successfully compensated.

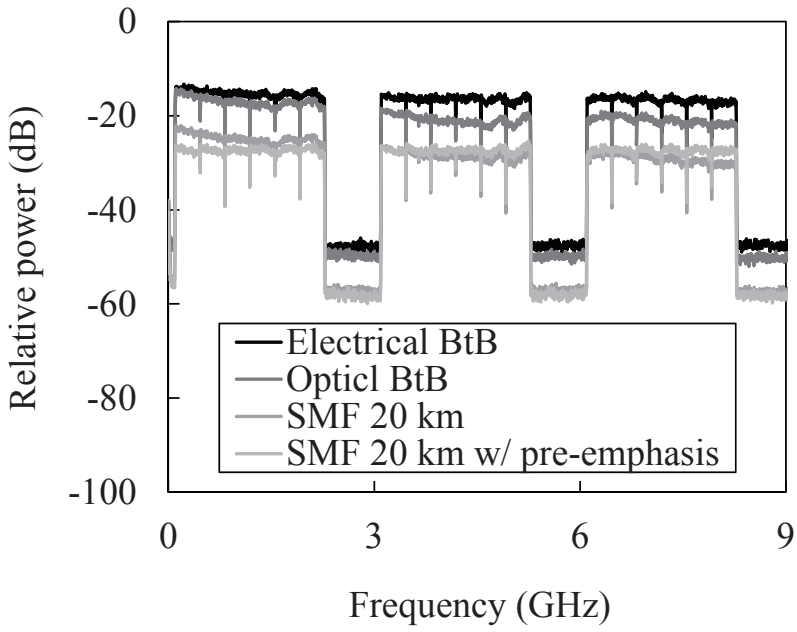

Fig. 5-12　RF spectra before and after the broadband IFoF transmission.

In order to confirm the proper RF driving power for the LN-MZM, root mean square (rms) EVM values for all signals were evaluated after the broadband IFoF link. In the experiment, the received power at the O/E was adjusted to +2.0 dBm. Figure 5-13 plots average EVM values from all signals when the RF input power to the LN-MZM changes. When the RF power increases up to around -5.0 dBm, the EVM performances gradually become better. That is because the electric signal power after the PD can be increased. However, when the RF power were set to more than around -5.0 dBm, the EVM performances tended to become worse. That is because signal distortions occurred due to the nonlinearity of the LN-MZM, and the influence caused the deteriorations of the EVM performances. In a common LN-MZM, the relationship between input voltage and output optical power is expressed by the square of cosine. Then, the proper received optical power at the O/E was evaluated, when the driving RF power for the LN-MZM was set to -5.0 dBm. Figure 5-14 plots average EVM values from all signals as a function of received optical power after the broadband IFoF transmission. In comparison with the reference results from the optical BtB condition, no significant EVM degradations are observed

after the SMF 20 km. When the received optical power increases up to +2.0 dBm, EVM performances gradually become better. From Figures 5-13 and 5-14, it is confirmed that better EVM performances can be obtained by properly adjusting the conditions in the IFoF transmission. Figure 5-15 presents the EVM measurement results for all IF channels before and after the broadband IFoF link. In the experiment, the driving RF power for the LN-MZM and the received optical power at the O/E were adjusted optimally. In the electrical BtB, IF signals with larger channel number, i.e., with higher frequencies, have worse EVM performances because the AWG itself had worse signal quality in higher frequencies. The minimum and maximum EVM values were 2.9% and 4.4%, respectively. In the optical BtB condition, the EVM values in lower frequencies are similar to those in the electrical BtB case. However, when the signal frequency becomes higher, the difference in EVM values can be found by 1.2% at maximum. The EVM degradation is considered due to the frequency response mainly from the O/E. After the broadband IFoF link, in comparison with the optical BtB condition, the maximum EVM deterioration of 0.6% are found in the eighteenth channel. To suppress the difference in EVM values among channels, a simple pre-emphasis technique is effective. Actually, the EVM values after the transmission successfully became within 3.8% to 4.5%. The following experimental results included the effect of this pre-emphasis. In addition, the received power at the OE was adjusted to +2.0 dBm.

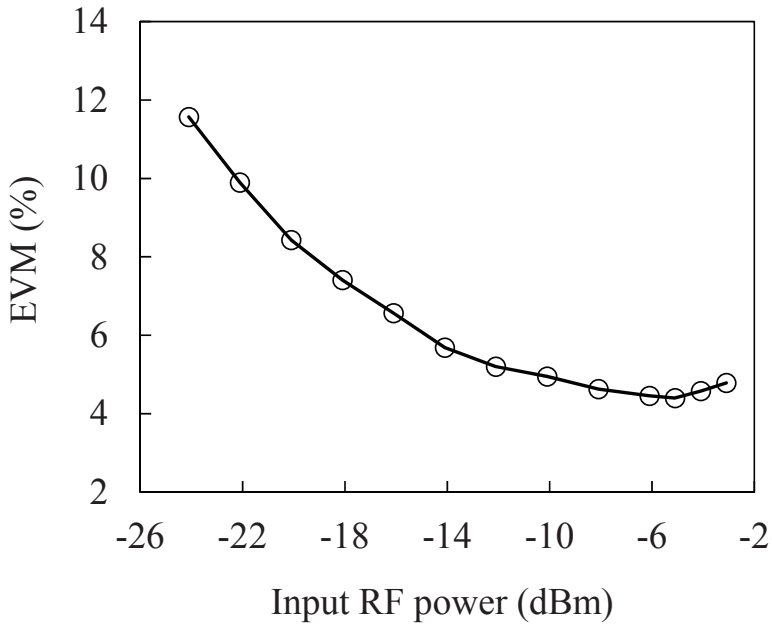

Fig. 5-13 EVM performances as a function of the RF power input to the LN-MZM.

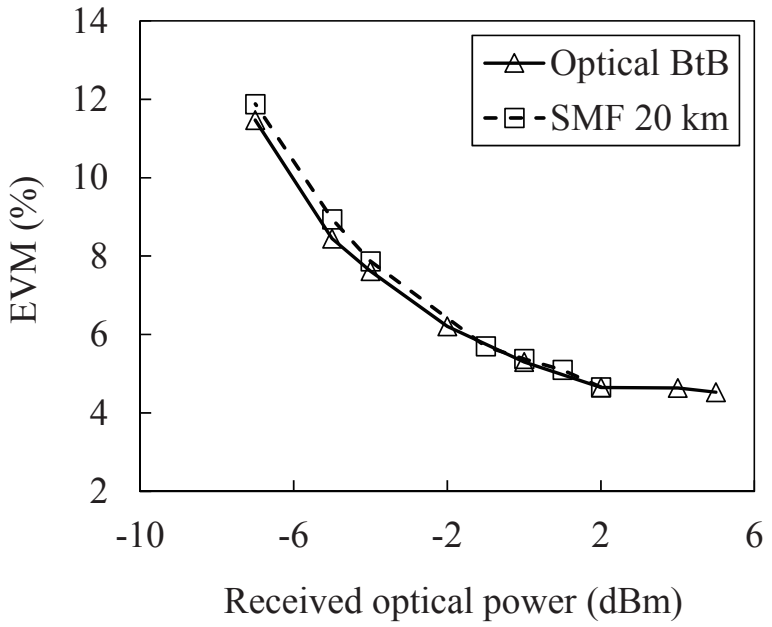

Fig. 5-14 EVM performances as a function of the received optical power at the PD after the broadband IFoF link.

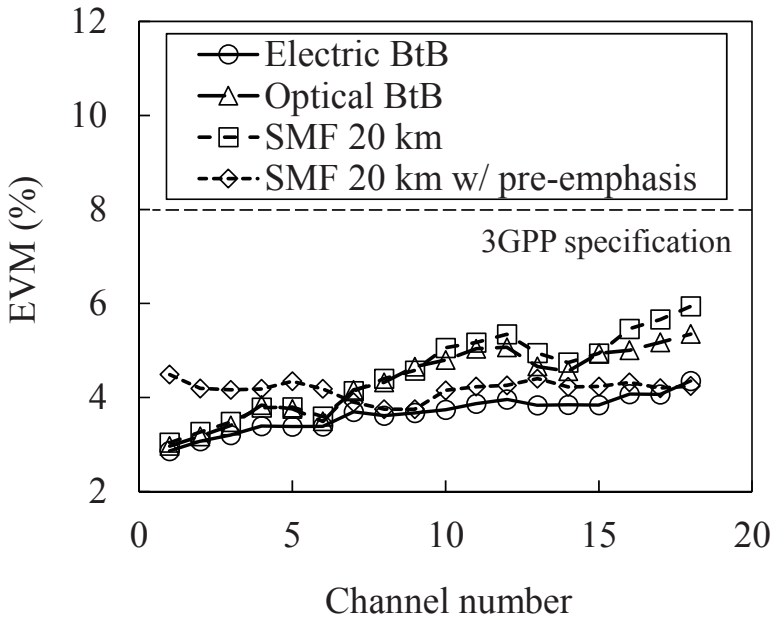

Fig. 5-15 EVM performances for each IF channel before and after the broadband IFoF link.

Measured RF spectra for each of the bands after the analog signal processing applied in the relay site are shown in Figure 5-16. Figure 5-16(a) presents the first band. An undesired signal is found at around 3 GHz because the LPF with a pass band of less than 3 GHz was not able to completely remove the seventh IF channel. Figure 5-16(b) depicts the second band. An undesired signal from the LO remains at 3 GHz because of the limitation of the LPF filtering performance. The obtained power difference in the band was mainly caused by the frequency response of the mixer. Figure 5-16(c) describes the third band. The power fluctuation in the band was caused by the same reason as the second band. Next, RF spectra measured after the narrowband IFoF link are shown in Figure 5-17. Figure 5-17(a) shows the RF spectrum of the second band. The relatively high noise power in higher frequencies was caused by the DML in the relay site. Measured RF spectra of the seventh, the ninth, and the twelfth IF channels after the DSP and LPF are depicted in Figure 5-17(b), (c), and (d), respectively. Each of the IF channels in the band was successfully obtained by the high filtering performance of the developed DSP. The power of the out-band frequencies was also effectively suppressed.

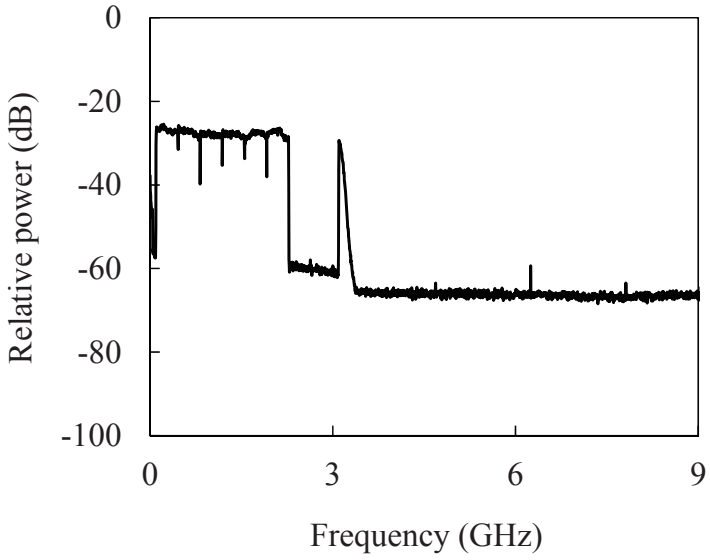
0
-20
-40
-60
-80
-100
Relative power (dB)
0
3
6
9
Frequency (GHz)

(a)

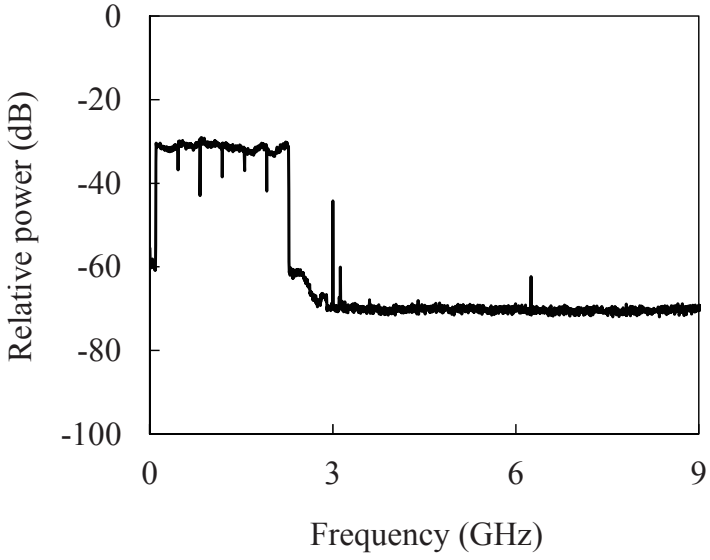
0
-20
-40
-60
-80
-100
Relative power (dB)
0
3
6
9
Frequency (GHz)

(b)

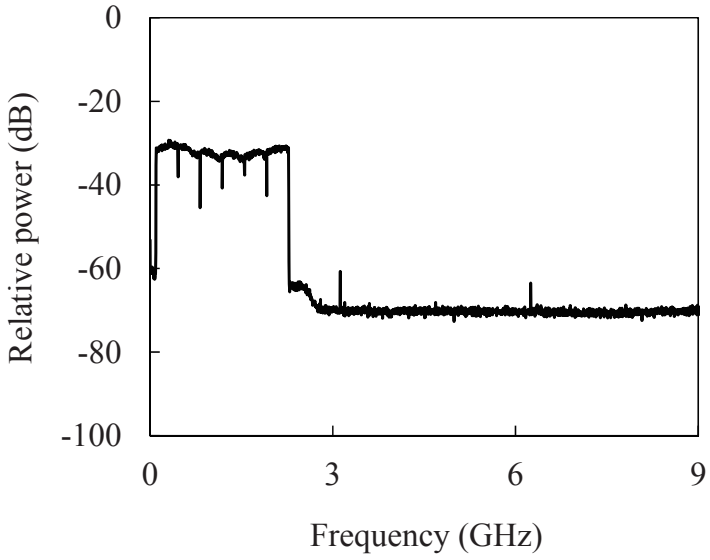

(c)

Fig. 5-16 RF spectra after the band extraction and down conversion (a) for the first band, (b) for the second band, and (c) for the third band.

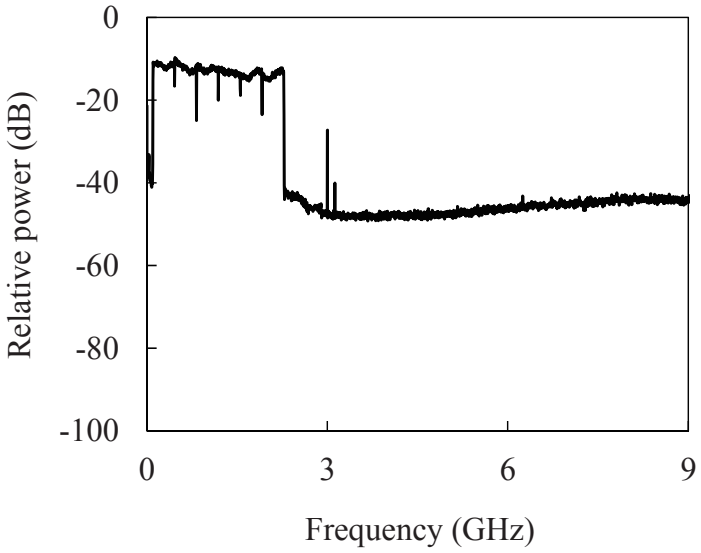
0
-20
-40
-60
-80
-100
Relative power (dB)
0
3
6
9
Frequency (GHz)

(a)

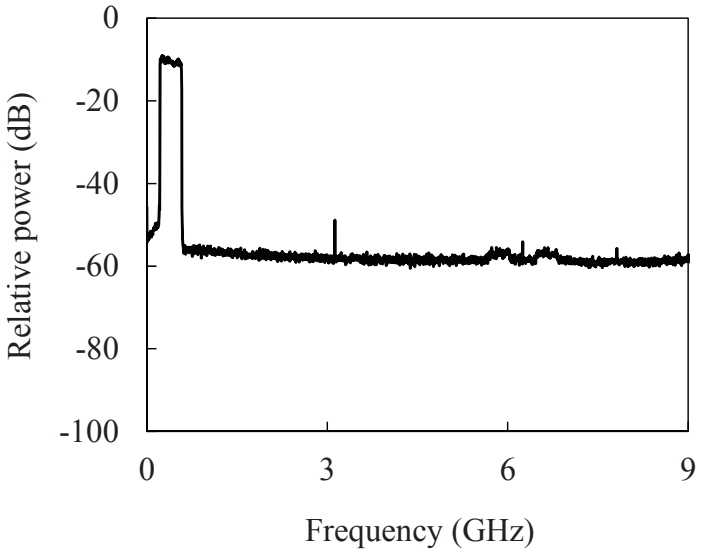
0
-20
-40
-60
-80
-100
Relative power (dB)
0
3
6
9
Frequency (GHz)

(b)

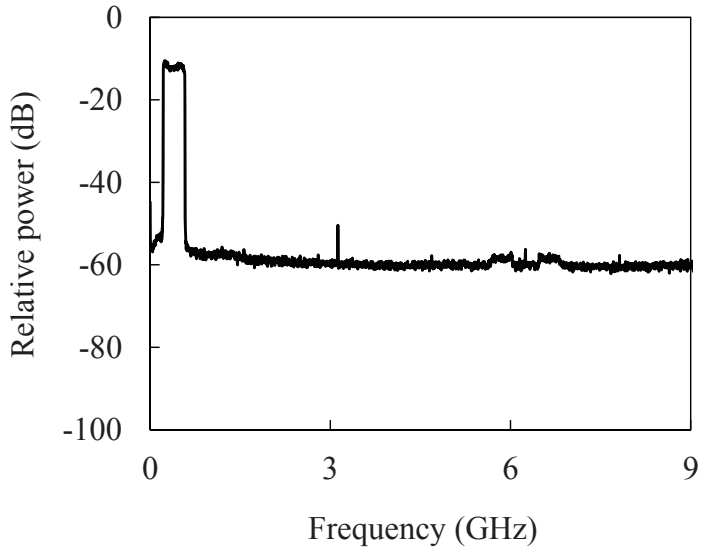

(c)

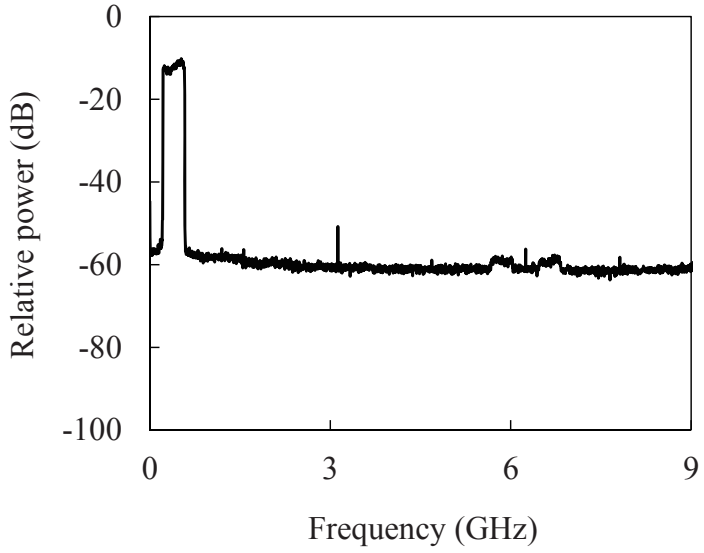

(d)

Fig. 5-17 RF spectra of the IF signals in the second band after the narrowband IFoF link: (a) six IF signals before the real-time DSP, (b) the seventh IF signal, (c) the ninth IF signal, and (d) the twelfth IF signal after the DSP equipment and LPF.

Figure 5-18 shows measured average EVM values of the second-band IF channels after the antenna-site O/E as a function of the received optical power at the PD. An EVM value of 4.5% was obtained in the best case where the received optical power was set to around +2.0 dBm. No big difference in EVM values is found even when the received optical power increases to more than -2 dBm because the EVM degradation due to the optical transmission was sufficiently small, in comparison with the EVM values before the narrowband IFoF tranamission. Figure 5-19 plots measured rms EVM values of the seventh IF signal after the DSP equipment and LPF as a function of the input RF power of the second-band IF channels to the DSP. The best EVM performance was obtained by the input RF power of around -15.0 dBm. The EVM degradations with the input RF power of over -15 dBm were caused by the distortions from the ADC. In such cases, the ADC is considered not to identify the actual level because the input RF power is over the maximum level defined in the ADC. From the experimental results of Figures 5-18 and 5-19, it is obvious that adjusting optical and RF powers properly is important for obtaining better EVM performances. Measured EVM performances for each of the eighteen channels before and after the narrowband IFoF link are described in Figure 5-20. In the measurement, the received optical power at the antenna-site PD and the input RF power to the DSP equipment were adjusted to +4.3 dBm and -15.5 dBm, respectively. After the analog signal processing, the EVM values of the first and the third bands become lower than those after the SMF 20 km. That is mainly because the quantization noise that was caused by the DSO decreased according to the reduction of the number of the input IF channels. On the other hand, the EVM values of the second band were not improved after the analog signal processing. Actually, although the EVM values just after the BPF were lower than those after the SMF 20 km, large EVM deteriorations by 0.6% to 1.3% were caused by the mixing process. The performance of the mixer for the second band and the subharmonics from the LO are considered to affect the EVM performances. After the narrowband IFoF transmission over a 1-km SMF, the maximum EVM deterioration was measured to be 1.4% for the thirteenth IF channel. Additionally, EVM degradations by 0.6% to 1.2% are found after the DSP equipment mainly because the quantization noise that was caused by the internal ADC and DAC was added to the IF signals. However, the minimum and maximum EVM values were measured to be 5.1% from the sixth channel and 6.2% from the twelfth channel, respectively, which meets an EVM criterion of 8% for a 64-QAM signal [15]. These EVM values remain enough margins for the following analog upconversion process.

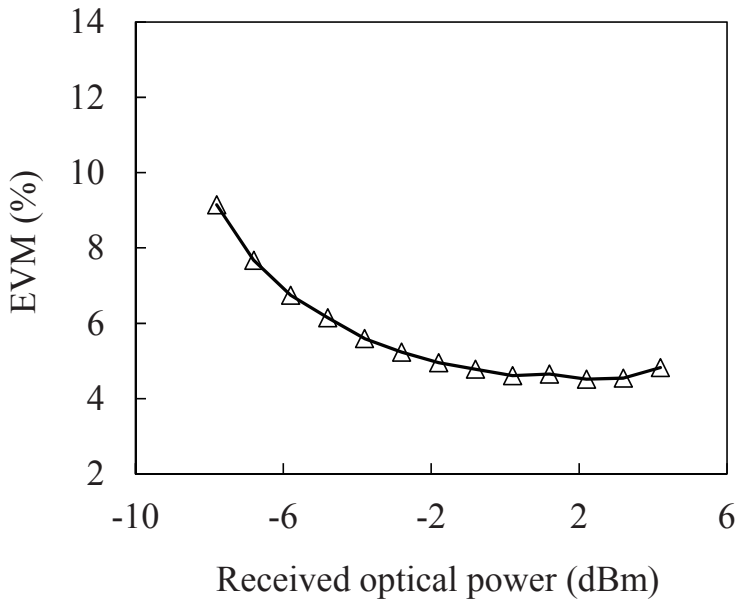

Fig. 5-18 EVM performances after the narrowband IFoF transmission as a function of the received optical power at the narrowband O/E.

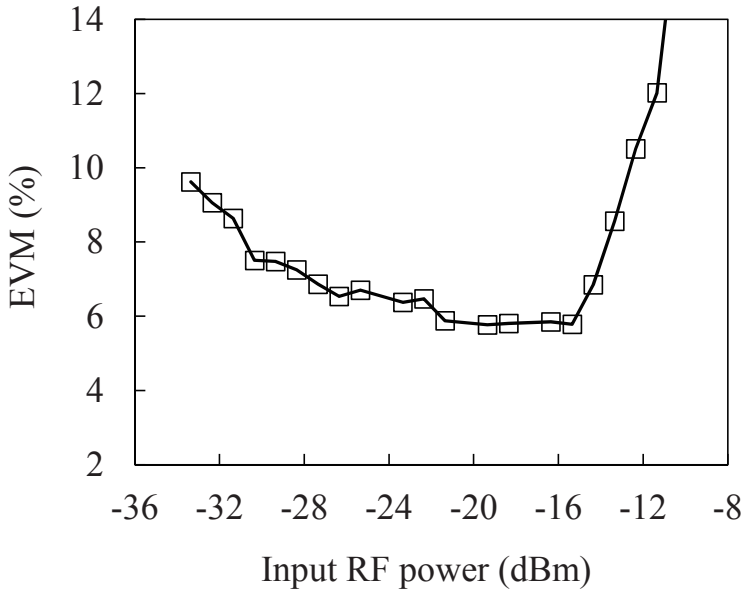

Fig. 5-19 EVM performances after the real-time DSP equipment and LPF as a function of the input RF power to the DSP.

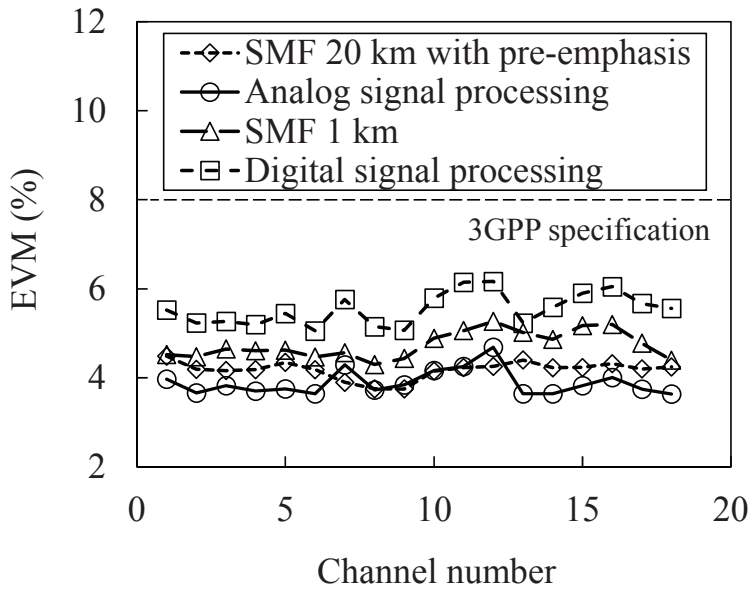

Fig. 5-20 EVM performances for each IF channel before and after the narrowband IFoF transmission.

Additionally, Figure 5-21 describes the processing delay in the developed DSP equipment. The time domain signal of the six IF channels in the first-band before the DSP equipment and one of the first IF channel after the equipment were measured by the DSO, and two of the results are described in Figures 5-21(a) and (b), respectively. When the end time of a continuous signal in Figure 5-21(a) is compared to that in Figure 5-21(b), the time difference is calculated to be around 2.8 μs. This delay value is small and almost negligible, in comparison with a latency of 1 ms required in 5G systems. From these experimental results, the cascaded IFoF MFH system with high spectral efficiency was successfully demonstrated.

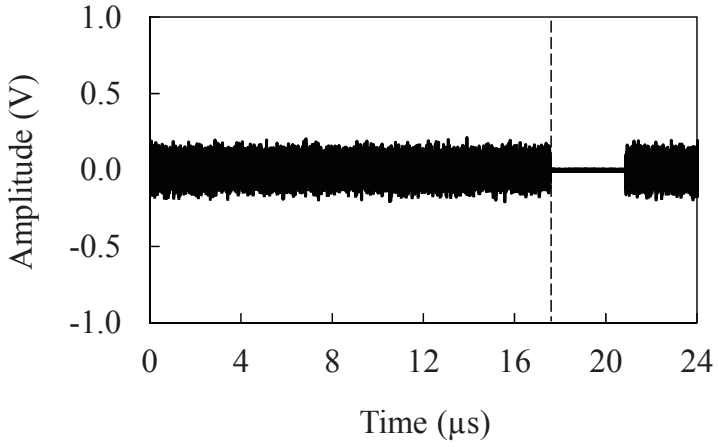

(a)

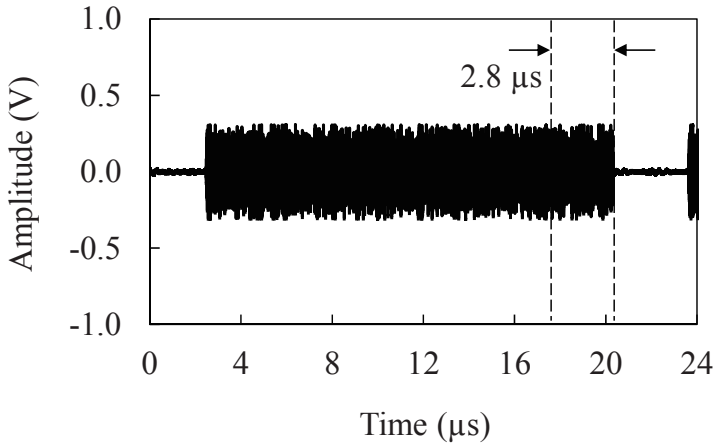

(b)

Fig. 5-21 Signal processing delay in the real-time DSP equipment: (a) a time-domain signal of six IF channels in the first band before the DSP equipment and (b) a time-domain signal of the first channel after the DSP equipment.

5-6 Cascaded IFoF systems for 5G mobile fronthaul

In this section, downlink IFoF transmission experiments are conducted using the secondly developed DSP equipment. Cascaded IFoF MFH systems with analog and digital signal processing that are effective for 5G mobile applications are experimentally verified [14].

5-6.1 Experimental setup

A signal modulation format of OFDM is also used in 5G mobile communication systems. However, the channel bandwidth and subcarrier spacing of an OFDM signal increase up to 400 MHz and 120 kHz, respectively [16]. Additionally, plural RF streams that are emitted from an antenna site should be supported. Therefore, the DSP equipment for an antenna site was replaced by the second prototype that is shown in Figure 5-9. An experimental setup in this section is similar to one in Section 5-5. Therefore, different conditions from the previous section are mainly explained using Figure 5-10. For plural IF signals generation, two types of AWGs were used. The first one had a sampling rate of 50 GSa/s and was used for generating six OFDM signals that are equivalent to 5G signals. On the other hand, the second one had a sampling rate of 120 GSa/s and was used for generating twelve dummy OFDM signals. Figure 5-22 depicts the schematic diagram of IF signals from the AWGs. In the top figure, the first and the second bands were generated by the second AWG for dummy signals, and the third band were from the first AWG for 5G signals. In the third band for 5G signals, each OFDM signal was generated by the parameter conditions where a subcarrier spacing, an IFFT size, and a cyclic prefix were set to 120 kHz, 4096 points, and 7%, respectively. Additionally, 2640 subcarriers and 528 subcarriers were used for 64-QAM modulated symbols and quadrature phase shift keying (QPSK) modulated pilots, respectively. Considering the number of subcarriers and the subcarrier spacing, the effective signal bandwidth became 380.16 MHz. Two 9.92-MHz bands were used as null subcarriers in a channel bandwidth of 400 MHz. In the first and the second bands, the parameters for generating an OFDM signal were needed to be different from the third band, due to the limitation of the available AWGs. The subcarrier spacing and IFFT size were set to 960 kHz and

512 points, respectively. The OFDM signals for the third band was multiplexed with OFDM signals for the first and the second bands by a combiner. Then, the SCM signals with an average RF power of -1.4 dBm were used to drive an LN-MZM. A DFB-LD with a carrier wavelength of 1567.5 nm was used for the light source. The modulated optical signal was launched into a 20-km SMF with an average RF power of + 6.0 dBm. The received optical power at O/E equipment after the 20-km SMF link was adjusted to 0 dBm by a VOA. The O/E equipment included a PIN-PD and an RF amplifier.

The output signal from the O/E equipment was input to a BPF for a band from 6 GHz to 9 GHz. The third band was extracted from the other bands by the BPF and downconverted to a frequency range from 0.1 GHz to 2.5 GHz by a mixer and an LO at 6 GHz. Then, undesired components from the mixing process were removed by an LPF with a passband of less than 3 GHz. The average power of the six OFDM signals after the LPF was adjusted to -3.9 dBm by an amplifier and ATTs. The six OFDM signals and a bias current of 50 mA were injected to a DML with a carrier wavelength of 1550.0 nm. The launched optical power to a 1-km SMF and the received optical power at O/E equipment after the 1-km SMF were set to +7.0 dBm and +3.0 dBm, respectively. The O/E also included a PIN-PD and an RF amplifier. The average RF power of the six OFDM signals from the O/E equipment was adjusted to -17.0 dBm by a variable ATT, and the signals were input to the secondly developed DSP equipment described in Figure 5-9. The OFDM signals #13 and #14 were converted to center frequencies of 400 MHz and 800 MHz, respectively, and output from the DAC #1. The OFDM signals #15 and #16 were output from the DAC #2 in the same manner as the OFDM signals #13 and #14. Additionally, the OFDM signals #17 and #18 were converted to a center frequency of 400 MHz and output from the DAC #3 and #4, respectively. Each of the output signals from the DACs passed through an LPF for removing undesired aliasing components, and then the EVM values of all signals were measured in the same manner as the experiment in Section 5-5.

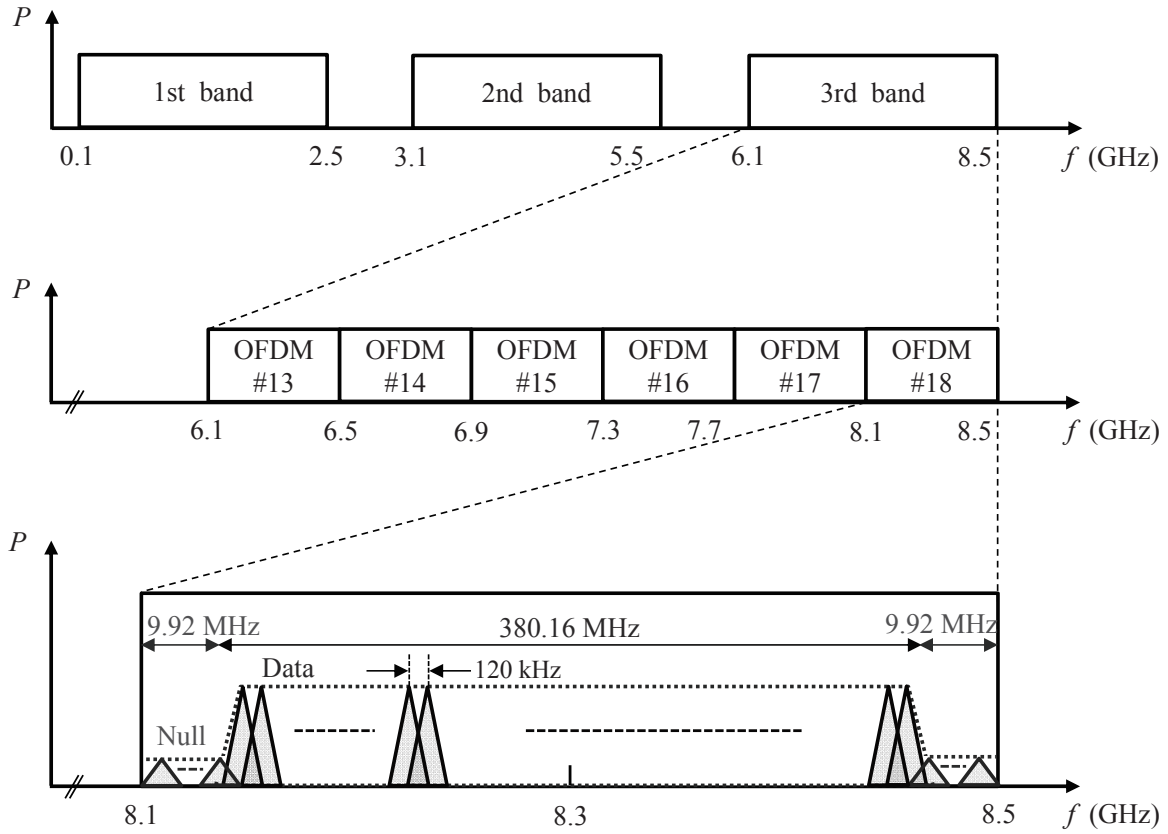

Fig. 5-22 IF signals transmitted over a broadband IFoF link in the second transmission experiment.

5-6.2 Results and discussion

Figure 5-23(a) shows measured RF spectra of eighteen IF signals before and after the broadband IFoF transmission over a 20-km SMF. In comparison with before the transmission, the spectrum after the transmission has relatively low powers in higher frequencies mainly because of the frequency response of the O/E equipment. Figure 5-23(b) depicts measured RF spectra of the thirteenth to the eighteenth IF signals before and after the narrowband IFoF link with a 1-km SMF. The RF power fluctuation among IF channels was caused by the frequency response of the analog down-conversion process. After the narrowband IFoF transmission, the noise level is

found to be relatively increased, compared with the signal level. The main reason was considered to be a high noise power from the DML that was used in this experiment. Figures 5-23(c) and (d) describe RF spectra measured after the DSP equipment and LPF, for the aggregated thirteenth and the fourteenth IF signals and the eighteenth IF signal, respectively. Undesired signal components were effectively suppressed by the digital filter and LPF for both cases. However, small undesired components from the DSP equipment remain in frequencies from 1.0 GHz to 1.6 GHz since the LPF after the DAC #1 passed frequencies of less than 1.6 GHz.

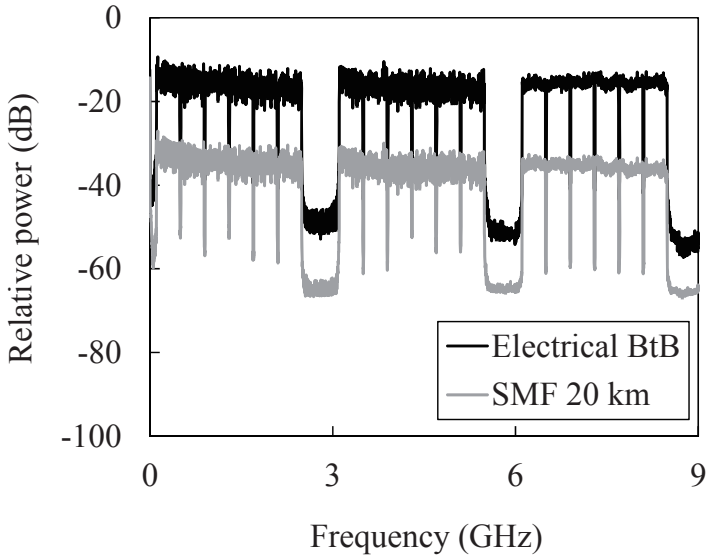

(a)

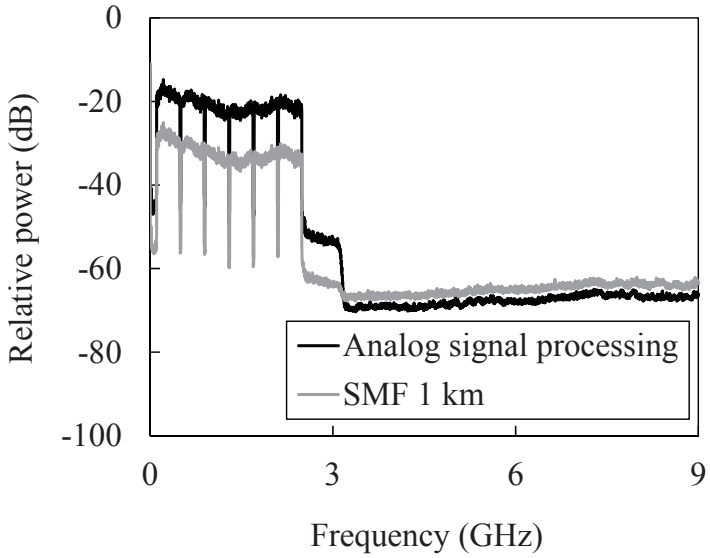
0
-20
-40
-60
-80
-100
Relative power (dB)
0
3
6
9
Frequency (GHz)
Analog signal processing
SMF 1 km

(b)

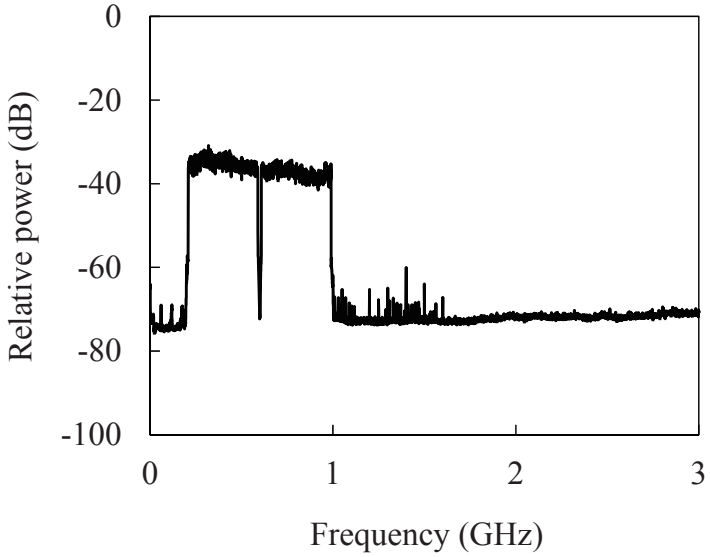
0
-20
-40
-60
-80
-100
Relative power (dB)
0
1
2
3
Frequency (GHz)

(c)

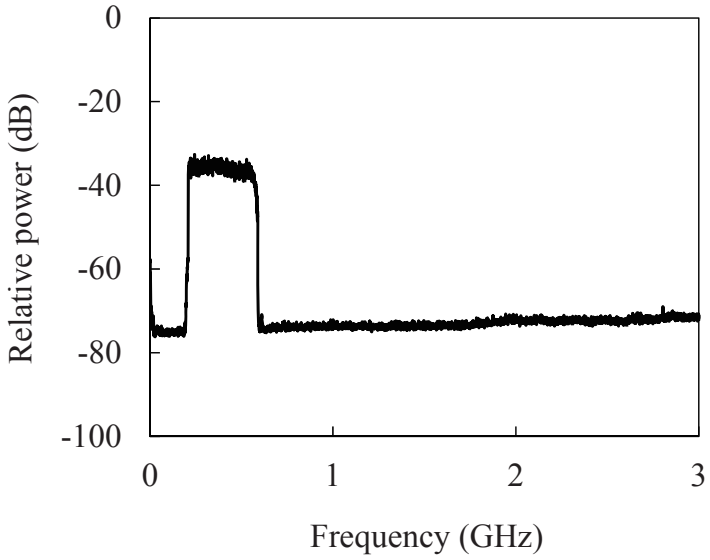

(d)

Fig. 5-23 RF spectra (a) before and after the broadband IFoF link, (b) before and after the narrowband IFoF link, (c) of the DAC #1 output with an LPF for removing undesired aliasing components, and (d) of the DAC #4 output with an LPF for reducing unwanted components.

Measured EVM performances of the six OFDM signals in the third band at various points are presented in Figure 5-24. After the broadband IFoF link with a 20-km SMF and narrowband IFoF link with a 1-km SMF, EVM values are various depending on the channel number. The EVM difference in the band is mainly from the frequency response of the analog frequency converter in the relay site. In the fifteenth and the sixteenth channels, large EVM degradations of over 1.0% are confirmed after the analog signal processing and the narrowband IFoF link. However, the EVM performances of the 5G OFDM signals are finally found to be 6.2% or less, after the DSP equipment and LPF. These EVM values meet an EVM criterion of 8% for 64-QAM signals from 3GPP. EVM margins of around 2% are expected to be sufficient for the following analog upconversion process.

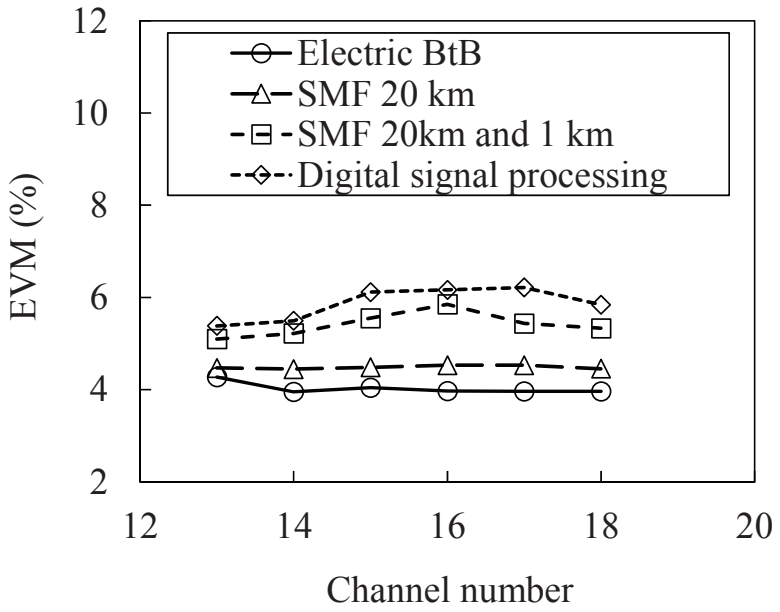

Fig. 5-24 EVM performances for each OFDM signal in the third band.

Figures 5-25(a), (b), (c), and (d) show constellation diagrams of the sixteenth 64-QAM OFDM signal, for electric BtB, after the broadband IFoF transmission, after the narrowband IFoF transmission, and after the DSP equipment and LPF, respectively. From these results, SNR degradations of the signal due to the optical transmission and signal processing are also visually confirmed.

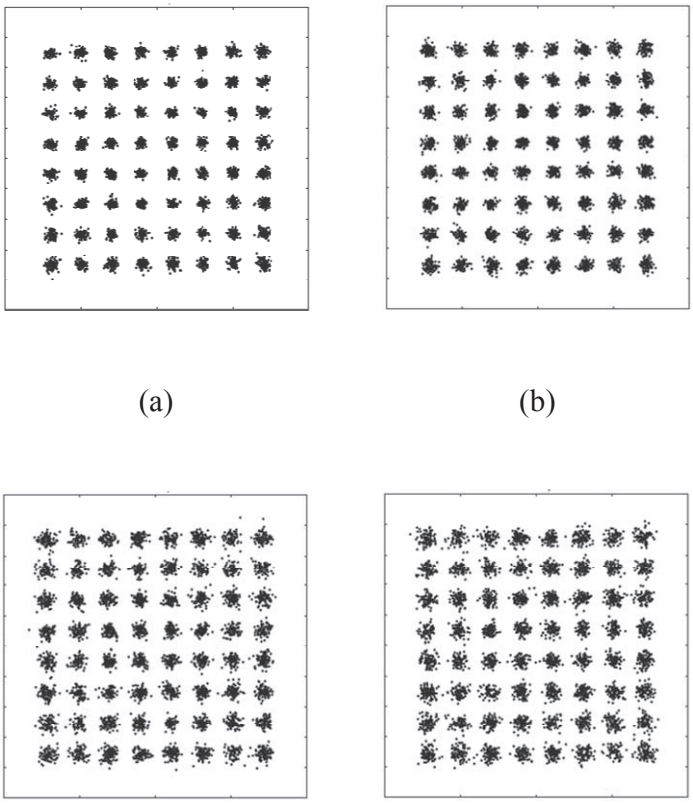

Fig. 5-25 Constellation diagrams of the sixteenth channel measured (a) before the broadband IFoF link, (b) after the broadband IFoF link, (c) after the narrowband IFoF link, and (d) after the digital signal processing.

Figures 5-26(a), (b), and (c) show time-domain waveforms of the six OFDM signals input to the real-time DSP equipment, two OFDM signals from the DAC #1, and an OFDM signal from the DAC #4, respectively. In the same manner as Figure 5-21, the waveforms were observed with a DSO. In comparison with Figures 5-26(a) and (b), the processing delay for the DAC #1 output was around 1.3 μs. On the other hand, in comparison with Figures 5-26(a) and (c), the processing delay for the DAC #4 output was about 1.9 μs. The delay difference is due to without or with the connection between two FPGA boards in the DSP equipment. These delay values will have few

impacts on a delay of 1 ms required by 5G mobile systems. Furthermore, the delays in this measurement are smaller than the delay measured in Figure 5-21. This is mainly because the number of the taps implemented in the digital band filter was only 155 for this experiment, as explained in Section 5-4.2. Through the experiments in this section, it was confirmed that the cascaded IFoF system with hybrid signal processing has potential as one of the MFH technologies for 5G. Additionally, the cascaded IFoF systems are expected to be effective for the future MFH systems that will require higher date rates and lower latencies than 5G, using SCM, WDM, and the other multiplexing technologies properly.

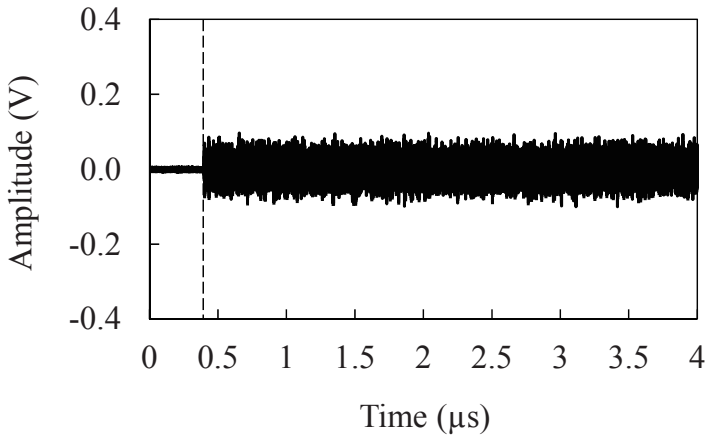

(a)

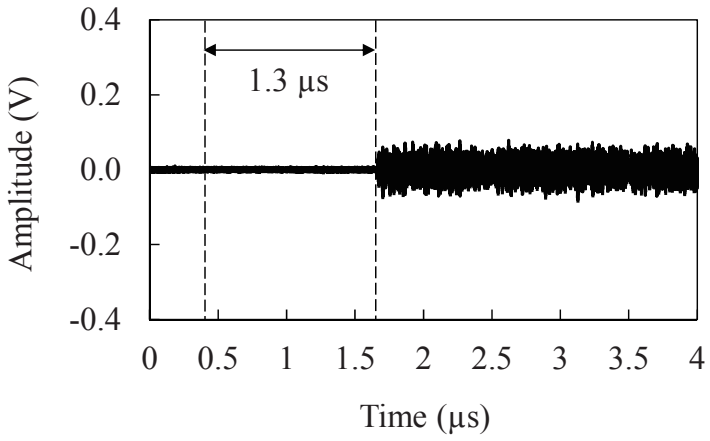

(b)

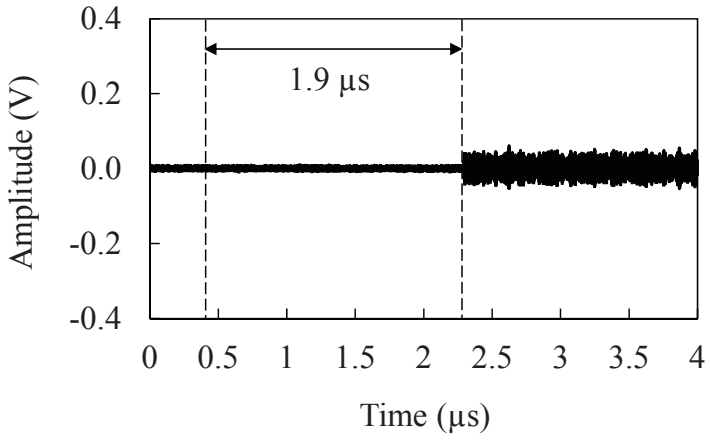

(c)

Fig. 5-26 Signal processing delay of the secondly developed real-time DSP equipment: (a) a time-domain signal of the six IF signals before the DSP, (b) a time-domain signal of two IF signals after the DAC #1, and (c) a time-domain signal of an IF signal after the DAC #4.

5-7 Conclusion

In this chapter, cascaded IFoF-based MFH systems with hybrid signal processing were

explained in detail. The hybrid signal processing, that consisted of analog signal processing in a relay site and digital and analog signal processing in antenna sites, was shown to be a reasonable scheme for 5G application through the calculations on required bandwidths for electric components in relay and antenna sites. It was also confirmed by calculations that the sum of required bandwidths for all optical components in a cascaded IFoF system can be narrower than that in a SCM-PON when four and more antenna sites are assumed.

To verify the effectiveness of the cascaded IFoF-based MFH systems, two types of downlink transmission experiments were conducted. One was for the high spectral efficiency MFH by real-time DSP that implemented an extremely sharp filter. In the experiment, eighteen 64-QAM f-OFDM signals with 360-MHz bandwidths and 3.6-MHz band gaps between adjacent IF signals were transmitted over a 20-km SMF for the broadband IFoF link and a 1-km SMF for the narrowband IFoF link. After the narrowband IFoF transmission and real-time DSP, EVM performances of less than 6.2% were achieved for all channels. A cascaded IFoF MFH system with high spectral efficiency that had an about 24-Gbit/s mobile user data was successfully demonstrated. The other experiment was for 5G mobile communication systems using real-time DSP that supported simultaneous and plural outputs of RF streams in an antenna site. The f-OFDM signals in the first experiment were changed to eighteen OFDM signals with 380.16-MHz bandwidths and 19.84-MHz band gaps between adjacent IF signals. The bandwidth of 380.16 MHz was the maximum value of an OFDM signal specified for 5G mobile systems. After the transmission of the OFDM signals over the same SMFs as the first experiment, EVM values for the thirteenth to eighteenth signals were measured to be less than 6.2%. Additionally, the measured processing delay of the DSP was 1.9 μs at maximum. The potential of the cascaded IFoF system to support 5G MFH with an over 20-Gbit/s mobile user data rate was experimentally shown.

5. References

[1] S. Ishimura, A. Bekkali, K. Tanaka, K. Nishimura, and M. Suzuki, "1.032-Tb/s CPRI-Equivalent Rate IF-Over-Fiber Transmission Using a Parallel IM/PM Transmitter for High-Capacity Mobile Fronthaul Links," *IEEE J. Lightwave Technol.*, vol. 36, no. 8, pp. 1478-1484, 2018.

[2] A. Bekkali, S. Ishimura, K. Tanaka, K. Nishimura, and M. Suzuki, "Multi-IF-Over-Fiber System With Adaptive Frequency Transmit Diversity for High Capacity Mobile Fronthaul," *IEEE J. Lightwave Technol.*, vol. 37, no. 19, pp. 4957-4966, 2019.

[3] P. Li, W. Pan, L. Huang, X. Zou, Y. Pan, Q. Zhou, Y. W. Chen, P. C. Peng, S. Liu, S. Shen, and G. K. Chang, "Multi-IF-Over-Fiber Based Mobile Fronthaul With Blind Linearization and Flexible Dispersion Induced Bandwidth Penalty Mitigation," *IEEE J. Lightwave Technol.*, vol. 37, no. 4, pp. 1424-1433, 2019.

[4] B. G. Kim, S. H. Bae, and Y. C. Chung, "Adaptive Blind CSO Cancellation Technique for RoF Systems Implemented by Using DMLs," *IEEE Photon. Technol. Lett.*, vol. 30, no. 20, pp. 1745-1748, 2018.

[5] H. J. Park, S. Y. Jung, D. W. Kwon, S. H. Cho, H. S. Chung, J. H. Lee, and S. K. Han, "Distortion Mitigation in Multiband OFDM RoF Transmission Employing Blind Post Equalizer," *IEEE Photon. Technol. Lett.*, vol. 28, no. 23, pp. 2708-2711, 2016.

[6] B. G. Kim, H. Kim, and Y. C. Chung, "Impact of Multipath Interference on the Performance of RoF-Based Mobile Fronthaul Network Implemented by Using DML," *IEEE J. Lightwave Technol.*, vol. 35, no. 2, pp. 145-151, 2017.

[7] M. Zhu, X. Liu, N. Chand, F. Effenberger, and G. K. Chang, "High-capacity mobile fronthaul supporting LTE-advanced carrier aggregation and 8×8 MIMO," in Proc. *Optical Fiber Communication Conference (OFC)*, M2J.3, Los Angeles, CA, Mar. 2015.

[8] T. Xu, A. Fumagalli, and R. Hui, "Dynamic optical networks based on digital subcarrier multiplexing," in *Proc. SPIE 10560*, 105600N, 2018.

[9] T. Xu, A. Fumagalli, and R. Hui, "Efficient real-time digital subcarrier cross-connect (DSXC) based on distributed arithmetic DSP algorithm," *IEEE J. Lightwave Technol.*, vol. 38, no. 13, pp. 3495-3505, 2020.

[10] S. H. Cho, H. Park, H. S. Chung, K. H. Doo, S. Lee, and J. H. Lee, “Cost-effective Next Generation Mobile Fronthaul Architecture with Multi-IF Carrier Transmission Scheme,” in *Proc. Optical Fiber Communication Conference (OFC)*, Tu2B.6, San Francisco, CA, Mar. 2014.

[11] M. Xu , J. H. Yan, J. Zhang, F. Lu, J. Wang, L. Cheng, D. Guidotti, and G. K. Chang, “Bidirectional Fiber-Wireless Access Technology for 5G Mobile Spectral Aggregation and Cell Densification,” *IEEE J. Opt. Commun. Netw.*, vol. 8, no. 12, pp. B104–B110, 2016.

[12] M. Befekadu, S. Straullu, S. Abrate, and R. Gaudino, “Experimental Optimization of DSP-Aggregated Front-hauling Transmission for up to 4x96 LTE radio waveforms,” in *Proc. European Conference on Optical Communication (ECOC)*, W.4.P1.SC7.73, Düsseldorf, Germany, Sept. 2016.

[13] K. Tanaka, A. Bekkali, H. Y. Kao, S. Ishimura, K. Nishimura, and M. Suzuki, “First Experimental Demonstration of 5G Mobile Fronthaul Consisting of Cascaded IF-Over-Fiber Links, Frequency Converters and a Channel Selector,” in *Proc. European Conference on Optical Communication (ECOC)*, Tu4B.6, Roma, Italy, Sept. 2018.

[14] K. Tanaka, H. Y. Kao, S. Ishimura, K. Nishimura, T. Kawanishi, and M. Suzuki, “Cascaded IF-Over-Fiber Links With Hybrid Signal Processing for Analog Mobile Fronthaul,” *IEEE J. Lightwave Technol.*, vol. 38, no. 20, pp. 5656-2286, 2020.

[15] 3GPP TS 36.104 v14.3.0 Release 14, “Technical Specification Group Radio Access Network; Evolved Universal Terrestrial Radio Access (E-UTRA); Base Station (BS) radio transmission and reception,” 2017.

[16] 3GPP TS 38.104 v15.2.0 Release 15, “Technical Specification Group Radio Access Network; NR; Base Station (BS) radio transmission and reception,” 2018.

Chapter 6

Conclusion

Optical access technologies to accommodate mobile BSs or antennas efficiently have been studied. In MBH, a PTP-based time synchronization technique over TDM-PON for avoiding conventional GPS antenna deployments has been experimentally evaluated. Furthermore, in MFH, the effectiveness of cascaded IFoF links with analog and digital hybrid signal processing for replacing conventional PtP CPRI links has been also investigated by transmission experiments. The conclusions of this dissertation are summarized as follows:

1. In Chapter 2, a cascaded IFoF system with hybrid signal processing was proposed for simplifying 5G and future MFH systems. In comparison with a conventional PtP CPRI-based system, the proposed system effectively reduced the number of system components with large cost impacts such as 8 to 1 for access fibers and 32 to 1 for broadband E/O and O/E when the 32 antenna elements per antenna site, four data streams per antenna site, and eight antenna sites were assumed. Additionally, the proposed system reduced the total fiber length by over 50% when the length ratio of the short fiber to the access fiber of 0.2 and four antenna sites were assumed. The total fiber cost of the proposed system was also estimated to be about 13% of that of PtP CPRI system when eight antenna sites, access fiber length of 5 km, and dark fiber usage ratio of 25% were assumed. The potential of the proposed system for simpler and more cost-effective MFH was confirmed.

2. In Chapter 3, a time synchronization technique using PTP packets was proposed in TDM-PON-based MBH systems. A prototype of 10G-EPON with the proposed synchronization function was developed and experimentally evaluated. In the 10G-EPON unit tests, the absolute time accuracy and time fluctuation of the ONUs for 72 hours were 13 ns and 17 ns, respectively. In the interoperability tests with a commercial PTP slave for 72 hours, the absolute time accuracy of 38 ns and the time fluctuation of 55 ns were achieved. Furthermore, in the interoperability tests between the 10G-EPON prototype and a commercial TD-LTE BS with a PTP slave function for 60

hours, the absolute time accuracy and time fluctuation of the BS were measured to be 119 ns and 230 ns, respectively. These experimental results verified the effectiveness of the proposed system for TD-LTE systems and showed the potential of the proposed system for future mobile applications.

3. In Chapter 4, the transmission performances of PtP IFoF-based MFH systems were numerically and experimentally evaluated. In the numerical calculations for CNR values, it was confirmed that 54 100-MHz IF channels were successfully transmitted when transmission conditions such as OMI per channel, received optical power after transmission and IF channel allocation were properly selected. In the IFoF transmission experiment using a commercial LTE BS and deployed fibers, 24 20-MHz OFDM signals including a real 64-QAM LTE signal were successfully transmitted over an optical fiber link, that consisted of 0.4-km in-building fiber and 7.4-km access fiber with -27.9-dB and -21.5-dB optical reflection points, by setting the transmission conditions properly. The applicability of IFoF technologies to 4G mobile systems was experimentally verified.

4. In Chapter 5, cascaded IFoF-based MFH systems with hybrid signal processing for downlink were experimentally evaluated. Two kinds of real-time FPGA for IF channel filtering and frequency conversion in antenna sites were developed; one was for high spectral efficiency MFH using an extremely sharp digital filter and the other was for 5G MFH supporting simultaneous outputs of plural RF streams for each antenna site. Eighteen 64-QAM f-OFDM signals with 360-MHz bandwidths and 3.6-MHz band gaps between adjacent signals were transmitted over cascaded 20-km and 1-km SMFs, and each signal was extracted and converted to an IF by the first developed FPGA. Eighteen 64-QAM OFDM signals with 380.16-MHz bandwidths and 19.84-MHz band gaps between adjacent signals were also transmitted over the same SMFs as the first experiment, and all signals were simultaneously extracted and converted to specific IFs by the second FPGA. In both experiments, EVM values of less than 6.2% were obtained, leaving sufficient margins for the subsequent analog frequency conversions. Through these experiments, the potential of the proposed cascaded IFoF systems for 5G and future MFH was confirmed.

In the future studies, the comparison of MFH systems should include different kinds of technologies such as evolved CPRI (eCPRI). The proposed time synchronization technique should be investigated on the applicability for 5G mobile systems. Theoretical analyses of the obtained time synchronization performances should be also conducted, changing some conditions such as clock stabilities, clock inaccuracies, packet rates, packet delays, and packet fluctuations, for exploring the optimal system design and the technical potential for the future applications. The uplink of the cascaded IFoF systems with hybrid signal processing should be configured and investigated in detail. Additionally, increasing capacity of the MFH links by simple and low-cost electric and optical components will be an issue for expanding the proposed MFH systems to the future 6G mobile systems.

Finally, the author strongly believes the studies in this dissertation will contribute to the development of the future optical access technologies and systems for MBH and MFH applications.

Abbreviations

ADC	analog-to-digital converter
ADSL	asymmetric digital subscriber line
ANT	antenna
APC	angled physical contact
A-RoF	analog radio-over-fiber
ATT	attenuator
AWG	arrayed waveguide grating
	arbitrary waveform generator
AxC	antenna carrier
BBU	baseband unit
BC	boundary clock
BF	beamforming
BPF	bandpass filter
BPSK	binary phase shift keying
BS	base station
BW	bandwidth
CATV	commercial community antenna television
CDMA	code division multiple access
C&M	control and management
CNR	carrier-to-noise ratio
CO	central office
CoMP	coordinated multi-point
CP	cyclic prefix
CPL	coupler
CPRI	common public radio interface
C-RAN	centralized radio access network
Cs	cesium
ctrl	control
CU	central unit

CW	control word
DAC	digital-to-analog converter
DAS	distributed antenna system
DBA	dynamic bandwidth allocation
Demux	demultiplexer
DFB-LD	distributed feedback laser diode
DML	directly modulated laser
D-RAN	distributed radio access network
D-RoF	digitized radio-over-fiber
DSO	digital sampling oscilloscope
DSP	digital signal processing
DU	distributed unit
EDFA	erbium-doped fiber amplifier
EEC	Ethernet equipment clock
eCPRI	evolved common public radio interface
eICIC	enhanced inter-cell interference coordination
eMBB	enhanced mobile broadband
E/O	electrical-to-optical converter
EPC	evolved packet core
EVM	error vector magnitude
FDM	frequency division multiplexing
FFT	fast Fourier transform
FIR	finite impulse response
f-OFDM	filtered OFDM
FPGA	field programmable gate array
FTP	file transfer protocol
FTTH	fiber to the home
FWHM	full width at half maximum
GM	grand master
GNSS	global navigation satellite system
GPS	global positioning system
GSM	global system for mobile communications
HE	head end

HSS	home subscriber server
IFFT	inverse fast Fourier transform
IFoF	intermediate frequency-over-fiber
IMDD	intensity modulation and direct detection
IP	internet protocol
IQ	in-phase and quadrature
LAN	local area network
LD	laser diode
LN-MZM	lithium niobate Mach-Zehnder modulator
LO	local oscillator
LPF	low pass filter
LTE	long term evolution
LTE-A	LTE-Advanced
L2	layer 2
L2SW	layer 2 switch
L3	layer 3
MAC	media access control
MBH	mobile backhaul
MC	media convertor
MFH	mobile fronthaul
MIMO	multiple-input multiple-output
MME	mobility management entity
mMTC	massive-machine type communication
M-ONU	master ONU
MPCP	multipoint control protocol
NNI	network-network interface
NTP	network time protocol
Mux	multiplexer
NCO	numerically controlled oscillator
NRZ	non-return to zero
NW	network
OAM	operation, administration and maintenance
OC	ordinary clock

OCS	oscilloscope
OCXO	oven controlled crystal oscillator
ODN	optical distribution network
O/E	optical-to-electrical converter
OFDM	orthogonal frequency division multiplexing
OLT	optical line terminal
OMI	optical modulation index
ONU	optical network unit
OTDR	optical time-domain reflector
PCRF	policy and charging rules function
PDCP	packet data convergence protocol
P-GW	packet data network gateway
PHY	physical layer
PIN-PD	PIN photodiode
PM	power meter
PON	passive optical network
ppb	parts per billion
ppm	parts per million
PRN	pseudo random noise
PtMP	point-to-multipoint
PtP	point-to-point
PTP	precision time protocol
QPSK	quadrature phase shift keying
Rb	rubidium
RF	radio frequency
RIN	relative intensity noise
RLC	radio link control
rms	root mean square
RRH	remote radio head
RTT	round-trip time
RU	remote unit
Rx	receiver
SA	spectrum analyzer

SCM	subcarrier multiplexing
	subcarrier multiplexed
SDO	standards development organization
SGSN	serving general packet radio service support node
S-GW	serving gateway
SMF	single mode fiber
SNR	signal-to-noise ratio
S-ONU	slave ONU
Sync-E	synchronous Ethernet
TC	transparent clock
TDD	time division duplex
TD-LTE	time division long term evolution
TDM	time division multiplexing
TDMA	time division multiple access
TD-SCDMA	time division synchronous code division multiple access
ToD	time of date
Tx	transmitter
UE	user equipment
UNI	user-network interface
URLLC	ultra-reliable and low latency communication
VCSEL	vertical cavity surface emitting laser
VDSL	very high bit rate digital subscriber line
VOA	variable optical attenuator
VSA	vector signal analyzer
W-CDMA	wideband code division multiple access
WDM	wavelength division multiplexing
WDMA	wavelength division multiple access
WiMAX	worldwide interoperability for microwave access
1PPS	one pulse per second
3GPP	3rd generation partnership project
4G	4th generation
5G	5th generation
64-QAM	64-quadrature amplitude modulation

Acknowlegements

This research has been conducted in the doctoral course of the Department of Electronic and Physical Systems, Graduate School of Fundamental Science and Engineering, Waseda University, under the guidance of Professor Tetsuya Kawanishi.

I would like to express the deepest appreciation to Professor Tetsuya Kawanishi for his thoughtful guidance and constructive suggestions. I would also like to express my sincere appreciation to Professors Katsuyuki Utaka and Takashi Tanii of Waseda University for their fluitful comments and discussions on my doctoral thesis.

I would like to express my sincere gratitude to Professors Yun Chur Chung and Hoon Kim and Dr. Byung Gon Kim of KAIST for fruitful technical discussions in a collaborate research between KAIST and KDDI Research, Inc.

I am deeply grateful to Dr. Masatoshi Suzuki, Mr. Yoji Kishi, Dr. Takehiro Tsuritani, Dr. Kosuke Nishimura, and Mr. Ryo Inohara of KDDI Research, Inc. for their continuous support for this work and helpful technical discussions. I am also particularly grateful to Dr. Shinobu Namba of KDDI Research, Inc., Mr. Naoya Nishi of KDDI Corporation, Dr. Abdelmoula Bekkali of Toyo Electric Corporation, Mr. Takashi Kobayashi of KDDI Corporation, Mr. Shota Ishimura, and Mr. Hsuan-Yun Kao of KDDI Research, Inc. for their fruitful discussions and technical assistances for the experiments related to this thesis.

Finally, I would like to thank my wife, Tomoko Tanaka, and my daughter, Mayuko Tanaka, for their deep understanding of this work and continuous support in my life.

List of publications by the author

1. Papers

[1] K. Tanaka, H. Y. Kao, S. Ishimura, K. Nishimura, T. Kawanishi, and M. Suzuki, "Cascaded IF-Over-Fiber Links With Hybrid Signal Processing for Analog Mobile Fronthaul," *IEEE J. Lightwave Technol.*, vol. 38, no. 20, pp. 5656-5667, 2020.

[2] K. Tanaka, N. Nishi, R. Inohara, and K. Nishimura, "Time Synchronization Technique for Mobile Base Stations over TDM-PON-Based Mobile Backhaul Using Precision Time Protocol," *IEICE Trans. Commun.*, vol. E101-B, no. 4, pp. 979-986, 2018.

[3] K. Tanaka, B. G. Kim, T. Kobayashi, A. Bekkali, S. Nanba, K. Nishimura, H. Kim, Y. C. Chung, and M. Suzuki, "Transmission of Multiple Mobile Wireless Signals by IF-over-Fiber Technique," *IEICE Trans. Electron.*, vol. J101-C, no. 2, pp. 107-118, 2018.

2. International conferences

[1] K. Tanaka, S. Ishimura, K. Nishimura, T. Kawanishi, and M. Suzuki, "Advanced IFoF systems for mobile fronthaul," in *Proc. International Conference on Photonics Solutions (ICPS)*, 21, Chiang Mai, Thailand, Nov. 2019.

[2] K. Tanaka, S. Ishimura, A. Bekkali, K. Nishimura, and M. Suzuki, "Evolution Scenario of Optical Access Infrastructure for Supporting Beyond-5G Mobile Systems," in *Proc. Opto-Electronics and Communications Conference (OECC)*, S1-6, Fukuoka, Japan, July 2019.

[3] K. Tanaka, A. Bekkali, H. Y. Kao, S. Ishimura, K. Nishimura, and M. Suzuki, "First Experimental Demonstration of 5G Mobile Fronthaul Consisting of Cascaded IF-Over-Fiber Links, Frequency Converters and a Channel Selector," in *Proc. European Conference on Optical Communication (ECOC)*, Tu4B.6, Roma, Italy, Sept. 2018.

[4] K. Tanaka, N. Nishi, R. Inohara, and K. Nishimura, “Novel Scheme of PTP Packets Distribution over TDM-PON for Time Synchronization among Mobile Base Station,” in *Proc. Optical Fiber Communication Conference (OFC)*, Th4B.3, Los Angeles, CA, Mar. 2017.

3. Review papers

[1] K. Tanaka, S. Ishimura, and K. Nishimura, “Radio-over-Fiber Technologies for Mobile Communication Systems,” *The Review of Laser Engineering*, vol. 43, no. 1, pp. 6-10, 2020.